AN ABSTRACT OF THE THESIS OF

FREDERICK ROLAND FICKETT (Name) for the Ph. D. (Degree)

in PHYSICS (Major) presented on October 18, 1967 (Date)

Title: LONGITUDINAL MAGNETORESISTANCE OF SINGLE-CRYSTAL MERCURY

Abstract approved: [redacted]
Dr. Melvin Cutler

The longitudinal magnetoresistance of single-crystals of mercury is investigated experimentally, both in the low field and the high field regions. The variation of the magnetoresistance with crystal purity, orientation, size and temperature below 4.2°K is presented. In the low field region the data are discussed in terms of existing theory. The data in the high field region are treated following the ideas of Pippard in terms of a simplified model of the mercury Fermi surface. Agreement of the experimental data with the model calculations is found to be quite good considering the simplicity of the model.

The results of an experimental investigation of the zero field resistance of the mercury crystals from 1.8°K to the melting point are also presented. Observed deviations from the Bloch-Grüneisen law at low temperatures and near the melting point are discussed. An anomaly is observed in the resistance versus temperature

curves near 4.2°K. A possible explanation of this behavior is presented.

A discussion of a number of new techniques related to the methods of growth, X-ray orientation and handling of the mercury crystals is also included.

Longitudinal Magnetoresistance of Single-Crystal Mercury

by

Frederick Roland Fickett

A THESIS

submitted to

Oregon State University

in partial fulfillment of
the requirements for the
degree of

Doctor of Philosophy

June 1968

APPROVED:

[redacted]

Associate Professor of Physics
in charge of major

[redacted]

Head of Department of Physics

[redacted]

Dean of Graduate School

Date thesis is presented October 18, 1967

Typed by Marion F. Palmateer for Frederick Roland Fickett

ACKNOWLEDGEMENT

I wish to thank Dr. Melvin Cutler for taking time from his own research on liquid semiconductors to direct this thesis. I am also grateful to Dr. Allen Wasserman for many illuminating theoretical discussions.

Thanks is also due to the Albany Metallurgy Research Center of the United States Bureau of Mines for providing fellowship support for this research. The project on alloy superconductors headed by Mr. Richard Siemens deserves special thanks on several counts, first for providing the equipment and liquid helium without which this project would have been impossible, and second for the long hours of assistance provided by Mr. Siemens and Mr. Donald Deardorff in the actual performance of the experimental runs.

TABLE OF CONTENTS

LIST OF FIGURES

LIST OF TABLES

LONGITUDINAL MAGNETORESISTANCE OF SINGLE-CRYSTAL MERCURY

CHAPTER 1

INTRODUCTION

Fermiology, the study of the properties of metallic Fermi surfaces, has become one of the major branches of solid state physics over the past decade. Early theoretical work by Lifshitz, Azbel' and Kaganov (1957) and by Lifshitz and Peschanski (1959) showed that measurements of the galvanomagnetic properties of metals made under suitable conditions could be related directly to the topology of the Fermi surface. It was further shown by Harrison (1960) that a Fermi surface constructed from a nearly-free-electron theory exhibited most of the features of the actual surface, at least in a qualitative way. Later calculations by Loucks (1967) using the relativistic augmented plane wave (RAPW) method gave a theoretical model which agrees quantitatively with experiment for a number of metals including mercury. The Fermi surface topology of a large number of metals has been outlined both experimentally and theoretically by this time. The most common experimental methods are measurements of the de Haas-Van Alphen effect and of the transverse magnetoresistance.

The availability of a well defined Fermi surface for a particular

metal leads to the possibility of investigating the scattering interactions of the electrons on the surface. Pippard (1964) suggested that measurement of the longitudinal magnetoresistance might give at least a qualitative picture of the mechanisms. Recent work by Powell (1966) has shown that for the case of copper the variation of the mean free path over the surface can be determined by longitudinal magnetoresistance measurements combined with a detailed knowledge of the topology. No other longitudinal magnetoresistance experiments on single crystals have been reported in the literature.

The research described here was an attempt to determine what sort of information could be obtained from measurement of the longitudinal magnetoresistance on a metal with a more complex Fermi surface than those of the monovalent metals. Mercury was chosen for the experiment because its relatively simple Fermi surface extending into only two zones might allow some approximate calculations to be made. While no detailed topology measurements have been made, the main features of the surface have been determined by de Haas-Van Alphen (Brandt and Rayne, 1965) and transverse magnetoresistance (Datars and Dixon, 1967, and Dishman and Rayne, 1966) experiments. Agreement of these measurements with an RAPW calculation by Keeton and Loucks (1966) is generally good.

The behavior of the longitudinal magnetoresistance of pure metals at a given temperature is expected to depend strongly on the

magnitude of the dominant phonon wave vector at that temperature. This information can be obtained from measurements of the variation of the lattice resistance with temperature. This information was not available in the literature so an experiment was done to measure the variation of the resistance of single crystals of mercury with temperature and the results of that experiment are also reported here.

CHAPTER 2

STATEMENT OF THE PROBLEM

The research reported here is an investigation of the electrical resistance of single crystals of mercury, its variation with temperature and crystal orientation, and the effect of a magnetic field parallel to the current direction through the crystal. The latter measurement is termed longitudinal magnetoresistance. The experiments involving magnetic fields are performed at 4.2° K and below, as it is in this low temperature region that the features of the Fermi surface have a significant effect on the conduction mechanisms.

Mercury is a superconductor with the relatively high transformation temperature of 4.15° K. This leads to difficulties, particularly in the magnetoresistance measurements, since it is often desirable to have the resistance at zero magnetic field. This resistance must, of course, be determined by indirect methods below the transformation temperature.

The low melting point of mercury required development of a rather specialized technology for handling the crystals and making the experimental measurements. The details of the various pieces of equipment and techniques are discussed in Chapter 3.

Chapter 4 is devoted to a discussion of the variation of the resistance of the mercury crystals with temperature over a temperature

range from 1.8° K to the melting point. A comparison to theory is given and observed deviations from the theory are discussed.

A brief discussion of the low field magnetoresistance measurements is given in Chapter 5. The observations are discussed in terms of current theory.

The high field magnetoresistance measurements are treated in Chapter 6. A plausible model of the mercury Fermi surface is developed and the implications of the measurements with respect to calculations from the model are discussed.

CHAPTER 3

EXPERIMENTAL TECHNIQUES

The extreme softness of solid mercury and its low melting point have required the development of specialized techniques for handling the crystals throughout the various phases of the experiment. These techniques are discussed in detail in this section.

Figures 1 through 4[1] show the experimental arrangements in block diagram form.

Crystal Growth and Storage

Mercury solidifies at 234.3° K. In the solid state, at temperatures down to at least 77° K, the metal remains extremely soft and is easily deformed. If two pieces of the metal come into contact at these temperatures a bond is formed of such strength that cutting is necessary to separate them. The samples for this experiment were required to be free-surface single crystals of nominal rectangular cross section. The crystals had to be grown in a strain-free manner and in such a fashion that subsequent handling would not result in deformation.

The mold used was of the Shubnikov type and is shown in

---

[1] All figures are at the end of the text.

Figure 5. The separate pieces of the mold are of plexiglass and all surfaces facing the crystal, except that of the ridge, have a Teflon (TFE) tape applied to facilitate removal of the pieces. The ridge width is 2.0 mm, and by use of various side pieces, crystals of thicknesses from 0.25 to 2.0 mm were grown. In use, one end of the mold is covered with the tape and the mold is bound together with the tape. The mold is filled with mercury of 99.99999% purity[2] (some alloy samples were also made, as discussed later, using the same method) with a hypodermic needle until a small ball of mercury is formed above the top end. It is necessary to have this ball, otherwise the crystal surface will invariably be pitted. If the sample is to be grown with the mold in a horizontal position, the open end is fitted with a cup of red wax to contain the liquid excess.

To grow the crystals, the mold is inserted into a Styrafoam chimney, the open bottom end of the chimney resting on CO_2 snow at 195° K, and the whole arrangement enclosed in a wide-mouth dewar. This configuration provides a sufficient temperature gradient and single crystals are generally obtained.

This method of growth results in a single crystal approximately 80% of the time. Due to the shape of the mold, the growth is initiated in a random fashion and, apparently for this reason, no

---

[2] United Mineral and Chemical Company

preferred orientation is noted. Andrew (1949), in his work on small wires, noted a preference for crystals to form, each with its trigonal axis normal to the temperature gradient.

When the TFE covered pieces of the mold are removed after the crystal is grown, the sample remains loosely bonded to the smooth surface of the plexiglass ridge. This arrangement provides a convenient method for handling the samples without having to touch the metal itself. There is no indication, either from X-ray work or from electrical measurement, that any strains are induced in the crystals due to a differential contraction of the ridge and the sample at the temperatures used in the experiment.

Measurement of some of the samples showed them to be of uniform cross section. There is a slight variation of crystal thickness with a maximum of 0.003 inch, due to the fact that the smooth surface of the original plexiglass sheet was used for the ridge; it exhibits this much waviness over the 1.25-inch length of the crystal. Crystals grown from dilute alloys of silver and cadmium (0.01 to 0.001 wt %) tend to be pitted and show strains induced by alloying. These strains tend to anneal out somewhat after a month or more of storage.

Until the crystals have been mounted for the experiment, they are stored under alcohol at approximately 195° K. After mounting the holders are stored in brass tubes surrounded by CO_2 ice.

Early in the experiment a series of resistance ratio measurements (R liquid nitrogen/R liquid helium) were made on crystals grown from mercury of advertised purities of 99.9, 99.999, 99.9999 and 99.99999%. No change was observed in the resistance ratio for the different purities, while the change due to the dilute alloys of Ag and Cd mentioned above was as much as 50%.

Before the X-ray methods had been perfected, it was thought that perhaps the easiest method of determining crystal orientation for the pure crystals would be to use the ratio of the resistance in the liquid state to that of the solid, much in the same fashion as Sckell (1930). To investigate whether the resistance ratio could be increased, an annealing oven was built which could hold the crystals at 0.5°C below the melting point for several hours. A zone-refining device was also developed for the same purpose. Neither of these methods showed any effect on the resistance ratio for reasons which are now clear and are discussed in Chapter 4.

Another series of tests was made to determine if the stainless steel hypodermic needle used for filling the molds might have contaminated the mercury. Molds were filled with carefully cleaned glass syringes and TFE needles, and crystals grown for comparison to those grown in the usual manner. In terms of electrical purity measurements to 1.80°K no noticeable contamination resulted.

Analysis of Crystal Orientation

All of the effects investigated in this experiment depend strongly on the relative orientation of the crystal lattice to the current direction. It is thus necessary to determine the orientation of the lattice with respect to the external dimensions of the sample rod.

Mercury crystalizes in a simple rhombohedral lattice. The lattice parameters, as given by Barrett (1957), are a_o = 2.9925 Å α = 70° 44.6' at 78°K. His measurements indicate no change in α and a 0.2% decrease in a_o upon cooling to 5°K. This structure has a single three-fold axis with three two-fold axes perpendicular to it and three mirror symmetry planes containing the trigonal axis and bisecting the 60° angles between two-fold axes. The space group is $\bar{3}$m. The reciprocal lattice is also simple rhombohedral with α = 104° 23'.

Photographs of models of the direct and reciprocal lattices are shown in Figures 6 and 7. The cell outlined by the black rods in Figure 6 is the face-centered rhombohedral cell which is often used in discussions of the mercury lattice. It can be regarded as a face-centered cubic cell distorted along a diagonal in the direction of the mercury trigonal axis. Crystallographic angles referred to this cell are given by Bacon, Hecksher and Crocker (1964). This particular type of distortion brings (111) planes quite close together. The

atomic separation in a (111) plane is 3.47 Å, while the distance between atoms in adjacent (111) planes is 3.00 Å; thus, the coordination number is six. As mentioned by Wycoff (1963), this is an opposite type of distortion of the cubic close-packed structure from that of the other (hexagonal) II-B metals, zinc and cadmium.

A second phase of mercury exists (Bridgman, 1935), the β phase, stable below 90° K, but the α-β transformation requires pressures of several thousand atmospheres at temperatures below 79° K (Shirber and Swenson, 1961, 1962), and does not occur at zero applied pressure as suggested by Bridgman.

The large size of the samples and the problems caused by the low melting point required that a Laue back reflection method be used for X-ray analysis of the samples. The techniques of the Laue method are discussed in detail by Cullity (1956). In general, Laue back reflection patterns are quite difficult to interpret for crystals of symmetry as low as that of mercury. A further problem was presented by the fact that the sample holding arrangement could not be permanently set up on the X-ray machine.

The procedure generally followed in Laue work is to change the orientation of the crystal with respect to the X-ray beam until a high symmetry axis, whose pattern is easily identified, is along the beam. A sample holder (Figure 8) was constructed for this purpose, but the problem of keeping the large crystal cold made its use so marginal

that it was used only as a last resort on crystals where the methods described below would not yield an orientation.

The general X-ray procedure is to use a tungsten target tube operated at 30 kv and 16 ma with a Polaroid cassette in the back reflection position. The exposure times of two to five minutes are such that a stream of cold nitrogen gas boiled from a dewar of liquid nitrogen by a heating element is sufficient to keep the crystal solid and free of ice for the exposure.

A sample holder was molded from expandable polystyrene beads with a front slot to accept the plexiglass ridge holding the sample. This holder and its track mount are shown in Figure 9. An enclosed space behind the sample is filled with dry ice snow and another Styrafoam piece just above the sample provides a path for the cold nitrogen gas such that it passes over the length of the sample in a stream three or four times the width of the sample. Other small pieces of Styrafoam serve to further isolate the sample from the warm room air. Note that the Styrafoam sample holder sits on a plastic tray from which it can be easily moved to a large dewar of dry ice for sample changes. The plastic base is milled out so that the Styrafoam sample holder is placed in the same position each time. The main feature of this holder is that there is no solid material between the sample face and the X-ray beam, thus making short exposures possible.

To further assist in the orientation of the samples, a goniometer (Figure 10) was constructed to allow back reflection patterns to be taken over a large range of angles on small single crystals of roughly hemispherical shape which were specially grown for this purpose. The smaller crystal size greatly simplifies the cooling problem. This goniometer allows mapping of the prominent zones of the mercury pattern over a large angular range. The small parts of these prominent zones which appear on the patterns from the samples in the Styrafoam sample holder can then be compared with these maps.

The orientation is determined by making stereographic projections of prominent zones from patterns made with a film-to-sample distance of 3 or 4 cm. Zone intersections (higher symmetry points) are then translated to the center of the projection in the usual manner. These projections are then compared to standard projections constructed from the crystallographic angle data of Arko, Cotner, and Weertman (1963). The standard (111) projection from their report is reproduced as Figure 11. For some orientations which are quite similar, such as (110) and ($\bar{1}$01), maps of the zone spots from the large-angle orienter are used in the manner described above.

The nature of the samples and the fact that the X-ray machine could only be borrowed for short periods of time did not permit an extremely accurate arrangement to determine crystal orientation

such as that devised by Powell (1966) for a similar experiment on copper. Further, the accuracy of the equipment available for the experimental runs did not warrant such a critical determination. The nets used for the projections were carefully checked against the original construction equations and the sample-to-film distance was accurate to within 1 mm. The major source of inaccuracy is in the orientation of the sample with respect to the film and X-ray beam. The usual optical methods of orientation could not be used here, and measurements on the system indicate that the maximum probable error from this source is $\pm$ 3°. An error of similar magnitude exists for the location of the (111) axis when it is not actually on the Laue photograph, as it must be projected back to the stereographic projection from a standard projection. Due to the way the apparatus is constructed, these errors are not cumulative in full and the error in the angle between the current direction and the (111) axis has a maximum value of $\pm$ 4°.

Lattices which are not cubic do not, in general, have their lattice directions parallel to the poles of the lattice planes. Mercury exhibits this parallelism only for the [111] direction and for directions in the (111) plane. Since the poles of the direct lattice planes are used both in the X-ray analysis and in the Brillouin zone construction, all nomenclature will be in terms of the poles unless it is explicitly stated to be otherwise. The transformation back to the

direct lattice is easily accomplished with the aid of the data given by Arko, et al. (1963).

The crystal orientations listed in Appendix A use the following convention: χ is the angle between the long axis of the sample rod and the (111) direction in the (reciprocal) lattice; and ϕ is the angle made by the projection of the rod axis on the plane normal to (111) with the $(\bar{2}11)$ direction and is positive counterclockwise from the $(\bar{2}11)$ direction. These relationships are easily seen by referring to the stereographic projection of the reciprocal lattice in Figure 11. All directions are stated so as to lie in the irreducible part of the projection defined by $(\bar{1}01)$, (111) and $(01\bar{1})$. In this experiment the current and the magnetic field are always along the rod axis.

Universal Sample Mounts

In the course of the experiment measurements are made with the sample crystal in four different sample holders. These holders and their functions are described in the following section of this chapter. So that comparisons between measurements in the different holders could be made easily and because lead attachment is relatively difficult a universal sample mount was designed which fits all of the sample holders and the storage tubes. Once the crystal has been mounted it is not removed until all measurements have been completed. A drawing of the mount is shown in Figure 12.

The leads are tinned with mercury by first dipping them in dilute nitric acid and then into clean mercury. Attachment of the leads to the crystal is done by "soldering" the the tinned leads to the crystal with a relatively warm iron.

It was determined early in the work that the low signal levels on the potential leads (0. 1 μv minimum) required essentially continuous leads from the sample to the meter in order to avoid large signals due to thermal effects in soldered joints. The method used was to take the potential leads (No. 34 copper wire) out of the dewar through an O-ring seal, the leads themselves being epoxied into a short small diameter stainless steel tube to insure a good vacuum seal. The ends of the leads were then clamped into a copper junction block and copper clips from the meter were connected to the block. This method of maintaining copper-to-copper joints reduced the thermal emfs to a suitably low level.

The current leads (No. 18 copper wire) were connected to the sample by means of strips of 0. 002 inch copper foil of the same width as the samples. The potential leads were placed approximately 0. 20 inches from the current connections.

The shorting effects of the current electrodes are not as serious in this type of experiment as they would be in a Hall or transverse magnetoresistance measurement. The theory of such effects has been treated in great detail by Gorkun (1961), and Putley (1960)

gives some simple criteria which are satisfied many times over by the arrangement used here.

A groove parallel to the sample is provided to hold a germanium thermometer or thermocouple for the resistance versus temperature measurements. A copper collar is placed on the stainless steel tube at the upper end of the mount. This collar is machined to give a good fit to the copper cups used as isothermal enclosures for the resistance versus temperature measurements which are described in a later section. A slot is provided in the collar for leads from the thermometric devices.

In the early phases of the experiments in the stainless steel dewars a two-resistor level detector of the bridge type (White, 1961) was installed on the crystal mounts to determine when the liquid level fell below the top of the samples. Several runs made with the detector in place allowed determination of the proper amount of liquid helium required for a given measurement.

Resistance and Magnetoresistance Sample Holders

The wide range of temperatures and magnetic fields used in the experiment required a large number of separate sample holders. These are described in this section and the figures. The high field superconducting magnet used here had an effective lower field of 1500 Oe due to power supply leakage and trapped flux. For this

reason the smaller magnet, described below, was constructed in order to keep the samples just slightly above their critical field for resistance measurements below the transition temperature with a minimum magnetoresistance effect. The small magnet was also used to investigate the low field magnetoresistance of the samples.

The separate sample holders are as follows:

1. A small holder (Figure 13) which fits tightly over the sample and has the usual foil current leads and short potential leads of No. 28 copper wire embedded in plexiglass cylinders. The cylinders are inserted into holes in the holder bringing the tinned leads into contact with the top surface of the crystal at a separation of 0.90 inches and accurately in line with the long dimension. The crystal resistance at 77°K is measured in this holder and, combined with mold measurements prior to growing the crystal, is used to determine the resistivity of the crystal for comparison to the X-ray orientations. The indentations made in the crystal by the potential leads provide a location for attaching the leads of the universal sample mounts.

2. Holder for resistance versus temperature measurements in the range 77 °K to 220° K. This holder is shown in cross section in Figure 14. An oxygen-free high-conductivity (OFHC) copper cup 3.5 inches long and 0.500 inches ID with 0.125 inch walls is wound with a length of resistance wire to provide a heat source. The

bottom of the cup is threaded to accept 3.0 inch long brass rods of varying diameters. The cup is tightly inserted into a hole in a Styrafoam dewar lid so that it is insulated along its entire length. The brass heat sink reaches from the bottom of the cup down into liquid nitrogen in the bottom of the dewar. For this arrangement a 0.25 inch diameter brass rod was found to give the best temperature control. Brass is used for the heat sink because of its ability to maintain a much greater temperature gradient than copper.

The sample mount with an attached copper-constantan thermocouple is inserted into the cup with the copper collar of the sample mount closing off the top of the cup. By using an adjustable, current-regulated d-c power supply for the heater the temperature can be varied over the range from 100° K to 220° K. At any setting the temperature can be held steady to ±1° K as indicated by the thermocouple. Calibration of the thermocouple with liquid gases and slush baths over the temperature range shows temperatures to be accurate to ±0.5° K. The high thermal conductivity of the OFHC copper guarantees that the enclosure will be nearly isothermal.

3. Holder for resistance versus temperature measurement in the range 4.2° K to 40° K. This holder is shown in cross section in Figure 15. An OFHC copper cup similar to that of the previous holder forms the sample enclosure. The cup is contained in a two-wall stainless steel dewar. A single stainless steel tube extends

5. 0 inches upward from the top of this dewar. In use, the holder is placed inside a four-wall glass helium dewar and the dewar is filled with liquid helium to just over the top of the upper tube of the holder so that the sample is in the liquid for the 4. 2° K reading. Then, using the heater at low power levels (approximately 0. 3 watts), the liquid is boiled off until the level is well down on the upper tube. A germanium resistance thermometer in the groove of the mount beside the sample is used to monitor the temperature in the cup enclosure. By adjusting the current to the heater, an equilibrium is reached between the heat input to the cup and the output up the dewar wall to the liquid. The temperature stability of the system is such that the temperature can be maintained to $\pm$0. 02° K up to 5° K; $\pm$0. 1° K to 20° K; and to $\pm$0. 2° K above that, as indicated by the thermometer.

The germanium thermometer was purchased uncalibrated and a similar factory-calibrated thermometer was used for calibration. The two thermometers were fitted side by side into the copper cup for this comparison. The absolute accuracy of the thermometer is calculated to be approximately $\pm$ 3%. The thermometer power supply, constructed in the laboratory, allowed constant monitoring of the thermometer current and the temperature reading. The holder is capable of temperatures to 100° K or higher, but the readings here stop at 40° K, which represents the upper limit of the thermometer.

4. Holder for resistance versus temperature below 4. 2° K and

for low field magnetoresistance. A small superconducting magnet 4. 20 inches long with a 0. 458 inch bore was wound with six layers of copper-clad NbTi wire. The small size of the bore does not allow field calibration with available instruments, but the design parameters give a magnet constant of 226 Oe/amp with a homogeneity of 0. 2% over the central 0. 5 inch. This value for the magnet constant is consistent with observed critical field values for mercury at various temperatures (Finnemore, Mapother and Shaw, 1960). The maximum field used was approximately 2400 Oe limited by the 10 amp current-regulated power supply used to power the magnet. Superconducting to normal joints were made by tinning the copper cladding with indium solder and crimping the tinned wires into a three inch length of copper tubing.

This magnet was designed to be used in the isolation dewar of the large magnet system as this dewar was already fitted with the pumping lines and control systems for work below 4. 2° K.

For measurements in this holder, the sample mount is fitted into a wooden tube, the OD of which fits the magnet bore tightly. The tube has a ridge slightly larger than the bore of the magnet which positions the sample vertically at the center of the solenoid.

The absolute accuracy of the field magnitude is estimated from the critical field data to be better than $\pm 5\%$. The relative accuracy is determined by the metering arrangement used for the magnet current

and is $\pm$0. 5%. A discussion of the temperature control and monitoring system is given in the following section of this chapter.

5. High field longitudinal magnetoresistance holder. A cross section drawing of the holder is shown in Figure 16. This holder is mounted within the isolation dewar which, in turn, is inside the high field magnet. The runs are made at fields up to 48 kOe at temperatures from 4. 2° K to 1. 8° K. At the lower temperatures and high fields, the error due to a slight misorientation of the sample from exact parallism with the field is extremely large due to the magnitude of the transverse magnetoresistance component. As an example, an error of approximately 1° at 1. 8° K leads to a value of R(48 kOe)/R(2 kOe) of 2. 2 versus 1. 6 for the parallel orientation. As a result, a special provision is made for sensitive adjustment of the orientation of the sample while it is at liquid helium temperature.

The head unit is constructed as follows: The sample mount is held at the end of a thin-wall stainless steel tube approximately 47 inches from the top of the dewar. This places the sample in the center of the magnet bore. This tube is carefully attached to the head plate in a manner such that the sample misorientation due to the head unit alone is less than 2°. The tube is fitted with a pivot just above the point where the isolation dewar necks down to enter the magnet bore. This pivot fits into a pivot ring firmly attached to the inner bore of the dewar. At the top of the dewar a bellows system

(Figure 17) and two sets of drive screws at right angles allow the sample to pivot through a total angle of approximately 2° in any direction while the system is under vacuum. The orientation procedure is as follows: The sample is in place and the dewar filled with liquid helium; the temperature is lowered by pumping to 1.8° K; and the field is brought up to 48 kOe. The sample is then oriented for a minimum sample voltage reading by means of the drive screws. The head is then locked in place with the screws and the system is returned to atmospheric pressure by admitting dry helium gas. The cold liquid remaining in the dewar is boiled off by means of a resistor near the sample, a new transfer is made, and the runs proceed without changing the orientation of the sample. A discussion of the justification for this procedure and a listing of the runs made is given in Chapter 6 where the data from the runs are treated.

Calculations from purposely misoriented crystals and observations of sharpness of the minimum upon orientation indicate that this method gives a maximum error of $\pm 0.1°$ in the sample orientation.

Magnet and Dewar System

The system is a commercial one.[3] The superconducting magnet is capable of a maximum field of 56 kOe with a homogeniety of

---

[3] Varian Associates, Inc.

better than 1% over the central inch. The available bore size is 1.5 inches without the isolation dewar in place and 1.2 inches with the dewar. Field magnitudes are determined from a volt-potentiometer reading across a standard resistor in series with the current supply. Multiplication of this reading by the manufacturer's magnet constant gives the field.

At fields below 20 kOe the accuracy of the field magnitude is limited by trapped flux to 1% at the lowest fields, and increases to 0.1% at fields above 20 kOe where the major limitation is the stability of the power supply. The reproducibility is estimated to be 0.1% over the entire field range.

The maximum field attainable with the magnet before quenching occurs is dependent on the rate at which the field is increased. The requirement that high field runs be made in a reasonable period of time leads to a maximum field of 48 kOe for the experiment.

All dewars are stainless steel and of standard design. Temperatures below 4.2° K are obtained in the isolation dewar by pumping through a 2.25 inch diameter line with a 264 l/min vacuum pump. Temperature regulation is provided by a cartesian manostat in the pumping line. The arrangement is such that the manostat can be by-passed to reach the lowest temperatures. The system reaches a minimum temperature of 1.7° K.

The temperature of the pumped liquid is measured with a

precision dial manometer[4] monitoring the vapor pressure above the liquid. The gauge is calibrated directly in degrees Kelvin with National Bureau of Standards data (Brickwedde, et al. 1960) and has a claimed accuracy of ±0.004° K. The gauge is calibrated at 25° C and has a maximum temperature effect of 0.4%/10° K. The manostat allows control of the temperature to ±0.001° K as measured by the gauge and the system can easily be held within this range for the length of time required for the runs.

Errors due to the hydrostatic pressure head and those inherent in the open type of vapor pressure monitoring, as discussed by Hoare and Zimmerman (1959), limit the accuracy of temperature measurement to approximately ±0.02° K.

Electrical Measurements

The d-c sample current, usually 2.0 amperes, is supplied by a current-regulated, low voltage supply with an external ten-turn current setting control for most of the measurements. A 12-volt auto battery and adjustable resistor system is used for the resistance versus temperature and low field magnetoresistance measurements where the regulated supply is needed to power the small magnet. The sample current is continuously monitored with a calibrated

---

[4] Wallace and Tiernan, Inc., Model FA145.

ammeter. The power supply has a stability better than ±0.005 amperes at 2.0 amperes. A reversing switch is provided in the line which can be operated either manually or automatically with a 15 second reading in each position.

The sample voltage, generally between 0.5 and 20 microvolts at 4.2° K and below, is read with a Kiethley 150A microvolt-ammeter connected to a time-based recorder. A Kiethley 148 nanovoltmeter was used early in the experiment but a small oscillation in the output which could not be removed caused us to favor the microvolt-ammeter. Both of these meters offer a stable zero suppressing mechanism which allows suppression of signals up to 100 times full scale which is useful in removing constant thermal emfs and in looking at small variations in a large signal such as those observed in the low field magnetoresistance work. The absolute accuracy of the 150A is ± 2% and the linearity is estimated to be better than ± 1%. The recorder accuracy is slated to be ±0.25% of full span. The exception to the use of this system is the measurement of resistance versus temperature above 77° K. In this temperature range the sample voltages are such that a millivolt potentiometer can be used. The accuracy of sample voltage measurement in this range is ±0.05% + 15 μ v.

Some high field magnetoresistance runs were made using an x-y recorder and plotting resistance versus field directly as the field was increased slowly. This method is reasonably successful at

higher temperatures although a small, constant voltage is introduced due to the changing flux through unavoidable loops in the potential leads and correction must be made for this effect. At lower temperatures, and thus low signal levels, slight thermal drifts made this method impractical. The majority of the runs used in this experiment were made point-by-point with several current reversals at each field point.

The low field magnetoresistance runs were about evenly divided between a point-by-point method of low accuracy, since the zero field signal cannot be suppressed, and an x-y recorder method with the zero field signal suppressed. The latter method has considerably higher accuracy, but if thermal drifts are present the curves have to be rerun several times. When this is done, the agreement between the two methods is good, although the accuracy of either method is not nearly as good as that of the high field runs.

CHAPTER 4

THE RESISTANCE AT ZERO MAGNETIC FIELD

The experimental investigation of the zero field resistance of the mercury crystals was originally used only to indicate the predominant type of scattering mechanism at a given temperature near 4.2°K for use in conjunction with the high field magnetoresistance measurements. The results were sufficiently interesting that the investigation was enlarged to cover the entire temperature range from the lowest attainable temperature to the melting point.

The chapter is divided into four sections; the first is a discussion of the general theory of resistance in metals with an emphasis on low temperature effects, the second part deals with the methods used to process the raw data, the third section presents the results along with additional theoretical discussion where necessary, and the final section is a summary of the results and some possible conclusions.

Theoretical Discussion

At zero magnetic field the electrical resistance of metals is usually determined by a combination of scattering mechanisms. We can group these loosely into two categories, scattering by phonons (lattice vibrations) and scattering by impurities. The impurities

may be chemical or mechanical in nature and size effects are included under this category as well. We begin our discussion with a treatment of the phonon scattering in general and of the Bloch-Grüneisen formulation in particular. We then consider briefly the theoretical aspects of some other related problems such as the effect of crystalline anisotropy, problems of measurement in the superconducting region, and the effect of impurities and size effects.

Variation of the Resistance with Temperature

The interaction between conduction electrons and the lattice phonons is responsible for the temperature dependent part of the resistivity of metals.

Both chemical impurities and lattice imperfections give a constant contribution to the resistivity which, in high purity metals, is quite small and is termed the residual resistivity. The theory of scattering by impurities is treated in many texts. A particularly readable account is given by Rosenberg (1963). For our purposes it is sufficient to say that the resistance due to the impurities has two properties; it is temperature independent, and the lattice (or ideal) and impurity resistivities are additive in the region where they are both of importance, i. e. ,

$$\rho = \rho_{\text{ideal}} + \rho_{\text{impurity}}. \qquad (4\text{-}1)$$

The latter statement, known as Matthiessen's rule, is not strictly obeyed. Deviations are to be expected at low temperatures where the approximation of a general relaxation time for the electron-phonon collisions is not valid (Sondheimer, 1950). Deviations are also to be expected and have been observed in the polyvalent metals. The rule may well hold for each band separately in these metals, but such a situation can result in deviations in the total resistivity. In any event, the deviations are generally extremely small (Meaden, 1965) over a very large temperature range and can be neglected for our purposes. Recently, Dugdale and Basinski (1967) have shown that deviations from Matthiessen's rule can be quite large in regions where the impurity resistance dominates but our measurements do not approach this region very closely.

The preceding discussion and that which follows do not apply to ferromagnetic or antiferromagnetic metals, or alloys with these metals, where an additional temperature dependent term arises due to a spin type of scattering. Another type of scattering with an uncertain temperature dependence is that due to the physical boundaries of the samples. This will be discussed in a later section in some detail.

The general treatment of transport usually starts from the Boltzmann equation in the steady state form:

$$\frac{1}{\hbar}\vec{F}\cdot\vec{\nabla}_k f + \vec{v}\cdot\vec{\nabla}_r f = \dot{f}_{coll.} \qquad (4\text{-}2)$$

where $\vec{F}$ contains all external forces, f is the distribution function, $\vec{v}$ the electron velocity and k the momentum coordinate. The first term presents no problem since the external forces on the electrons are generally known. The second term, the diffusion term, will give a contribution if the distribution function has a spatial dependence; boundary effects contribute through this term as do thermal gradient effects. The right hand term, the change in the distribution function due to scattering collisions, is where the difficulty lies. In a complete description of a conduction problem we will have collisions between electrons, many-body effects, collisions with zone boundaries and impurities and, finally, the electron-phonon collisions. Clearly, any complete theory of conduction has to take at least the most important of these effects into account in a quantitative way. This involves computing the transition probability for scattering from any state $\vec{k}$ to another state $\vec{k}'$. For elastic scattering, a relaxation time, τ, can be introduced which results in important simplifications at least in the case where τ does not vary with $\vec{k}$. In general, however, and particularly at low temperatures, inelastic scattering should be considered and the relaxation time approximation replaced by a more detailed scattering integral approach.

If we consider, for the moment, the electron-phonon

interaction, we can see the magnitude of the difficulty involved in any attempt to create a general theory for metallic conduction which can be used to discuss actual conductivity data. The models and the various theoretical approaches to the problem of electron phonon interactions are discussed thoroughly by Ziman (1960). Several problems are evident. First, it is necessary to have a good idea of the phonon spectrum of the metal under consideration; the spectra are not isotropic and their determination, primarily by neutron diffraction, is involved and only limited data are available. Pines (1964) gives an excellent discussion of this topic. Second, even with a correct phonon spectrum one must know how to take Umklapp processes into account. Current theories differ on the fraction of the resistivity of monovalent metals which can be attributed to these processes, but it appears to be between 0.6 and 0.8, certainly it cannot be neglected. On a more optimistic note, theoretical calculations by Hasegawa (1964) on potassium which take account of Umklapp processes agree with experiment with a maximum deviation of 25% over the temperature range from 3° K to 273° K. It is still a large step to polyvalent metals but Bross and Bohn (1967) give a theoretical calculation which, when compared to experimental values for aluminum, gives agreement to within 40% over a temperature range from 30° K to 300° K. It is evident from these treatments that the more sophisticated theories must be applied to each metal in turn and none

is yet sufficiently general that it can be used as a "standard" means of intercomparing resistance data from a large number of metals.

The Bloch-Grüneisen formula is usually used as a "standard" for treatment of resistivity data due to its relatively simple form. In spite of the large number of unrealistic assumptions made in its derivation, the formula gives quite good agreement with experiment, particularly in the high and low temperature limits, for many metals. The relaxation time approximation is used. Most treatments assume elastic scattering, but a full treatment accounting for the energy lost or gained by the electron is used for the formula below and the result is not greatly different. The phonon spectrum is accounted for by assuming a Debye model and Umklapp processes are totally neglected. It is further assumed that only one "kind" of electron is responsible for the conduction, i. e., a one band model is used.

Using the assumptions of the preceding paragraph, the relaxation time is evaluated and the result for the ideal resistivity can be written in the form (Ziman, 1960; Wilson, 1965):

$$\rho = \frac{C}{M\theta_R}\left(\frac{T}{\theta_R}\right)^5 \int_0^{\theta_R/T} \frac{z^5 dz}{(e^z - 1)(1 - e^{-z})} \equiv \frac{K_G T}{\theta_R^2}\, G\left(\frac{\theta_R}{T}\right) \qquad (4\text{-}3)$$

where M is the atomic mass, C is a constant, $K_G = C/4M$ and θ_R is a characteristic temperature. $G\left(\frac{\theta_R}{T}\right)$ is called the Grüneisen function;

$$G\left(\frac{\theta_R}{T}\right) = 4\left(\frac{T}{\theta_R}\right)^4 \int_0^{\theta_{R/T}} \frac{z^5 dz}{(e^z - 1)(1 - e^{-z})} . \qquad (4\text{-}4)$$

The constant K_G (or C) contains the details of the electron phonon scattering mechanism; it is therefore not generally a constant over a wide temperature range. Most comparisons to experimental data either remove K_G or assume it to be constant and absorb its variations in the temperature variation of θ_R.

The integral is such that $\rho \sim T$ at high temperatures and $\rho \sim T^5$ at low temperatures. The proportionality to T at high temperatures is usually observed and variations are generally explainable in terms of changing values of the Debye θ as a result of thermal expansion of the lattice or in terms of a density of states effect (Meaden, 1965). The temperature dependence of the phonon resistivity of many metals at low temperatures has been measured. Some of the metals obey the T^5 law but most have shown an exponent less than 5. Recent experiments by Alexandrov and D'Yakov (1963), however, indicate that when samples of sufficient purity are used most nonmagnetic metals will show a T^5 dependence. Agreement of the Bloch-Grűneisen theory with experiment at intermediate temperatures is not generally good and agreement over the entire temperature range is unknown for any metal yet investigated.

Deviations of actual experimental data from this very idealized form are usually expressed as variations in θ_R as a function of temperature. There are several methods of preparing these plots from experimental data, all of which make use of tabulated numerical values of the function G and its derivatives. The form of the final curve is unfortunately strongly dependent on which of the methods is used. Before comparison can be made to other values of θ_R or even to values of the Debye temperature, θ_D, where the situation is the same, one must know the method by which the values were obtained from the data. An excellent discussion of this problem, complete with examples, is given by Kelly and MacDonald (1953).

Two effects have been considered in a general way that can cause quite a different power law at low temperatures for polyvalent metals. The first is electron-electron scattering, which has been considered particularly in the case of the transition metals. The s and d electrons in the transition metals are quite different in character due to the narrowness of the d band, which results in a high effective mass and poor conduction properties of the d electrons. Scattering interactions between these groups of electrons can thus affect the resistivity. The predicted temperature variation of this component is T^2 and some experimental confirmation of this behavior has been found (Mott and Jones, 1958). In divalent metals, where the bands are more similar in character, the e-e

interactions do not affect the charge transport to any degree and such a component is not expected for mercury.

A second effect which cannot be easily neglected here is the effect of phonon assisted band-to-band scattering. Wilson (1938), has given a theoretical treatment of this effect, primarily for transition metals although none of the major assumptions of the theory require this, with the result that the low temperature resistivity has a T^3 term added to the T^5 variation from the Bloch-Grüneisen formulation. Such a mechanism has been suggested for bismuth and antimony by White and Woods (1958) to explain their low temperature resistivity data.

It is interesting to note that all of the non-hcp metals, which have a small area of free Fermi surface in one zone and a small overlap into the next zone only, apparently do not exhibit a T^5 dependence of the ideal resistivity. White and Woods give an exponent of 2.7 for Bi and 2.8 for Sb. Justi and Kramer (1940) made measurements on barium which indicate a dependence with lower exponent than 4 but they had insufficient data to determine the exact dependence in the low temperature region. To the best of our knowledge, no data is available on As, Ca and Sr, although calcium and arsenic crystals of sufficient purity for such measurements have been used for de Haas-van Alphen experiments (As: Berlincourt, 1955; Ca: Condon and Marcus, 1964).

Variation of the Resistance with Crystal Orientation

The usual experimental arrangement for resistance measurement is such that the direction of the current density vector $\vec{J}$ is determined rather than that of the electric field. Noncubic crystals such as mercury do not, in general, given an electric field parallel to $\vec{J}$ due to the crystalline anisotropy. As a result, the measured voltage is due to the component of the field in the $\vec{J}$ direction. The resulting resistivity for the mercury structure as outlined in the next chapter is

$$\rho_{measured} = \rho_{\perp} \sin^2\chi + \rho_{||} \cos^2\chi \qquad (4\text{-}5)$$

where χ is the angle between the trigonal axis and the current direction.

Resistance Measurements on Superconductors below the Transition Temperature

A number of resistance measurements have been reported on superconductors below their transition temperatures but essentially no discussion is given of the effect of the magnetic field required to maintain the samples in the normal state.

The usual method of determining R at H=0 below T_c is to plot R versus H at the temperature of interest and fit the data to

a quadratic curve of the form

$$R = R(0)(1 + \alpha H^2) \qquad (4\text{-}6)$$

obtaining $R(0)$ and α in the process. This form is discussed in more detail in the next chapter. The problem with this method, at least in the case of mercury ($T_c = 4.15°K$), is shown in Figure 18. In this figure ΔR is taken with respect to an extrapolated zero field value. The superconducting region is indicated approximately by the dashed lines. At temperatures below 2.7°K the field dependence is no longer quadratic at $H = H_c$ and the measured curve is already bending over toward saturation. Thus, the curve cannot be properly fitted, and determination of $R(0)$ is not possible with any degree of certainty even if the procedure could be justified on theoretical grounds.

It is by no means obvious that an extrapolation of $R(H)$ to $R(0)$ by any method is justified. At the very least it implies that the phonon and impurity scattering of "normal" electrons is not affected by the transition. While this may be plausible for the impurity scattering it is rather hard to accept in the case of the phonon component. Recent ultrasonic attenuation measurements on lead by Fate and Shaw (1967) indicate a different phonon limited mean free path in the normal and superconducting states in agreement with some

earlier calculations. The impurity limited mean free path is not changed on passing through the transition.

The Residual Resistance Ratio

It has become standard procedure in metals research at low temperatures to state the purity of the sample in terms of the ratio of its resistance at room temperature to that at liquid helium temperature. The justification for the procedure is that normally at liquid helium temperature the phonon contribution to the resistivity is effectively zero and the residual resistivity then directly measures the purity of the sample. The technique is very powerful in general as it is capable of detecting impurity levels far below those of the most sophisticated chemical analysis. Further, the method takes account of all impurities acting to scatter the electrons, the mechanical as well as the chemical ones. A last point in its favor is that, to a good approximation, the shape factor of the sample is removed.

The method loses some of its significance, however, when applied to mercury crystals of reasonable purity. Mercury has a low Debye temperature which varies from approximately $\theta_D = 120°\,K$ at $T = 80°\,K$ to $\theta_D = 50°\,K$ at $T = 3°\,K$ as reported by Smith and Wolcott (1956). This variation probably accounts for the wide discrepancy in published values of θ_D. In any event, the lattice contribution to the resistivity in this case is by far the dominant term at 4.2° K, and

apparently the chemical impurity levels must be at least on the order of parts per ten thousand before they have any effect on the resistivity ratio as mentioned earlier in the discussion of sample growth techniques. It is significant that all mercury experiments since 1913 on pure samples of reasonable size have given essentially the same value for this ratio. Table 1 illustrates this behavior for a wide range of sample sizes and purities.

Table 1. Resistance ratio measurements.

Sample No.	Nominal Cross Section	Stated Purity	R(77°K)/R(4.2°K)
17	1 x 2 mm	5N[1]	172[2]
23	1 x 2 mm	Lab[3]	171
29	0.25 x 2 mm	6N	173
32	0.5 x 2 mm	Ag alloy[4] 0.1 wt. %[5]	60
40	0.125 in. dia.	6N	173
77	0.5 x 2 mm	Ag alloy 0.01 wt. %	121
80	0.5 x 2 mm	Cd alloy 0.01 wt. %	138
82	2 x 2 mm	7N	168
84	0.5 x 2 mm	7N	168
85	1 x 2 mm	7N	171

[1] 5N = 99.999%, 6N = 99.9999%, etc.

[2] Accuracy of these measurements is ± 2%.

[3] Distilled mercury from general supply.

[4] It is doubtful that all of the silver dissolved.

[5] The percent composition indicated for each alloy sample is that of the liquid from which the crystal was grown.

Another difficulty arises with mercury in that it is unrealistic to use the ratio to room temperature for two reasons. First, mercury shows the largest change in resistivity upon melting of any metal, and second, the resistivity anisotropy of the crystals would cause such a ratio to depend on the crystal orientation to a large degree. So that while for most other metals an almost direct comparison can be made between them by the casual reader when resistivity ratios are stated, mercury does not allow this. The ratio used here has the resistance at liquid nitrogen temperature as the high temperature value.

The use of the ratio for the pure metal still has some significance in this work as it should be an indicator of the presence of boundary scattering and strain effects at low temperatures. In the case of the alloy samples, we see that, as in other metals, the ratio is a fairly sensitive indicator of impurity level.

Size Effects.

At low temperatures the mean free path of the conduction electrons in very pure metals can become quite large, on the order of 1 mm in some cases. Thus, for reasonable sample sizes, scattering of the electrons at the sample boundaries may play a significant role in the conduction process. If such reflections are specular, the momentum in the direction of the applied field is not affected and the

resistivity should maintain its bulk value. However, if at least part of the scattering is diffuse the momentum loss will show up as an additional resistivity over that of the bulk material. A review of the theoretical approaches to boundary scattering for different sample configurations and results derived from available experimental data are given by Sondheimer (1952).

There are several types of experiments which can be used to obtain information on mean free path magnitudes. None of these give the mean free path directly and a theoretical interpretation must be made.

The most direct experiment uses the boundary scattering itself. Resistivity measurements are made on samples of varying sizes and shapes and the change in the resistivity with size is then interpreted theoretically to give a value for ℓ/σ_0, where ℓ is the the mean free path and σ_0 is the bulk conductivity. Such measurements have been made on mercury wires by Andrew (1949) and interpreted theoretically by Dingle (1950). Application of the theory requires that an assumption be made as to the value of ϵ where ϵ is the probability of elastic scattering at the boundary (hence, $1-\epsilon$ is the probability of diffuse scattering). Treatment of the results for wires of diameter greater than 2×10^{-3} cm leads to a value $\ell/\sigma_0 = 3.6 \times 10^{-11}\ \Omega\text{-cm}^2$ if $\epsilon = 0$ and $\ell/\sigma_0 = 8.7 \times 10^{-11}\ \Omega\text{-cm}^2$ if $\epsilon = 1/2$.

A second experiment to give values of ℓ/σ_0 is the anomalous

skin effect measurement. Experiments on mercury were done by Pippard (1947) and interpretation by Reuter and Sondheimer (1948) gives a value $\ell/\sigma_0 = 2.7 \times 10^{-11} \Omega - cm^2$.

A third experiment which, with a good theory, should be capable of interpretation in terms of mean free path effects is longitudinal magnetoresistance measurements in the low field region on samples of varying sizes. A theory in terms of the free electron model was developed by Chambers (1950) and a series of experiments on several metals were made by Alexandrov (1963). No data on thin mercury samples by this method are available.

All of the various theoretical treatments compare best with experiment when the scattering is assumed to be perfectly diffuse at the boundary, i. e., when $\epsilon = 0$. This conclusion is rather general; it applies to a large number of other metals as well as to mercury.

Using the value of 3.6×10^{-11} for ℓ/σ_0 and a representative resistivity of $36 \times 10^{-9} \Omega - cm$ at 4. 2° K from our data we find that $\ell \approx 1 \times 10^{-2}$ mm and at 1. 8° K, $\ell \approx 2 \times 10^{-1}$ mm.

Thus, there is a possibility of a size effect which could represent as much as 50% of the total resistance at the lowest temperatures according to the development by Sondheimer (1952).

Treatment of the Data

The part of the experiment described in this chapter is devoted

to determining the variation of the zero field resistance of the mercury crystals with temperature. The range of measurement is from 1.8°K to 220°K in three distinct steps as outlined in Chapter 3. At the lower temperatures it is necessary to consider the effects of impurities, size and the small magnetic field necessary to maintain the sample in the normal state.

The type of crystals used in this experiment do not allow extremely accurate absolute determination of the resistivity due to difficulties in measuring the geometric factor. This problem and the fact that the functional form of the resistance variation is not known, required that a technique be used for comparing the data from various samples which would not be affected by these difficulties. The method decided upon was the following: Log-log plots of the data for the various samples are made on tracing paper with scales chosen to give slopes close to unity in the temperature region under consideration. The plots are then placed one over the other and moved vertically until the best agreement is obtained. A composite curve is then drawn and the limits of variation of 90% of the data points are used as error bars. This method is somewhat equivalent to the method of plotting $R(T)/R(T_0)$, where T_0 is some characteristic temperature, but it removes the strong dependence of the curves on the data point at T_0. Differences in the magnitude of the resistivity due to crystal orientation will be removed by the method as long as

the ratio $\rho_{\perp}/\rho_{||}$ is a constant. If the ratio does depend on temperature, i.e., if $\rho_{\perp}$ is a different function of T than $\rho_{||}$, the method should show this up strongly as no matching of the curves should be possible. This method, which we call the overlay technique, is used on the R-T data in the two regions up to 77 °K.

The following is a discussion of the treatment of the data in each temperature region in more detail.

Temperature Regions

77° K to 220° K. In this region we expect a linear variation of the resistance with temperature. Plots are made of R/T versus T. The results for two samples are shown in Figure 19.

4. 2° K to 40° K. The overlay technique is used here and the region is broken at 10° K to allow plots which show reasonably small slopes. The upper end of the region is extended to include the 77° K point, but there are no data points above 40° K. Composite plots are shown in Figure 20 and Figure 21. Data points are shown for a single sample on these plots and in Figure 22. The vertical scale of the three figures is appropriate for a crystal with nominal cross section 0. 5 x 2. 0 mm.

Below 4. 2° K. The overlay technique is used here in the range from 2. 6° K to 4. 2° K. The composite plot is shown in Figure 22. The resistance component due to the magnetic field required to keep

the sample normal is handled in the following manner: R-H data similar to that shown in Figure 18 are fitted by computer at a number of temperatures where the behavior is still quadratic to determine roughly the variation of a with T for a given sample.

Using this data, the temperature is determined at which the error in the resistance measurement due to the magnetoresistance effect becomes greater than 3% and data points at temperatures below this are not used in the data interpretation. This procedure is used rather than one which corrects for the magnetoresistance effect because all of the resistance data points can be used down to the 3% error temperature rather than those few representing temperatures at which the magnetoresistance measurements are made. Furthermore, this limit is usually $T = 2.6°K$ which is not far above the point where the magnetoresistance correction cannot be made.

There is a temptation to use equation 4-6 and extrapolated values of a from a versus T plots to correct the data at lower temperatures, but the theoretical behavior of the coefficients with temperature is not well enough known to justify such a procedure. A more thorough discussion of these low field magnetoresistance effects is given in the next chapter.

Nonlinear least squares analysis was made by computer on the $2.6°K$ to $4.2°K$ data to determine the best fit to a functional dependence of the form

$$R = R_{impurity} + aT^{n}. \qquad (4\text{-}7)$$

The data points were given a $1/R^2$ weighting appropriate to a constant percentage error. An attempt was also made to fit a form $R = R_{impurity} + bT^3 + cT^5$ by this same method.

Resistance Versus Temperature in General

The slopes of the curves at the limits of the various regions are checked to determine how closely they match. A log-log plot of the resistance over the entire temperature range is given for one sample in Figure 23. Composite curves are used to determine the value of θ_R, the characteristic temperature of the Bloch-Grüneisen function, and its temperature variation. The various methods of comparing experimental data to the Bloch-Grűneisen function are discussed by Kelly and MacDonald (1953) and outlined by Meaden (1965), who tabulates a number of functions related to the Grüneisen function.

As stated previously (equation 4-3) we can write the Bloch-Grüneisen relation as

$$\rho = \frac{K_G T}{\theta_R^2} G\left(\frac{\theta_R}{T}\right). \qquad (4\text{-}8)$$

The temperature dependence of K_G and θ_R are not known and the various methods differ mainly in how they treat this aspect of the

problem.

The first method used here, to get a rough indication of the variation of θ_R with T starts from the logarithmic derivative of the experimental R versus T curves. From equation 4-8,

$$\frac{d\ln\rho}{d\ln T} = 1 + \frac{d\ln G}{d\ln T} - 2\frac{d\ln\theta_R}{d\ln T} = 1 - \frac{d\ln G}{d\ln(\theta_R/T)} - \frac{d\ln\theta_R}{d\ln T}\left[2 - \frac{d\ln G}{d\ln(\theta_R/T)}\right]. \tag{4-9}$$

Assume that θ_R is constant, then

$$\frac{d\ln\rho}{d\ln T} = 1 - \frac{d\ln G}{d\ln(\theta_R/T)}. \tag{4-10}$$

Tabulated values of the right hand side of equation 4-10 as a function of θ_R/T then allow a rough graph of θ_R versus T to be made from the data. From such a graph, a relatively large region where θ_R is constant as a function of temperature is determined--say θ_0 at T_0. The next step in the most general procedure would be to go back to equation 4-9 and determine a new θ_R versus T, but this is not justified by the accuracy of the data. We use another method which assumes that K_G is a constant and solves the Bloch-Grüneisen relation, equation 4-8, for K_G at two different temperatures to get:

$$\left(\frac{T_1}{\theta_1}\right)^2 G\left(\frac{\theta_1}{T_1}\right) = T_1 R(T_1)\left[\frac{T_0}{\theta_0^2 R(T_0)} G\left(\frac{\theta_0}{T_0}\right)\right]. \qquad (4\text{-}11)$$

Since the term in brackets is evaluated from the previous plot, this equation allows us to arrive at a new plot for θ_R versus T which is more accurate since θ_R is not assumed to be a constant in this derivation.

The plots by the two methods are given in Figures 24 and 25. The values used for the final fit by equation 4-11 were $\theta_0 = 23.5°K$ at $T_0 = 7.5°K$. The form of the Grüneisen function does not allow this determination to be carried into the linear region with any accuracy and thus these plots stop at 40°K.

Results

Detailed descriptions of samples, referred to by number, in this and following sections are given in Appendix A. Again, we first consider the variation of resistance with temperature. We look at each region separately.

Temperature Regions

The Region 77°K to 220°K. (See Figure 19.) A total of nine samples were run in this region (samples Nos. 72, 73, 75, 77, 80, 82, 83, 84 and 85), covering a wide range of sizes, purities, and

orientations. Measurements were made on the samples shown in Figure 19 at approximately twice the number of temperature points of the other samples. No data points were taken between 77° K and 100° K. The behavior shown in the figure is observed in all samples--there is a linear region between 110° K and 170° K. The average value in this region is indicated by the solid lines on the graphs. At 77° K the R/T versus T curves have fallen off considerably and it is thus unlikely that the linear region extends much below 100° K. Above 170° K the resistance is rising faster than linearly with temperature for all samples. Several mechanisms have been suggested in the literature to explain deviations of this sort which occur in a number of other metals (Jones, 1956).

The first is that thermal expansion of the sample effectively decreases θ_D in this region and the temperature dependence becomes

$$R \sim T[1 + 2\alpha_t \gamma T] \qquad (4\text{-}12)$$

where α_t is the thermal expansion coefficient and γ is Grüneisen's constant

$$\gamma = -\frac{d\ln\theta_D}{d\ln V} . \qquad (4\text{-}13)$$

By Debye theory and the Maxwell relations γ can be written in terms of observables as

$$\gamma = \frac{a_t V}{\chi C_v} \tag{4-14}$$

where χ is the isothermal compressibility, C_v the specific heat, and V the molar volume. A rough calculation using values of C_v calculated from the data of Busey and Gaigue (1953) gives $\gamma = 4.3$.

Thus,

$$2a_t\gamma = 6.4 \times 10^{-4} C^{\circ -1}. \tag{4-15}$$

Values of γ for many other metals are tabulated by Mott and Jones (1958) and comparison to their table shows that the value of γ derived here is a bit high but within reason.

The second mechanism arises in metals where the integrand in the expression for the conductivity derived from the Boltzmann equation

$$\sigma_{ij} = \frac{e^2}{4\pi^3} \int \tau \bar{v}_i v_j \frac{\partial f^\circ}{\partial \epsilon} \vec{dk} \tag{4-16}$$

may not be slowly varying over an energy range kT and thus the energy derivative of the distribution function cannot be treated as a delta function at $\epsilon = \epsilon_f$. Such a situation arises in two-band systems when the bands overlap and the Fermi energy falls near the maximum or minimum in the density of states curve created by this overlap. The argument is that the relaxation time τ is inversely proportional to the density of states $L(\epsilon)$ and thus can be changing rapidly with

energy near the Fermi energy. There is currently some question as to whether or not a strong minimum actually exists in the net density of states for divalent metals as has been stated by Slater (1965) and others. The question has not yet been adequately resolved and we thus include the possibility of this mechanism.

A development which takes the density of states minimum into account leads to the following expression for the resistance:

$$R \sim T\left\{1 - \frac{\pi^2 k^2 T^2}{6}\left[3\left(\frac{1}{L}\frac{dL}{d\epsilon}\right)^2 - \frac{1}{L}\frac{d^2L}{d\epsilon^2}\right]_{\epsilon_f}\right\} . \qquad (4\text{-}17)$$

Now, if ϵ_f falls near a minimum in the net density of states curve $(dL/d\epsilon)_{\epsilon_f}$ will be small and the second derivative will be positive and thus the term in the small brackets will be negative and the resistance will rise faster than linearly.

Unfortunately the accuracy and range of the data is not high enough to decide between these two mechanisms in spite of the fact that the correction term is linear in T in the former case and quadratic in T in the latter. As an example, the data for sample No. 84 can be fit to within the experimental error by either

$$R = 14.9\ T[1 + 22 \times 10^{-4} T]\ (\mu\Omega),\ T > 176^\circ K \qquad (4\text{-}18)$$

or

$$R = 18.1\ T[1 + 4.4 \times 10^{-6} T^2]\ (\mu\Omega),\ T > 174^\circ K. \qquad (4\text{-}19)$$

Deviations of this type observed in some of the alkali metals

have been explained by MacDonald (1953) in terms of the creation of lattice vacancies near the melting point. He derives the form

$$\Delta R/R = T^{-1} \exp(-U/kT) \qquad (4\text{-}20)$$

where U is the vacancy activation energy. The data for sample No. 84 also fits this form if U = .06 ev, a relatively low, but not entirely unreasonable, value.

The Region 4.2° K to 40° K. (See Figures 20 and 21.) A total of six samples (sample Nos. 71, 77, 80, 82, 83 and 84) were studied in this region. This group represents a wide range of crystal orientation, size, and purity. To the accuracy of the experiment, no dependence of the form of the curve on either size or crystal orientation was observed. The Ag alloy sample began to show an impurity resistance below 7° K and thus was not used in preparing the composite curve of Figure 21. Deviations of the Cd alloy sample from the pure Hg curves are still within the limits of error down to 4.2° K.

The Region Below 4.2° K. (See Figure 22). The composite pure Hg curve is made up from eight samples (sample Nos. 82, 83, 84, 85, 87, 88, 89 and 90) run with $H \approx H_c$. The solid curve over the region from 2.6° K to 4.2° K fits all of the samples very accurately. The 90% deviation limits are smaller than the data point circles. This leads to the conclusion that the functional dependence of the resistance on temperature is not affected by crystal orientation. Variation of the crystal size from a minimum cross section of

1/2 mm x 2 mm to a maximum of 2 mm x 2 mm also has no effect on the R-T relationship. Above 2.6° K the magnetoresistance correction is small enough that it could not be observed on the scale of Figure 22.

All of the comparisons made between samples are done using the uncorrected data above 2.6° K. Correction for the magnetoresistance is possible down to 2.2° K but the accuracy below 2.6° K is not high, as indicated by Figure 18. Thus the data for only one sample is shown below 2.6° K as indicated by the dashed curve.

The fact that the slope of the composite curve on the log-log plot is still increasing with decreasing temperature at 2.6° K leads to the conclusion that the impurity resistance is still a small fraction of the total resistance at this temperature and thus the plot is treated in the following section as if it represented the ideal resistance only. The decrease in slope of the curve below 2.6° K for the single sample shown is almost certainly due to magnetoresistance effects rather than to impurities.

The Cd alloy sample behavior is also shown in Figure 22 and it exhibits the typical impurity behavior in this region. The magnetoresistance correction for this sample is considerably smaller than for the pure Hg at the lower temperatures.

The large number of data points make the changes in slope of the composite curve quite obvious. Most of the earlier measurements

on metals in this temperature range were made at only a few points. The R-T behavior was then usually given in the form

$$R_{observed} = AT^n + R_{impurity}. \qquad (4\text{-}7)$$

Least squares analysis of all the samples investigated here, including the Cd alloy, gives agreement to this form when $n = 3.7 \pm .1$ but with a small negative value for $R_{impurity}$. The only purpose of this calculation was to arrive at a form which would allow easy comparison to the values reported for other metals.

An attempt to fit our data with a form $R_{ideal} \sim bT^3 + cT^5$ consistent with a band-to-band scattering contribution was not successful.

Resistance as a Function of Temperature in General.

The measured resistivity at 86° K is in agreement, within the rather high experimental error, with Grüneisen's (1945) values of $\rho_{||} = 5.6\,\mu\Omega$-cm and $\rho_{\perp}$ 7.4 $\mu\Omega$ - cm. The relative variation of the resistance with crystal orientation is in good agreement with Grüneisen's value of $\rho_{\perp}/\rho_{||} = 1.32$ for the few samples where a complete set of mold measurements were made before the crystals were grown.

It appears that there is no change due to crystal orientation in the functional dependence of the resistance on temperature over the

entire temperature range and thus the value of $\rho_{\perp}/\rho_{\parallel}$ should be constant over this range. This is not the case with the other II-B metals, Zn and Cd which have a reasonably strong maximum in $\rho_{\perp}/\rho_{\parallel}$ at 25°K to 30°K (Alexandrov and D'Yakov, 1963). The c/a ratio for Zn and Cd decreases as a function of temperature (Pearson, 1958), but there is no data to verify the existence of any anomaly in the rate of change in the low temperature region.

The Grüneisen characteristic temperature, θ_R, below 40°K is here determined to be between 20°K and 26°K. The only other quoted value of θ_R in the literature is 37°K given by Mott and Jones (1958). This value is obtained from the data presented here if the rough method of taking the ratio of ρ values at one high (77°K) and one low (4.2°K) temperature is followed. The method assumes that both K_G and θ_R are constant. This is undoubtedly the way the value was derived since very little low temperature data is available on mercury in the literature.

The only resistance versus temperature data for solid mercury available in the literature is that of Onnes and Holst (1915). The temperature range of their measurement was from 4.2°K to 234°K, but with such large gaps that no reliable temperature dependence can be determined. Their data, properly normalized, falls on the curves given here well within the error limits.

The form of the curves shows that, as might be expected from the low Debye temperature and the high purity, the major mechanism of the resistance of mercury is the electron-phonon interaction to the lowest temperatures investigated. This is the reason that residual resistance ratio measurements are of little value for this metal.

A final point to consider is the effect of boundary scattering. We saw earlier in this chapter that it could possibly give a large contribution to the resistance at low temperatures. It appears that, for samples such as those investigated here, the boundary effects are quite small. There are several arguments to indicate that this is the case; the first from Table 1 shows no dependence of the resistance ratio on sample size and the composite curve of Figure 22 indicates no dependence down to 2.6° K; secondly, the low field magnetoresistance plots would be expected to show a drop in R as H is increased and this is not observed. The argument that such a decrease would be swamped by the bulk magnetoresistance should not hold for the longitudinal configuration as this bulk effect itself is quite small.

Anomalous Behavior Near 4.2° K

When one attempts to match the slopes of the composite curves of Figures 21 and 22 at 4.2° K it appears that an almost discontinuous change of the slope is required at 4.2° K. A plot of a single sample (No. 84) through this region is shown in Figure 26; this slope change

is seen for all samples run through the two regions, including the Cd alloy sample. The slope measurements are not very precise in the region 4.2° K to 5.0° K due to a lack of data points, but there is no question that the slope changes quite rapidly with increasing temperature from a value of approximately 3.3 to one of approximately 5.0 in this region. This change is evident in the rough θ_R calculation shown in Figure 25, which is related directly to the slope of the composite curves.

It is suggested that the change may well be related to the onset of superconductivity at $T_c = 4.15°K$ in some manner. It is unfortunate that the method of temperature measurement is changed at 4.2° K as it opens the door to a number of spurious effects which might be responsible for this behavior in spite of the fact that it persists when all reasonable errors are taken into account.

It has generally been assumed that no change of this sort occurred when a superconductor was taken through the zero field transition temperature but kept in the normal state by application of an external field. Most superconductors are not available in sufficient purity to have much of a lattice contribution to the resistivity at T_c and thus the number of metals in which such an effect might be observed is currently very small. Lead is probably the only other element which is readily available that might be tested.

A number of experiments were tried which used the existing

equipment to take a mercury sample through the 4. 2° region with one method of thermometry. These experiments were inconclusive because of a host of difficulties but several of them strongly suggest that a slope change exists. Similar measurements were made on polycrystalline samples of indium and lead but again no conclusive results were obtained.

The statement to the effect that no change in the R-T behavior is observed in mercury on going through T_c is attributable to de Haas, Sizoo and Onnes (1926) and was made on the basis of measurements on one sample of mercury from 1. 56° K to 4. 35° K. Their sample was only 0. 04 mm in diameter and either size or impurity effects would have completely removed any hint of the behavior observed here. Their data, plotted to our scales, show that the resistance of their sample is well into the impurity region at 4. 2° K--more so than the Cd alloy sample investigated here.

The recent literature contains a number of anomalous effects observed or predicted for R-T curves at low temperatures. The magnetic field dependent anomaly observed in gallium by Newbower and Neighbor (1967) which seems to approach T_c as the field is raised is a possible comparison but their observed change takes place over a rather small temperature range. The theory advanced by Gurzhi (1965) shows that when the electron-phonon mean free path is of the same order as the mean free path for impurity scattering a

plateau can occur in the R-T curve of massive samples. It is unlikely that these conditions are satisfied by the mercury samples. Further, a significant shift in the temperature at which the plateau begins should be expected when the purity of the sample is decreased. No large shift is observed for our Cd alloy sample but a shift of as much as 0.5°K could occur and not be detected due to the limited amount of data available in the 4° K to 5° K region.

Summary of Results and Conclusions

The variation with temperature of the resistance of single crystal samples of pure mercury and dilute alloys with Ag and Cd has been investigated. No dependence of the R-T curves on crystal orientation is observed in spite of the fact that the lattice parameter changes slightly over the temperature range. Thus we conclude that $\rho_{\perp}/\rho_{||}$ is a constant down to 2.6° K. The value fixed by other experiments of $\rho_{\perp}/\rho_{||} = 1.32$ is in good agreement with our measurements. It is suggested that changes in the ratio observed for other anisotropic metals may be due to the onset of impurity scattering as the major resistive mechanism.

The value of the Bloch-Grüneisen characteristic temperature as a function of temperature below T = 40° K was calculated and shown to vary between $\theta_R = 20°$ K and $\theta_R = 26°$ K which makes it the lowest reported for any metal. This is not surprising in view of

the extremely low values reported for the Debye temperature.

The resistance of all samples investigated shows the expected linear behavior in the region 110° K to 170° K. Above this region the resistance rises faster than linearly. Of the explanations offered we tend to associate the increase with a combination of lattice expansion and vacancy formation, both of which can be termed "premelting" effects. This combination should result in better numerical values both for the correction term of equation 4-18 and for the vacancy activation energy. Computation of the correction term due to the density of states minimum is not possible with the information available and, as mentioned earlier, it is possible that a sufficiently deep minimum may not exist at all.

Investigation of the resistance in the region below 4.2° K shows the expected behavior for the alloy samples; the temperature dependence is starting to disappear. The data for the pure mercury samples indicate that there is essentially no contribution from impurity scattering down to 2.6° K at least. This suggests that all reasonably pure bulk samples of solid mercury should have the same residual resistance ratio when it is defined by R(77° K)/R(4.2° K), and this is observed to be the case. The temperature dependence of the resistance is still changing below 4.2° K but the predicted T^5 behavior is not observed. The best single exponent for this region was determined to be $3.7 \pm .1$.

It was determined that correction for the magnetic field

required to keep the samples in the normal state could only be made down to 2. 2° K. There is no quadratic region below that temperature for the pure samples.

Lack of any indication of a size effect when the sample size was varied and lack of any negative low field magnetoresistance indicates that boundary scattering is not a problem for crystals of the size used for the experiment. Data from other experiments presented earlier indicated that the size effect might be large. Apparently some of the assumptions made in deriving the expected value of ℓ at a given temperature were not justified.

No agreement was found with the form of the resistance variation to be expected if band-to-band transitions were important in the low temperature region. This is in agreement with calculations of the maximum phonon wave vector available at a given temperature which indicate that these transitions should not be important. These calculations are discussed in Chapter 6.

A very rapid slope change on the log-log plots was noted near 4. 2° K resulting in a plateau-like behavior. It is suggested that the anomaly is possibly associated with the superconducting transition. Recent experiments and theoretical work have indicated that the phonon limited mean free path is likely to be shorter in the superconducting state than in the normal state. If we hold with the long accepted assumption that the scattering time is not directly affected

by a magnetic field then it is possible that upon application of the small magnetic field the superconducting mean free path persists in spite of the fact that the sample itself is in the normal state.

CHAPTER 5

LOW FIELD LONGITUDINAL MAGNETORESISTANCE

The extrapolation of the low field longitudinal magnetoresistance used in the previous chapter was performed by fitting the data to the quadratic form

$$R = R(0)[1 + \alpha H^2]. \qquad (5\text{-}1)$$

The main purpose of the low field experiments was to determine R(0) and, as mentioned earlier, the experiment was not extremely precise. However, it does lead to some approximate values for α both as a function of crystal orientation and of temperature.

It seems worthwhile to spend some time here discussing the dependence of α on the various parameters. This discussion, aside from its inherent interest, will serve as an introduction to some of the problems encountered in the high field region treated in the next chapter.

The first part of the chapter is devoted to a theoretical treatment of the problems of electrical conduction in the presence of a low magnetic field, through a lattice of known symmetry. Specific evaluations are made for the mercury lattice symmetry and the dependence of α on crystal orientation is shown. The expected variation of α with temperature is calculated under a rather restrictive

set of assumptions. Comparison of the results to the form predicted by Kohler's rule is made.

The second part of the chapter describes the data processing procedures. The results are described in the third part and comparison is made to the theory. Possible explanations of observed deviations from the theory are discussed.

Theoretical Discussion

There are two distinct questions to consider here: (1) How does crystal symmetry affect the transport properties of the metal in a magnetic field and; (2) What specific statements can we make about the electrical conductivity by choosing a particular theoretical model for the metal. The answers to these questions will determine what variations we should expect for α and, for that matter, whether an equation of the type 5-1 is justified at all.

We consider the problem of symmetry first. We are interested in determining how the resistivity tensor defined by

$$E_i = \rho_{ij}(H)\, J_j \qquad (5\text{-}2)$$

is affected by the symmetry of the crystal. We work with ρ since this is the quantity usually measured. The Onsager relations, which are quite general relations from irreversible thermodynamics accounting for time reversal symmetry, require that

$$\rho_{ij}(H) = \rho_{ji}(-H). \tag{5-3}$$

We expand the resistivity tensor in a Taylor series in powers of the magnetic field and defer until later the question of convergence since it depends on the details of the charge transport mechanism. We can write the expansion to second order as

$$\rho_{ij}(H) = \rho_{ij} + R_{ijk}H_k + A_{ijkl}H_kH_l + \ldots \tag{5-4}$$

where clearly

$$\rho_{ij} = \rho_{ji} \; ; \; R_{ijk} = - R_{jik}$$

$$A_{ijkl} = A_{jikl} = A_{ijlk} \; .$$

These results are quite general so far. The point group operations for the symmetry of the crystal under consideration (D_{3d} in this case) are then applied to the coefficient tensors to further reduce the number of independent components. This procedure is discussed in general by Smith, Janak and Adler (1967) and by Kao and Katz (1958) and a particular application to the trigonal class was made by Juretschke (1955). The crystal coordinate system chosen is one for which the trigonal axis is the Z axis and the X axis lies in a reflection plane. The result of this calculation is that the number of independent components are as follows:

$$\rho_{ij} - 2$$

$$R_{ijk} - 2$$

$$A_{ijkl} - 8$$

Note that for a cubic point group the numbers are 1, 1 and 3 respectively.

Now, our longitudinal configuration has $\vec{H}$ parallel to $\vec{J}$ and at an arbitrary angle χ, to the trigonal axis; $\vec{E}$ being measured along $\vec{J}$. The coefficients of interest are ρ_{ij} and A_{ijkl}, all the diagonal R_{ijk} being zero. ρ has been discussed in the last chapter so it remains to look at the A_{ijkl}. If $\vec{J}$ makes an angle χ with the trigonal (Z) axis and its projection on the X-Y plane makes an angle ϕ with the X axis as defined previously, then after some algebra we find

$$E_{measured} = [A_{1111}\sin^4\chi + (A_{1133} + A_{3311} + 4A_{2323})$$
$$\sin^2\chi\cos^2\chi - 2(A_{2322} + A_{2223})\sin 3\phi$$
$$\cos\chi\sin^3\chi + A_{3333}\cos^4\chi]H^2J \quad . \qquad (5\text{-}5)$$

This expression shows quite clearly that the most information we can obtain about the separate A_{ijkl} by any number of longitudinal measurements is the value of the diagonal elements A_{1111}, $(=A_{2222})$ and A_{3333}. To separate the elements of the terms in parentheses in

equation (5-5) requires a number of transverse magnetoresistance measurements. The important point in terms of this experiment is that the coefficient a which is the bracketed term above divided by $\rho_{measured}$ at zero field is not a simple function of crystal orientation or even of the magnetoresistance coefficients.

The usual theoretical calculations which start from the Boltzmann equation compute $\sigma(H)$ rather than $\rho(H)$ and it should be stressed that, while the symmetry relations are identical, the actual relations between the tensor coefficient components in the two cases are by no means simple. Juretschke (1955) shows that the relations between the components are roughly as follows:

Zero order in H, σ goes like $1/\rho$ where ρ is $\rho(0)$.

First order in H, σ goes like R/ρ^2.

Second order in H, σ goes like terms or sums of terms of the two forms A/ρ^2 and R^2/ρ^3.

This situation has to be taken into account when any serious comparison of theory to experimental data is made.

In the following discussion all of the conductivity tensor coefficient components are labeled σ and the order in the expansion in terms of the magnetic field is indicated by the number of subscripts. This method of notation is slightly different than that used in equation (5-4).

The actual form of the coefficients by any available theory is

quite complex and subject to a large number of assumptions. In order to get a feeling for the quantities involved, one calculation due to Jones and Zener (1934) will be outlined briefly. The linearized form of the Boltzmann equation (setting $f = f^0 + f'$ and keeping lowest order nonzero terms on the left hand side) for the case of thermal equilibrium in a magnetic field and with the relaxation time approximation is (in MKS units):

$$\frac{e}{\hbar} \vec{v} X \vec{B} \cdot \vec{\nabla}_k f' + \vec{v} \cdot e\vec{E} \frac{\partial f^0}{\partial \epsilon} = - \frac{f'}{\tau} \qquad (5\text{-}6)$$

which is written in operator form as

$$(1 + \tau \Omega) f' = - \tau \vec{v} \cdot e\vec{E} \frac{\partial f^0}{\partial t} \qquad (5\text{-}7)$$

where

$$\Omega \equiv \frac{e}{\hbar} \vec{v} X \vec{B} \cdot \nabla_k = \frac{e}{\hbar} v_j B_k \epsilon_{ijk} \left(\frac{\partial}{\partial k_i}\right) \qquad (5\text{-}8$$

formal solution yields

$$f' = - (1 + \tau\Omega)^{-1} \tau \vec{v} \cdot e\vec{E} \frac{\partial f^0}{\partial \epsilon} \qquad (5\text{-}9)$$

which we can expand, again formally, to give

$$f' = - [\, 1 - \tau\Omega + (\tau\Omega)^2 - \ldots \,] \, \tau \vec{v} \cdot e\vec{E} \frac{\partial f^0}{\partial \epsilon} \, . \qquad (5\text{-}10)$$

We ignore the convergence problem for the time being and insert this value of f into the expression for the current density

$$J_i = \frac{e}{4\pi^3} \int v_i \, f \, d\vec{k} \, . \qquad (5\text{-}11)$$

From this we can find σ_{ij}, do the Taylor expansion in powers of the magnetic field and use $\vec{B} = \mu_0 \vec{H}$ to perform the derivatives with respect to H with the final result for the tensor coefficient component of the quadratic term

$$\sigma_{ijkl} = \frac{e^4 \mu_0^2}{4\pi^3 \hbar^2} \left[\tfrac{1}{2}(\epsilon_{mnk}\epsilon_{rsl} + \epsilon_{mnl}\epsilon_{rsk})\right]$$

$$\times \int \frac{\partial f^0}{\partial \epsilon} \tau v_m v_r \frac{\partial}{\partial k_n}(\tau v_i) \frac{\partial}{\partial k_s}(\tau v_j) d\vec{k} \quad . \qquad (5\text{-}12)$$

This form is not very useful for comparison to experiment but it does indicate the general makeup of the coefficients. The coefficients depend on the Fermi surface shape and on the behavior of τ over the surface. A single spherical band metal with a constant relaxation time clearly has vanishing longitudinal coefficients as is also true for ellipsoidal bands and two-band metals with spherical bands and no interband transitions.

It turns out that, under conditions of a constant relaxation time and a single spherical band, the linearized Boltzmann equation can be solved exactly (the magnetoresistance coefficients are zero). This solution gives a rough indication of the convergence criterion we should expect for the expansion in powers of the field. Smith, Janak and Adler (1967) discuss the relationship in detail; the resulting criterion is

$$\omega\tau = \frac{|e|B}{m}\tau < 1 \qquad (5\text{-}13)$$

where ω is the cyclotron resonance frequency. This is the standard criterion used in the theory of metals for the limit of the low field region.

We are interested in the temperature variation of the coefficients of the resistivity tensor. Since we do not have an exact expression for the Fermi surface, equation (5-12) must be simplified by assumptions in order to arrive at a form which we can compare with experiment. The best assumption, and one which can be surprisingly good, is that τ is constant over the entire Fermi surface at a given temperature. Using this assumption we note that all the $\sigma_{ijkl}(\sim\tau^3)$ will have the same temperature dependence. For simplicity assume that all fields are in the direction of the trigonal axis then Juretschke (1955) shows, as mentioned earlier,

$$\sigma_{3333} = A_{3333}/\rho_{33}^2 \qquad (5\text{-}14)$$

where $\rho_{33} = 1/\sigma_{33}$, the zero field resistivity and conductivity respectively. Furthermore, the constant a for this orientation is

$$a = A_{3333}/\rho_{33}. \qquad (5\text{-}15)$$

So that, from (5-14)

$$a = \rho_{33}\sigma_{3333} \qquad (5\text{-}16)$$

and thus $\alpha \sim T^2$. So we should expect that

$$\alpha(T) \sim \rho(T)^{-2}. \tag{5-17}$$

Note that such behavior is in accord with Kohler's (1938) rule for the magnetoresistance

$$\frac{\Delta R}{R(0)} = F\left[\frac{H}{R(0)}\right] \tag{5-18}$$

where the form of F is unchanged by variation in the temperature or the purity of the sample. The form of F is dependent on the relative orientation of $\vec{J}$ and $\vec{H}$ and on the crystal orientation. The rather restrictive assumptions under which this rule can be expected to hold have been discussed by Chambers (1956), and it is unlikely that they are satisfied for mercury. It has, however, been shown to hold approximately for quite a large number of metals particularly in the low field region.

Treatment of the Data

The resistance versus magnetic field data at a given temperature are fitted by the nonlinear least-squares method to the quadratic form over the region from $H_c(T)$ to a maximum field $H_{max}(T)$. The value of H_{max} at a given temperature was determined by investigation of the fit of the computed curve to the data as a function of the highest field data point used. The values of H_{max} used for the pure mercury samples were 2400 Oe (maximum H of magnet) at 4.2° K,

2000 Oe at 3.7° K, 1500 Oe at 2.7° K and < 1000 Oe at 2.2° K. All of the alloy sample data could be used down to 2.2° K.

The values of α determined from the fittings are then plotted and the overlay method described on page 44 is used to investigate their temperature dependences.

Results

R-H runs were made at six temperatures between 2.2° K and 4.2° K on three samples (sample Nos. 87, 88 and 89) and at four temperatures on the Cd alloy sample (No. 80). At least five other samples were run at each of three temperatures in this same range. The agreement of the quadratic computer fit with the experimental data is surprisingly good considering the rather low precision of the measurement. In essentially all cases the fit was well within the expected experimental error at each data point.

The composite plot of α versus T by the overlay method is shown as Figure 27. This plot is designed for looking at the slopes and determination of the value of α at any point requires knowledge of α at one temperature for that sample. α values are given in Appendix A for all samples measured and are shown on the figure for the two samples whose data points are plotted.

The composite plot for pure mercury is fitted with a straight line as the number of points available do not warrant a more complex

fit. The slope of the line is 6.1 but the scatter of the points for the individual samples is relatively large as indicated by the error bars which represent the 90% deviation limits. The slope for the Cd alloy sample is 3.7.

The fact that the overlay method does work reasonably well here indicates that a general expression for α of the form

$$\alpha = A\ (\text{orientation})\ F(T) \tag{5-19}$$

is obeyed. This form is reasonable if the magnetoresistance coefficient integrals, the A_{ijkl} of equation (5.5), all have approximately the same dependence on T. An investigation of the behavior of the low field transverse magnetoresistance would be most helpful in further clarifying this point. Unfortunately no work of this sort has yet been done.

If the theoretical proportionality of α to $R(0)^{-2}$ expressed in equation (5.17) is to hold, then b calculated from the form

$$\alpha\, R(0)^{b} = \text{constant} \tag{5-20}$$

should have the value $b = 2$. The calculation yields its best fit with $b = 3/2$ as the exponent rather than the value $b = 2$ predicted by the theory. Thus, Kohler's rule (5-18) is not obeyed for mercury in the low field region. It is likely that the deviations from Kohler's rule are the result of the extreme distortion of the Fermi surface from the spherical shape for which the rule is valid. The next chapter discusses the shape of the Fermi surface in detail.

CHAPTER 6

HIGH FIELD LONGITUDINAL MAGNETORESISTANCE

The high field region is defined by $\omega\tau > 1$ and is generally attained for high purity metals at temperatures near liquid helium temperature and in fields of tens of kilo-Oersteds. In this region, the mathematical expansion of the previous chapter is no longer valid and the details of the conduction mechanism become strongly dependent on the shape of the Fermi surface.

The magnetoresistance in the longitudinal configuration is qualitatively different from the more familiar transverse magnetoresistance. Whereas the latter measurement gives details of the Fermi surface topology, the former can only be interpreted in terms of the scattering processes taking place on the Fermi surface. Unfortunately, the theory is not well developed even for the simple metals and a good deal of the interpretation relies on rather gross assumptions. When a very fine grid measurement of the Fermi surface is available for simple metals the longitudinal magnetoresistance measurements can give a good indication of the anisotropy of the mean free path over the surface as shown by Powell (1966) who has performed the only other longitudinal magnetoresistance investigation known to the author.

The work reported here is an attempt to apply the method of

longitudinal magnetoresistance to a divalent metal. For even the simplest of the divalent metals the Fermi surface is significantly more complex than it is for the monovalent metals and consequently the investigation can yield only roughly quantitative results. This does not detract from the significance of the experiment. Essentially all of the Fermiology experiments to date have been devoted to outlining the shape of the metallic Fermi surfaces. The next generation of experiments would logically be expected to be one in which the effect of the Fermi surface topology on the interactions of the conduction electrons will be investigated. It is hoped that this experiment will indicate some of the problems and successes of the longitudinal magnetoresistance approach to an examination of the interactions in complex metals.

Mercury has several advantages over other divalent metals for this type of experiment. It has a Fermi surface which is sufficiently simple that an approximate model can be constructed which is mathematically tractable. Further, the metal is available in very high purity at low cost and the cost of crystal growing equipment is minimal.

The chapter is divided up as follows: In the first part a theoretical discussion is given of the behavior of the longitudinal magnetoresistance for a general Fermi surface. A model is developed for the mercury surface and calculations from this model are presented.

A qualitative discussion is given of the expected effect of temperature variation on the results. The second part of the chapter outlines the treatment of the experimental data. Results from the experiment are presented as the third part. Finally, a summary of the results is given and some conclusions derived from the results are discussed.

Theoretical Discussion

Introduction to Concepts

We begin our discussion with a very simplified introduction to the Fermi surface and the effect of fields and scattering mechanisms.

Energy considerations require that electrons in a metal have wave functions which are spread throughout the metal. They are thus localized in momentum space, as well as k-space. The periodicity of the lattice leads to planes of energy discontinuity in k-space. These planes form closed polyhedra in three dimensions known as Brillouin zones (BZ). An electron arriving at such a plane will be Bragg reflected. For a given crystal each BZ contains the same volume and is exactly large enough to hold two electron states for each atom in the crystal.

Since metallic electrons are governed by Fermi-Dirac statistics, only those within kT of the Fermi energy can take part in normal transport processes. The energy, E, is proportional to k^2 for plane wave states so that it is reasonable to represent the distribution

as a spherical surface in k-space. We might expect, then, that we can represent a monovalent metal by a spherical Fermi surface completely inside a Brillouin zone, as shown in cross section in Figure 28A. However, when better account is taken of the lattice potential, the states depart from plane waves and the surface bulges toward the nearer zone boundaries and may actually contact the boundary in "necks" as shown in Figure 28B.

The significance of these neck regions is better understood on a band picture. In the neck regions, the Fermi level falls within the band gap between the first and second bands. This is a region of forbidden energies and so no electron states exist on the areas of contact between the Bragg planes and the necks. Figure 28 is schematic, made up of a sphere and cylinders. The actual Fermi surface has a smooth transition between these regions. Real metals do not have simple cubic BZs and thus the distribution of the necks in general does not turn out to be as uniform as indicated here. One possible type of deviation is indicated in Figure 28C.

The models just presented are not as idealized as one might expect from their simplicity. Many of the observed galvanomagnetic effects in monovalent metals can be explained in detail by models such as these.

We have talked thus far about monovalent metals only. Mercury is divalent and has one atom per unit cell. Since the zone can

hold two states per atom, we should expect the zone to be full and the substance to be an insulator. It turns out that the crystal potential is sufficiently weak for the distribution to maintain an almost spherical shape and thus to bulge through the first zone boundaries and form pockets of electrons in the second zone. For such a situation our two dimensional model would look like that shown in Figure 29A. A more reasonable calculation taking the lattice potential into account will modify this model to that shown in Figure 29B giving some neck areas. Now each zone will react in its own fashion to electric and magnetic fields. Again, in reality these are three dimensional figures and the zones are more complex than the simple cubic one used here.

We are using a wave vector (k) space description here and thus we should look carefully at how applied electric and magnetic fields and scattering mechanisms affect the electronic states on the Fermi surface. For simplicity of discussion we treat the carriers as positively charged. The argument used here closely follows that given by Ziman (1962) and Figure 30 is essentially from that text.

Standard quantum mechanical arguments show that a Bloch electron in the state $\psi(\vec{k})$ has an average particle velocity given by

$$\langle \vec{v}(\vec{k}) \rangle = \frac{1}{\hbar} \vec{\nabla}_k \epsilon(\vec{k}). \qquad (6\text{-}1)$$

Note that the velocity vector is thus directed along the outward normal to a constant energy surface. Application of an external force,

$\vec{F}$, changes the state of the electron according to

$$\vec{F} = \hbar \dot{\vec{k}}. \tag{6-2}$$

We are concerned here with the effects of electric and magnetic fields so equation 6-2 becomes

$$\hbar \dot{\vec{k}} = e\vec{E} + \frac{e}{c}\vec{v} \times \vec{H}. \tag{6-3}$$

If we now consider the electric field alone, an electron in the state $\vec{k}$ will change its state at the rate

$$\dot{\vec{k}} = \frac{e}{\hbar}\vec{E}. \tag{6-4}$$

If the average relaxation time for the electron is τ, then each state will be displaced a distance $\frac{e}{\hbar}\vec{E}\,\tau$ from its zero field position. Reference to Figure 30A shows that the resulting effect on the whole Fermi surface is a displacement of the surface in the direction of the field by an amount

$$\delta\vec{k} = \frac{e}{\hbar}\vec{E}\,\tau \tag{6-5}$$

and the current flows.

The density of states per unit volume of k-space is $1/4\pi^3$ and thus the segment $\vec{dS}$ of the Fermi surface contributes a net number of states to the transport of $(1/4\pi^3)\vec{dS} \cdot \delta\vec{k}$. We can state this slightly differently by saying that the contribution to conduction of

any portion of the Fermi surface is proportional to $\vec{v} \cdot \vec{E}$.

One point, which is not obvious without numerical values, is that application of a reasonable (1 volt/meter) electric field alters the Fermi velocity by less than 1%. Thus we choose to regard the effect of an applied electric field as creating a net excess of electrons with a velocity component in the direction of the field but which still have the Fermi velocity. Another way of saying this is that the displacement of the surface shown in Figure 30A is greatly exaggerated with respect to the size of the surface shown. In what follows we will use Pippard's (1964) terminology and refer to this process as a creation of conduction states.

States can be removed from conduction by scattering interactions which take them to another part of the surface where the velocity is opposite to the field. A single impurity scattering can do this as can scatterings by phonons of short wavelength and thus large wave number $(\vec{q})$.

This process is illustrated in Figure 30B; an electron in state $\vec{k}'$ absorbs a phonon and is scattered to state $\vec{k}$. Its velocity component in any given direction is significantly altered since it is scattered through a relatively large angle. Of course, energy conservation must be obeyed but the phonon energy is so small compared to the electron energy that the electron effectively remains on the Fermi surface. These "large q" phonons predominate at higher

temperatures satisfying $T > \frac{1}{2}\theta_D$. This process is termed large angle scattering. At lower temperatures the phonon scattering is due to phonons of small wave number and multiple scatterings by these phonons are necessary to move an electron through a large angle and hence remove it from conduction. This region, below $\theta_D/10$ in high purity metals, is termed the small angle scattering region.

Now consider the effect of applying a magnetic field parallel to the electric field. In coordinate space we know that the electrons will move in helical paths along the field direction rotating about the field lines with angular frequency ω. The situation in terms of a Fermi surface description is illustrated by Figure 30C. Recall that in our description the electric field just creates an excess of electrons with a velocity component in the field direction. The magnetic force, from equation 6-3, changes $\vec{k}$ at the rate

$$\dot{\vec{k}} = \frac{e}{c\hbar} \vec{v} \times \vec{H} . \qquad (6\text{-}6)$$

The motion is thus normal to the field direction and to the electron velocity at that point on the surface. Since we know that the electron remains on the Fermi surface, we conclude that it must follow an "orbit" defined by the intersection of a plane normal to H with the Fermi surface as illustrated in Figure 30C. Thus in a magnetic field, the states created by the electric field are driven around the Fermi surface in orbits lying in planes normal to the field direction. The

condition $\omega\tau > 1$ is the same as requiring that the electron complete a number of orbits before a scattering interaction takes place.

Return for a moment to the simple Fermi surface models of Figure 28. As far as electrical conductivity is concerned there is not much difference between the surfaces (A) and (B) of Figure 28. The essential difference is that an excess of states with $\vec{v}$ along the field will not be created in the regions of contact when an electric field is applied. Thus the metal in (A) would have a slightly lower resistance. With this same figure consider the effect of a magnetic field perpendicular to the plane of the figure. Electrons on the surface in (A) will sweep around in circular orbits while in (B) they will be Bragg reflected to the opposite side of the zone many times and may follow orbits which are vastly different than those in (A). Note, however, that the orbits eventually close on themselves, i. e., the electron traverses all available sections of the orbit. An even more drastic thing happens with a contact situation like that in Figure 28C. Now the orbit never closes on itself and we have the phenomena of open orbits which is so important in transverse magnetoresistance studies. The effects of these orbit types on the various galvanomagnetic measurements are given in some detail by Ziman (1962).

A statement usually made in the literature is that the longitudinal magnetoresistance should saturate; that is the resistance should become independent of magnetic field after an initial rise. That this

should be the case can be seen by considering the two quite different Fermi surface models shown in Figure 31. These models illustrate in a simple manner the two most important longitudinal magnetoresistance mechanisms discussed by Pippard (1964).

First consider the cylindrical surface shown in Figure 31A. Application of an electric field creates an excess of states with velocities in the direction of the field and a current flows. The magnetic field causes the electrons to circle the surface in orbits with their planes perpendicular to the field. If the high field condition is satisfied we see that the velocity in the field direction will average to zero for each orbit and thus the resistance will become infinite. On a more realistic, i. e. less symmetrical, model of a surface the averaging will not give a zero net velocity but it will give an increase in the resistance with field until the high field condition is satisfied at which point the resistance will saturate. In other words, the velocities will average in the same fashion as on the cylindrical surface but the resulting average velocity will not be exactly zero.

Another saturating effect due to neck regions can be seen with the Fermi surface shown in Figure 31B. This is the model suggested by Pippard (1964) for copper. The surface is spherical and the necks are represented by circular areas of the surface on which no conduction states exist. If an electron is scattered into the neck regions it is Bragg reflected to the other side of the zone, its velocity in the field

direction is essentially reversed, and it is removed from conduction. To see the effect of a magnetic field on this model it is convenient to consider the electrons as stationary and the surface as rotating with angular velocity ω about H. The necks thus have the effect of sweeping up electrons as they move around and removing them from conduction. Clearly, a field will be reached where the necks are sweeping out a band across the surface before the electronic states created in these areas can be scattered out. At this point they have accomplished all that they can and a further field increase will not affect the resistance. Again we have saturation.

There are several features of this model which illustrate the suitability of the longitudinal magnetoresistance measurement as an indication of the type of scattering. First we see that the value of $\sigma(\infty)/\sigma(0)$ should change drastically with orientation since with a proper orientation most of the surface could be removed from conduction by the sweeping necks acting independently. Of course, the saturation field will be greater when the necks act independently. Second we can see that the effects of the necks is qualitatively different depending on whether we are in a large angle or a small angle scattering region. In the case of large angle scattering the field results in removal from conduction only of states in the band swept out by the necks as discussed above. In the small angle scattering region we consider the electrons as moving on the surface by a diffusion

process as a result of a large number of small angle scattering interactions. In this case states created outside of the neck regions can wander into these regions and be removed from conduction. The only other way they can be removed is to diffuse to the equatorial plane. When the necks are moving around with sufficient velocity, any of the states created in the polar region of Figure 31 B will eventually be removed from conduction as they diffuse into the band swept out by the necks. Thus, in this case of small angle scattering, the effect of the necks is greatly increased over that in the large angle case for the same orientation. For his copper model Pippard predicts an increase in $\sigma(0)/\sigma(\infty)$ by about a factor of 4.5 in going from large to small angle scattering.

Before leaving this discussion, we should note that the models used here have been very simple and have represented one zone only. We have said nothing about the field magnitudes required to observe the saturation effects. The calculation of these fields is a formidable problem. The only attempt to date was made by Pippard (1964) on a further simplification of the neck model presented here.

Mathematical Treatment

The ideas just outlined can be made at least partially quantitative. The derivations are discussed at length by Pippard (1965) and are only outlined here. If we consider the case where a relaxation

time approximation can be used, the Boltzmann equation of Chapter 5 leads directly to

$$\vec{J} = \frac{e^2}{4\pi^3} \int \tau(\vec{k})\, \vec{v}(\vec{k})\, [\, \vec{E}\cdot\vec{v}(\vec{k})\,]\, \frac{\partial f_0}{\partial \epsilon}\, d\vec{k} \qquad (6\text{-}7)$$

for the case of zero magnetic field. Thus the longitudinal conductivity is

$$\sigma_{zz}(0) = \frac{e^2}{4\pi^3 \hbar} \int_{\epsilon_f} \frac{\tau(\vec{k}) v_z^2(\vec{k})}{|\vec{v}(\vec{k})|}\, dS \qquad (6\text{-}8)$$

which we can write as

$$\sigma_{zz}(0) = \frac{e^2}{4\pi^3 \hbar} \int_{\epsilon_f} \tau(\vec{k})\, v(\vec{k}) \cos^2\theta\, dS \qquad (6\text{-}9)$$

where θ is the angle between z, the direction of the field, and the Fermi surface normal. For brevity we drop the explicit k dependence and rewrite 6-9 as

$$\sigma_{zz}(0) = \frac{e^2}{4\pi^3 \hbar} \int_{\epsilon_f} \tau v_z \cos\theta\, dS. \qquad (6\text{-}10)$$

Now,

$$dS = k_f^2 \sin\theta\, d\theta\, d\phi = ds\, \frac{dk_z}{\sin\theta} \qquad (6\text{-}11)$$

where ds is a path element perpendicular to z on the Fermi surface and $dk_z/\sin\theta$ is a path element perpendicular to ds on the surface. The conductivity can now be written as an integral over closed orbits on the surface in the form

$$\sigma_{zz}(0) = \frac{e^2}{4\pi^3\hbar} \int dk_z \oint \tau v_z \cot\theta \, ds. \qquad (6\text{-}12)$$

Now in the high field region the only change to this form is that v_z is replaced by an average $\overline{v}_z$, the average being taken over the orbit.

The result of the calculation for $\overline{v}_z$ is

$$\overline{v}_z = \frac{\oint \cot\theta \, ds}{\oint \frac{1}{v} \operatorname{cosec}\theta \, ds} \quad . \qquad (6\text{-}13)$$

which leads to the form for $\sigma(\infty)$

$$\sigma(\infty) = \frac{e^2}{4\pi^3\hbar} \int dkz \left[\frac{\left(\oint \cot ds\right)^2}{\oint \frac{1}{\tau v} \operatorname{cosec}\theta \, ds} \right. . \qquad (6\text{-}14)$$

Combination of this equation and 6-12 leads to Pippard's final form for the saturation magnetoresistance

$$\frac{\rho_{zz}(\infty)}{\rho_{zz}(0)} = \frac{\int dk_z \oint \ell \cot\theta \cos\theta \, ds}{\int dk_z \left[\frac{\left(\oint \cot\theta \, ds\right)^2}{\oint \frac{1}{\ell} \operatorname{cosec}\theta \, ds} \right]} \qquad (6\text{-}15)$$

where $\ell = \tau v$ is the mean free path on the Fermi surface. This expression is quite complex for any but the simplest surfaces but note that it involves only the surface geometry and the mean free path. Clearly a number of approximations must be made before this expression can be used for a complex Fermi surface. We will discuss these in the next several pages when the model is presented.

For the case of small angle scattering and where open orbits are present the previous development does not hold and an analytical treatment is very difficult if not impossible. Fortunately, the model treated here allows use of the relaxation time approximation for the major contribution to the ratio. Other contributions are handled in a more qualitative way as we shall see shortly after discussing the Fermi surface model for mercury.

The Fermi Surface Model

The first Brillouin zone of mercury along with the standard nomenclature is shown in Figure 32. There are six pseudohexagonal faces in (100) type directions, two hexagonal faces on the (111) axis and six rectangular faces on (110) type axes.

This zone is a distortion of the more familiar zone of a face centered cubic structure. The fcc zone would be obtained by compression of the mercury zone along the (111) direction. All eight six-sided faces become true hexagons and the six rectangular faces become square. The relationship between the mercury lattice and the fcc structure was discussed in more detail in Chapter 3.

On the nearly free electron model, the Fermi surface bulges through the zone only on the pseudohexagonal faces. There are no necks on this model. A more realistic model is provided by the relativistic augmented plane wave (RAPW) calculations of Keeton and

Loucks (1966). The result of their calculation is shown in Figure 33, taken from their report. The white areas are regions of necking contacts and the crosshatched areas represent the regions where the surface breaks through into the second zone. As mentioned earlier, this model has been verified to a large extent both by de Haas-van Alphen and transverse magnetoresistance measurements.

The model used here is illustrated in Figure 34 which is a plane containing the (111) and (100) axes. The neck areas are approximated by cylinders and the free surface areas are spherical. For purposes of calculation the small necks are ignored. The pertinent dimensions of Figure 34 in units of π/a as measured from Keeton and Loucks' paper are:

Radius of the spherical surface - 1.31

Zone 1, Radius of base of zone 1 cap - .47

Height of zone 1 cap - .09

Radius of zone 1 neck - .71

Length of zone 1 neck - .18

Zone 2, Radius of base of zone 2 cap - .54

Height of zone 2 cap - .12

Radius of zone 2 neck - .54

Length of zone 2 neck - .09

The model is not entirely realistic, there is some overlap of the cylinders in the first zone for instance, but it allows some crude

calculations to be made for the resistivity which would not be possible with a more complex model. The calculations show an internal consistency which implies that the approximations made in the model are not unreasonable.

Scattering by Phonons

In order to determine what type of scatterings are possible on the surface we use the approximate expression for the maximum phonon wave vector to be expected at a given temperature

$$q \approx \frac{2\pi}{a} \left(\frac{T}{\theta_D}\right). \tag{6-16}$$

θ_D is taken to have its minimum observed value given by Smith and Wolcott (1956) of 50° K. Thus, in units of π/a, $q_{max}(4.2° K) \approx .17$ and $q_{max}(1.8° K) \approx .07$. Measurements of critical distances on the model show that in the temperature region below 4.2° K there should be no scatterings between the second zone lenses. Even without the small necks Umklapp scattering on the first zone caps will continue well below 1.8° K. Although the phonon wave vectors are quite small compared to the radius of the Fermi surface, they are still of significant size compared to the dimensions of the areas available for conduction states and thus the scattering interactions can be still termed large angle. In other words, a single scattering can remove a state to a portion of the surface which is significantly different in

character from the region from which it was scattered. On a single spherical surface we would be well into the small angle region at these temperatures. Finally there should be no phonon assisted band-to-band transitions. This statement is in agreement with the results found in Chapter 4.

All of these results lead to a picture of the Fermi surface in which the second zone lenses contribute to the conduction independently of each other and independently of the first zone. On all parts of the surface it is not unreasonable to speak of the phonon scattering interactions as being effectively large angle. Thus a relaxation time approach may be used to attempt a calculation of the contribution of the various parts of the surface to the conduction process.

Calculations from the Model

It is possible to use the model proposed here to calculate $\sigma(0)$ and $\sigma(\infty)$. There is little question that the mean free path of the conduction electrons will be different in the neck regions than on the spherical surfaces. There is also the possiblity of a difference in the relaxation times in the two zones and, with a more exact model, the mean free path will vary over each part of the surface within a given zone.

The calculations were made using the following set of assumptions: Over a particular region in a given zone (i. e., over a cap or

a neck) the mean free path is constant. The mean free path on the neck regions is different from that on the caps. The first and second zone mean free paths are the same, i. e. $\ell_{neck}(\text{zone } 1) = \ell_{neck}(\text{zone } 2)$ and $\ell_{cap}(\text{zone } 1) = \ell_{cap}(\text{zone } 2)$. We define a parameter X by

$$\ell_{neck} = X\ell_{cap}. \tag{6-17}$$

The assumptions have no firm foundation. To the best of our knowledge there is no experimental evidence either for or against the form chosen here for divalent metals. The assumptions are based on a collection of ideas from various experiments and theoretical treatments. Experiments on the noble metals indicate a different mean free path in the necks from that on the spherical regions (Powell, 1966; Dugdale and Basinski, 1967). Pippard (1964) had some success in a very rough magnetoresistance calculation for aluminum assuming a constant mean free path over the major contributing zone. The assumption that mean free paths on each type of segment is the same in the two zones is based purely on the fact that it is not expected that the two bands of mercury will have significantly different behavior. Also, it is desired to keep the number of parameters of the theory to an absolute minimum consistent with available information.

Calculation of $\sigma(0)$

We initially calculate the zero field conductivity for the separate portions of the surface letting X = 1. Equation 6-12 in the form

$$\sigma_{zz}(0) = \frac{e^2}{4\pi^3\hbar} \tau v \int \cos^2\theta \, dS \qquad (6\text{-}18)$$

can be integrated over each segment of the surface and a general expression derived for the contribution of the segment to the conductivity in any given direction. The problem is geometrically complex but straightforward. The results for several high symmetry orientations are given in Table 2.

Table 2. Contribution to $\sigma(0)$ for X = 1

z	First Zone Caps	First Zone Necks	Second Zone Caps	Second Zone Necks	Total $\sigma(0)$	Normalized $\sigma(0)$
(111)	.186	.366	.155	.105	.812	1.00
($\bar{2}$11)	.006	.256	.330	.074	.666	.82
($\bar{1}$01)	.006	.257	.328	.073	.664	.82
(100)	.036	.274	.301	.079	.690	.85
(110)	.087	.303	.255	.087	.732	.90

$\sigma_{||}/\sigma_{\perp} = 1.22$

The results given here and in the rest of the similar tables are normalized so that a spherical surface of the same size with no necks and no zone intersections and with $\ell = \ell_{cap}$ over the entire surface

would give $\sigma(0) = \sigma(\infty) = 1$. The ratio of conductivity parallel to (111) to that perpendicular to (111) from this calculation is 1.22 as opposed to the measured value of 1.32.

We next determine what value of X in the assumption of equation 6-17 will give us the value, 1.32, for the ratio. The result is X = 2.9. Recalculation of the contributions to $\sigma(0)$ under this assumption are shown in Table 3. Agreement at intermediate orientations with equation 4-5 is excellent.

Table 3. Contributions to $\sigma(0)$ for X = 2.9.

	First Zone		Second Zone		Total	Normalized
z	Caps	Necks	Caps	Necks	$\sigma(0)$	$\sigma(0)$
(111)	.186	1.06	.155	.305	1.71	1.00
$(\bar{2}11)$	.006	.742	.330	.214	1.29	.75
$(\bar{1}01)$	.006	.746	.328	.212	1.29	.75
(100)	.036	.795	.310	.229	1.36	.80
(110)	.087	.879	.255	.253	1.47	.86

$\sigma_{||}/\sigma_{\perp} = 1.32$

Calculation of $\sigma(\infty)$

When we turn to consideration of the effect of a longitudinal magnetic field the problem becomes very difficult. The integrals of equation 6-14 must be performed over the orbits and thus the calculation cannot be done separately for each segment of the surface. The complete argument for the approach used on each zone surface is given in Appendix B. What we do, in summary, is to assume that

all of the first zone surface is removed from conduction due to the large necks except for orientations very close to (111). We find an "average" orbit for each of the second zone lenses whose contribution will approximately represent that of the entire lens. On this basis we calculate $\sigma(\infty)$ and recalculate $\sigma(0)$. The results of the calculations for both $x = 1$ and $x = 2.9$ are presented in Figures 35 and 36. The graphs show $\sigma(0)/\sigma(\infty)$ along the two major paths from the (111) plane to the (111) axis. The angular coordinate is the angle between (111) and z. These plots are normalized to unity in the (111) direction with the first zone contribution included.

Note that the parameter X defined in equation 6-17 has been restricted to apply only to the velocity contribution to the mean free path. By definition

$$\ell = \tau v \qquad (6\text{-}18)$$

and the calculation as given in Appendix B does not depend on τ. This is not surprising as we would not expect the magnetic field to have any direct effect on τ. Thus, agreement of the experimental magnetoresistance curves with the form derived from the model for the case $x = 2.9$ would imply that the variation in the mean free path was due to a variation in the Fermi velocity rather than in the relaxation time if the assumptions made in the calculations are correct.

It is difficult to justify the assumptions and the approach used here in any absolute sense. The best that can be said is that they do

not give disagreement with any of the known properties of mercury and the assumed behavior of the mean free path is in keeping with the results of recent work on other metals. Let us close this section with the comment that at least this treatment indicates some of the problems inherent in any attempt to relate experimental data on polyvalent metals back to basic mechanisms.

The Approach to Saturation

We have mentioned earlier that the approach to saturation of the longitudinal magnetoresistance is a very difficult problem. Essentially no quantitative work has been done for any realistic models. There are some investigations which can be made relevant to this problem. If we accept the fact that the longitudinal magnetoresistance does saturate in sufficiently high fields, we then can ask what we can do experimentally to change the field value at which the saturation occurs. The easiest way of doing this is to vary the temperature and thus the electron-phonon relaxation time.

Recall that we have looked at such behavior in the case of the low field magnetoresistance in Chapter 5. In that case the curves had a known mathematical form and a quantitative approach could be used. In the high field region where the form of the magnetoresistance is determined by the Fermi surface this is not possible. Thus the following discussion is more qualitative in nature.

Within the temperature range available here, we should expect no drastic changes in the magnetoresistance since there are no radical changes in the character of the scattering. The reasons for this are as follows: (1) We have already seen that the phonon scattering is effectively large angle due to the small size of the available Fermi surface areas. Actually, it would be more accurate to describe it as intermediate angle scattering, but it is likely that the relaxation time approximation is still justified. (2) Over our available range of temperatures (4.2° K to 1.8° K) the maximum phonon wave vector changes by a factor of 2.3 but it is still too small at the highest temperatures to give any interband or between lens scattering. (3) We have shown in Chapter 4 that at the lowest temperature there is very little impurity scattering. (4) Finally, we have already argued that the first zone contribution quickly saturates and hence contributes very little to the magnetoresistance regardless of the scattering region. Thus, it is reasonable to conclude that the only effect of lowering the temperature will be to cause the saturation to occur at lower field values, i.e., the high field region is reached more quickly.

The crystals which have had impurities purposely introduced may be of some help in the interpretation. In at least the low temperature end of the range the scattering in these samples should be mostly due to the impurities and this type of scattering can produce all of the transitions mentioned above. Thus we might expect the

magnetoresistance behavior of the alloy samples to be significantly different from that of the pure metal samples.

Treatment of the Data

The data is initially used to determine the variation of the magnetoresistance ratio R(H)/R(0) with angular orientation of H.

Values of R(H) in the saturation regions at a number of temperatures are determined from graphs of the high field magnetoresistance data for a number of samples. At temperatures below the transition temperature, but above 2.6° K, values of R(0) are determined by extrapolation of the low field magnetoresistance data. For the curves made at temperatures below 2.6° K we use R at the critical field. This value is taken directly from the resistance versus temperature data.

The temperature variation of the magnetoresistance for a given sample is investigated by plotting all of the resistance versus field curves on a single log-log-graph. The limit of the high field region is determined from the resistance versus temperature data and added to the graph. Additional information is obtained by comparison of the graphs for the various samples.

Results

The observed behavior of the longitudinal magnetoresistance

for a given sample is considerably more complex than our simple theory would indicate. Consider the curves shown in Figure 37 for the pure mercury sample. At 4.2°K the curve has not reached saturation. At 2.7° K the curve appears to approach saturation near 20 kOe and then start to increase again. Finally, at 2.2° K, there is a very short saturation region before the curve begins to rise again. This behavior is observed for all samples and we will say more about it when we discuss the temperature variation in general.

The lack of a final saturation is not unusual. It has been observed for some orientations in copper crystals by Powell (1966) and in polycrystalline potassium as reported by Justi and Auch (1963). No explanation has been given for this behavior and it stands as a basic problem in this type of measurement.

In order to attempt a comparison with theory, a number of ratio values are plotted as a function of the angle between the magnetic field and the (111) direction in Figures 38 and 39. Obviously, each point on a curve represents a single sample. The ratio values used are:

1. R(20 kOe)/R(0) for T = 2.7° K,
2. R(48 kOe)/R(0) for T = 2.7° K, and
3. R(48 kOe)/R(H_c) for T = 2.2° K.

The first of these is an attempt to investigate the first saturation; the second and third should indicate a minimum magnitude to be

expected for the ratio if the curves are in fact headed for a final saturation. All of the curves exhibit a behavior in qualitative agreement with the calculations from the model shown in Figures 35 and 36. The leveling off of the curve at small angles seems to begin at higher angle values than predicted by the theory, but this is probably due to the neglect of any first zone effect until the caps contribute. Both of the curves shown for 2.7° K agree best with the theory for $X = 1$ shown in Figure 35. The curve at 2.2° K has the steeper slope necessary for agreement with the theory for $X = 2.9$ but the agreement is not good.

The data points for the two alloy samples are shown in Figure 39 also. At 2.2° K the alloy samples are still in the first saturation region. These samples saturate at much lower values of $R(H)/R(0)$ than pure samples of the same orientation at the same temperature. Figure 37 shows this behavior very clearly.

The effect of temperature on the field curves is shown for three samples in Figures 40, 41 and 42. The saturation region is not as clear on these log-log plots of the raw data as it is on a ratio plot. It is seen as a slight leveling of the curves here. The solid line represents the expected field at which the high field region is first reached, i.e., the value of H at which $\omega\tau = 1$. This value is calculated by using the resistivity at 4.2° K to estimate τ, the composite R-T curve of Chapter 4 then gives τ at lower temperatures.

The values derived for $\omega\tau$ agree with approximate values stated by Dishman and Rayne (1966) and by Dixon and Datars (1967). Note that on all the curves this line is a good indicator of the beginning of the first saturation region. The dotted line to the right of the $\omega\tau \approx 1$ line is drawn parallel to the solid line and the region between the lines indicates roughly the extent of the saturation region. Note that this region becomes larger as H moves farther away from (111); in order of increasing angle we have No. 90 (22°), No. 94 (55°) and No. 84 (65°).

Summary of Results and Conclusions

If we take the R(20 kOe)/R(0) measurement at 2.7° K as indicative of the true saturation in the sense we have described it in the theory, then several conclusions can be drawn. First, the assumption of the theory that the neck velocity is considerably higher than that on the spherical caps is probably not true and the variation in the resistance should be blamed more on differences in the relaxation times in the two regions. Recent work on simple metals, both theoretical (Jones and Sondheimer, 1967) and experimental (Dugdale and Basinski, 1967), suggests that relaxation time anisotropies may play a significant role in the conduction properties.

The angular variation of the magnetoresistance predicted by the model is borne out reasonably well by the data. The first zone

seems to contribute to the magnetoresistance at a larger angle than that assumed in the theory. The data is not sufficiently accurate to attempt any comparison with the theoretical variation of the magnetoresistance with longitude on the Fermi surface.

Samples where impurity scattering is dominant show a much lower saturation value for the magnetoresistance. The theory developed here is not applicable to alloys, but we would expect this behavior since the scattering is essentially unrestricted large angle scattering which would override any small angle contribution. This result further bears out the accuracy of the qualitative arguments given by Pippard (1964) for simple surfaces and summarized at the beginning of this chapter.

The mechanism responsible for the increasing magnetoresistance beyond the first saturation is unexplained as mentioned earlier. The orientation method described in Chapter 3 rules out a transverse magnetoresistance effect. In the case of mercury it is tempting to blame the absence of saturation on some first zone effect in which the large necks do not give exact cancellation for all orbits. In view of the fact that similar behavior is observed for some monovalent metals as well, such an explanation is not expected to have general validity. Further experimental work is planned on potassium crystals which, it is hoped, will provide some answers. From the data presented here there is no indication that a second saturation

occurs, although the possibility cannot be discounted. If such a saturation could be observed, it would indicate the presence of a group of electrons with a significantly smaller relaxation time.

The final conclusion, and perhaps the most important, is that use of the longitudinal magnetoresistance as a quantitative indicator of scattering effects in metals with complex Fermi surfaces is unlikely to be immediately productive, for a vast number of extremely high precision measurements are needed, each one requiring growth of a crystal with a different orientation, and a good theory which can differentiate quantitatively between the contributions from the various zone surfaces does not exist. Finally, a significant amount of data is needed from other types of experiments which will allow us to determine the exact topology of the surface.

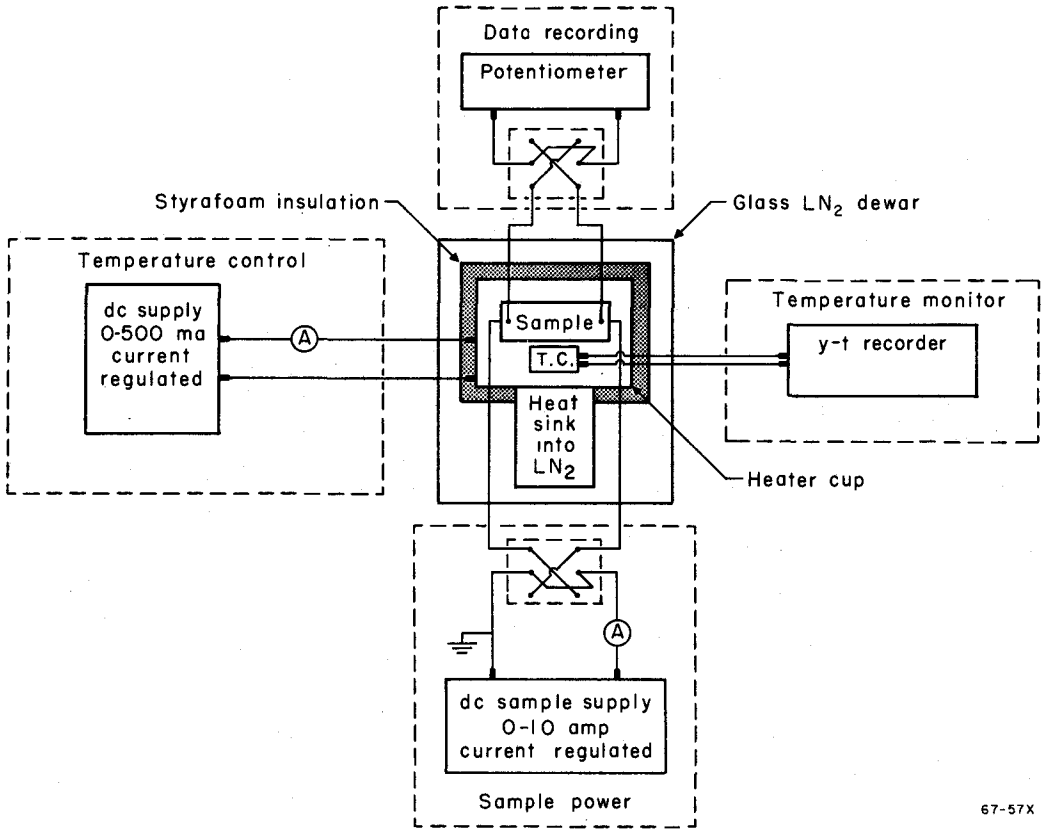

Figure 1. Resistance versus temperature measurement 77°K to 220°K.

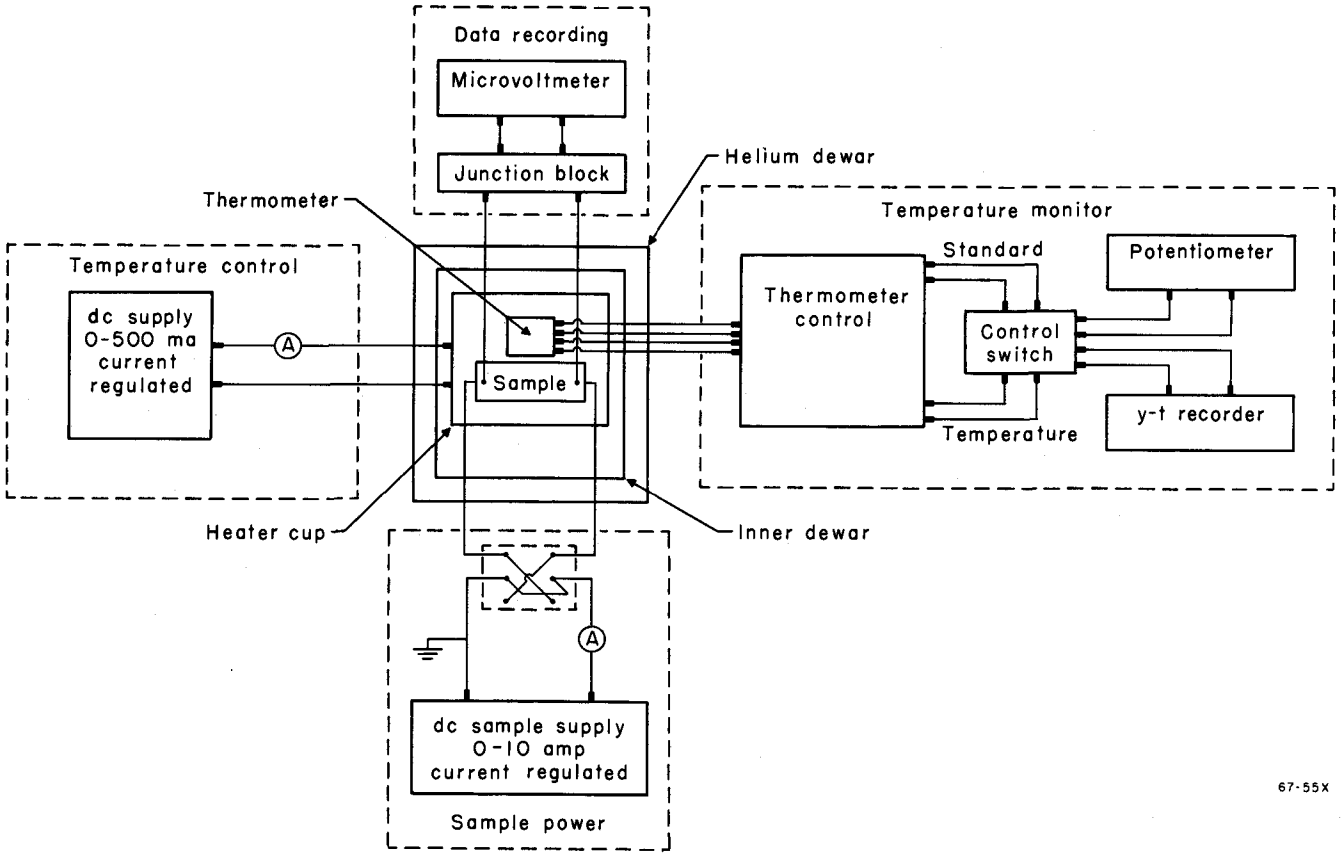

Figure 2. Resistance versus temperature measurement 4.2°K to 40°K.

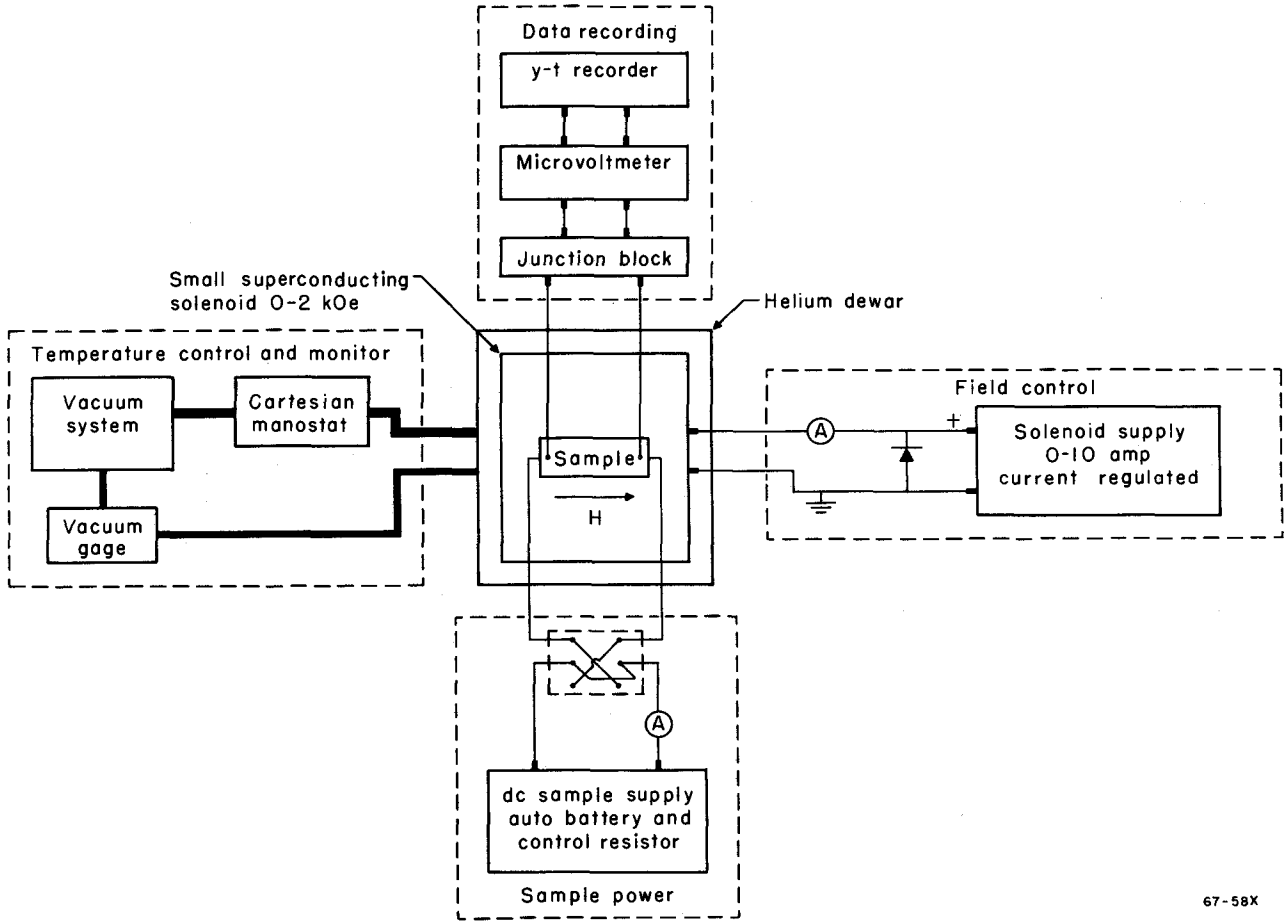

Figure 3. Resistance versus temperature 1.8°K to 4.2°K and low field magnetoresistance measurement.

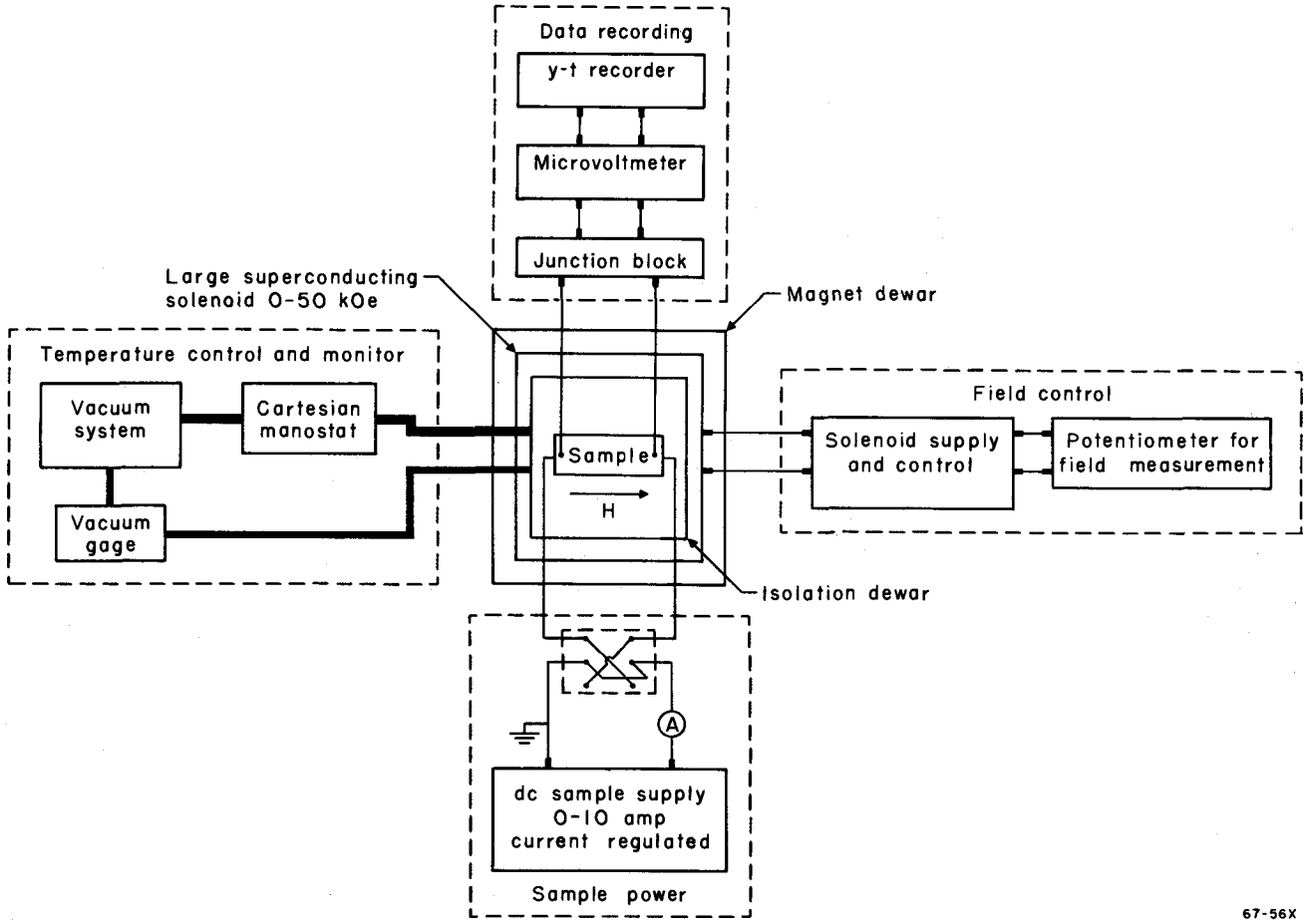

Figure 4. High field longitudinal magnetoresistance measurement.

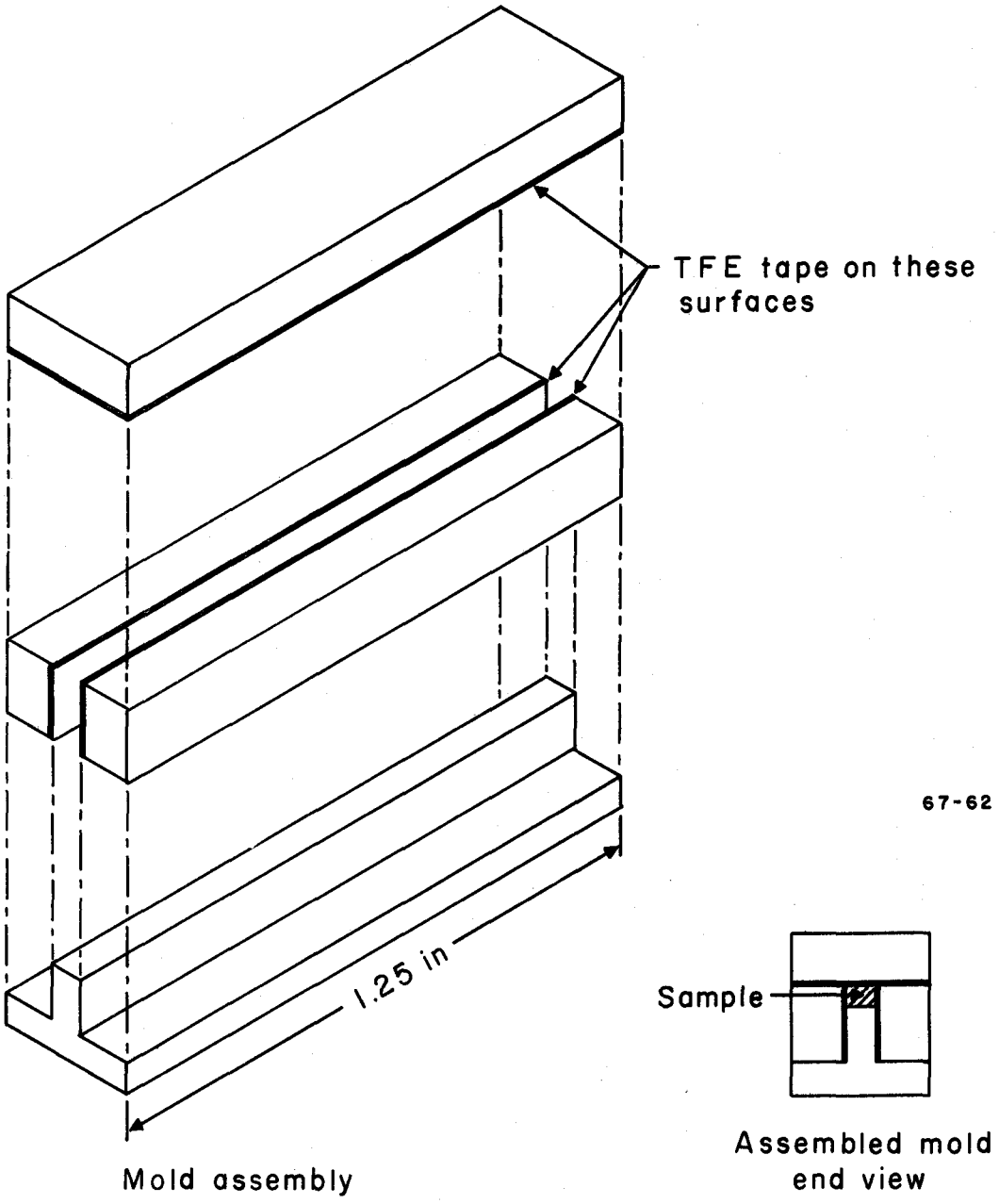

Figure 5. Crystal growth mold.

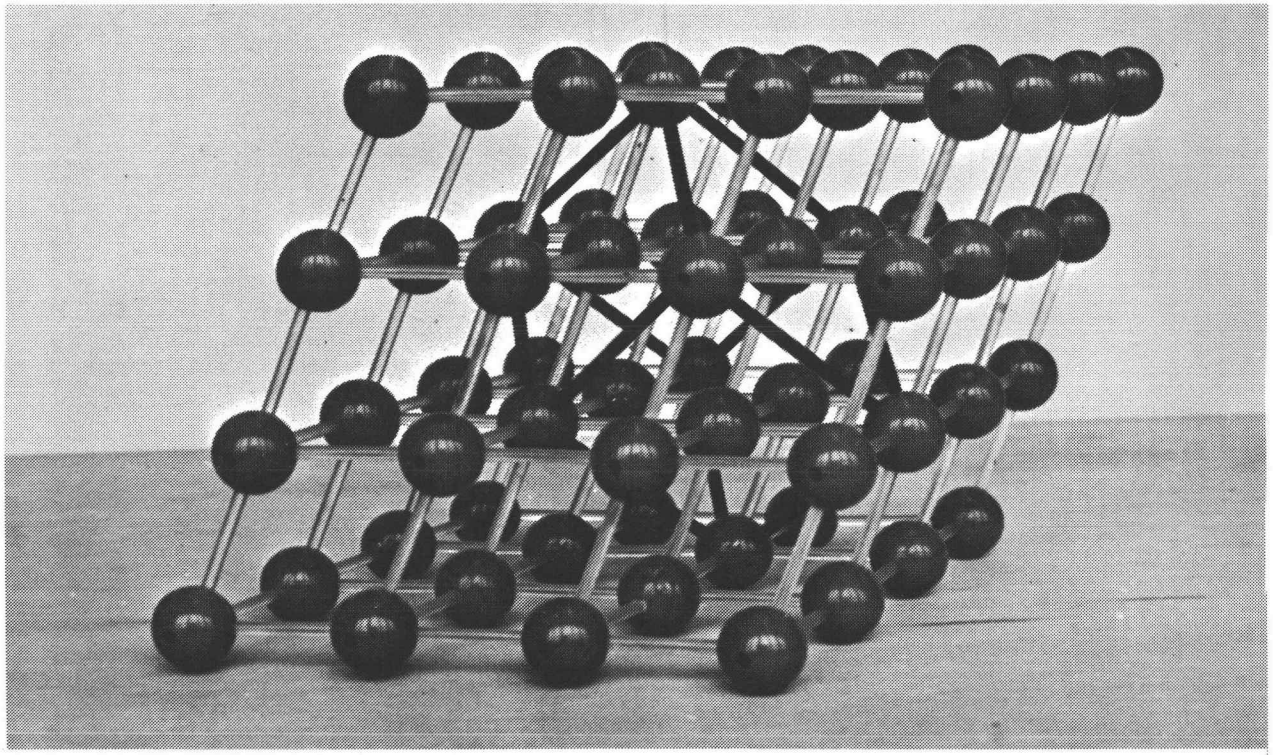

Figure 6. Direct lattice of mercury.

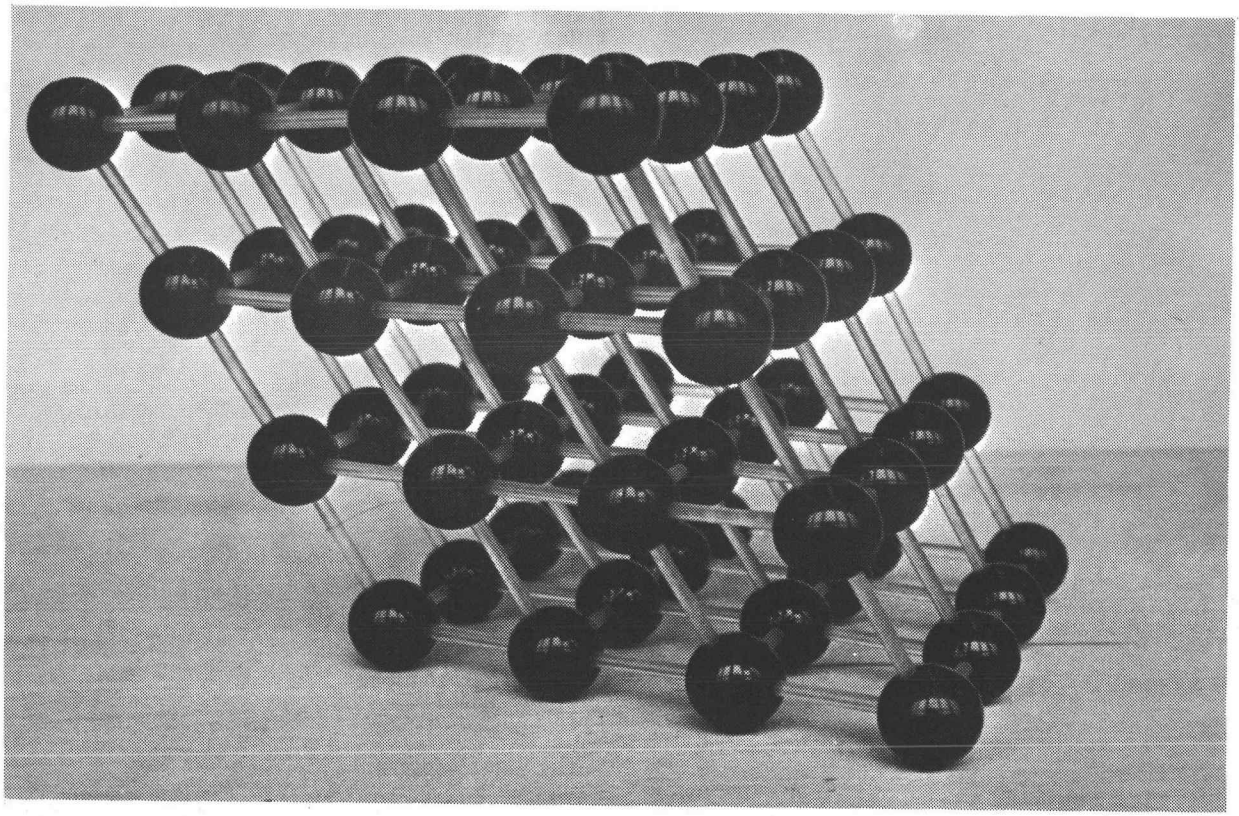

Figure 7. Reciprocal lattice of mercury.

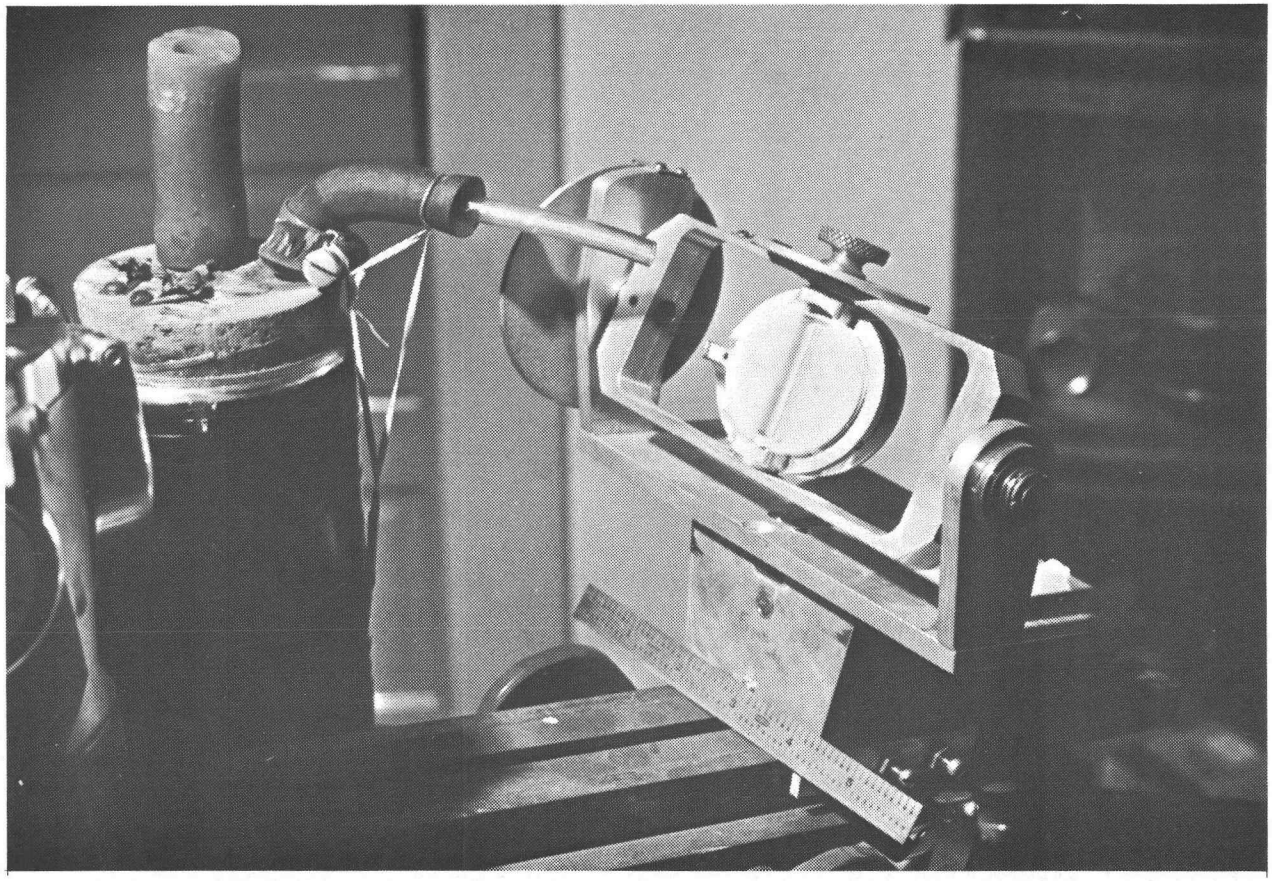

Figure 8. X-ray orienter for samples.

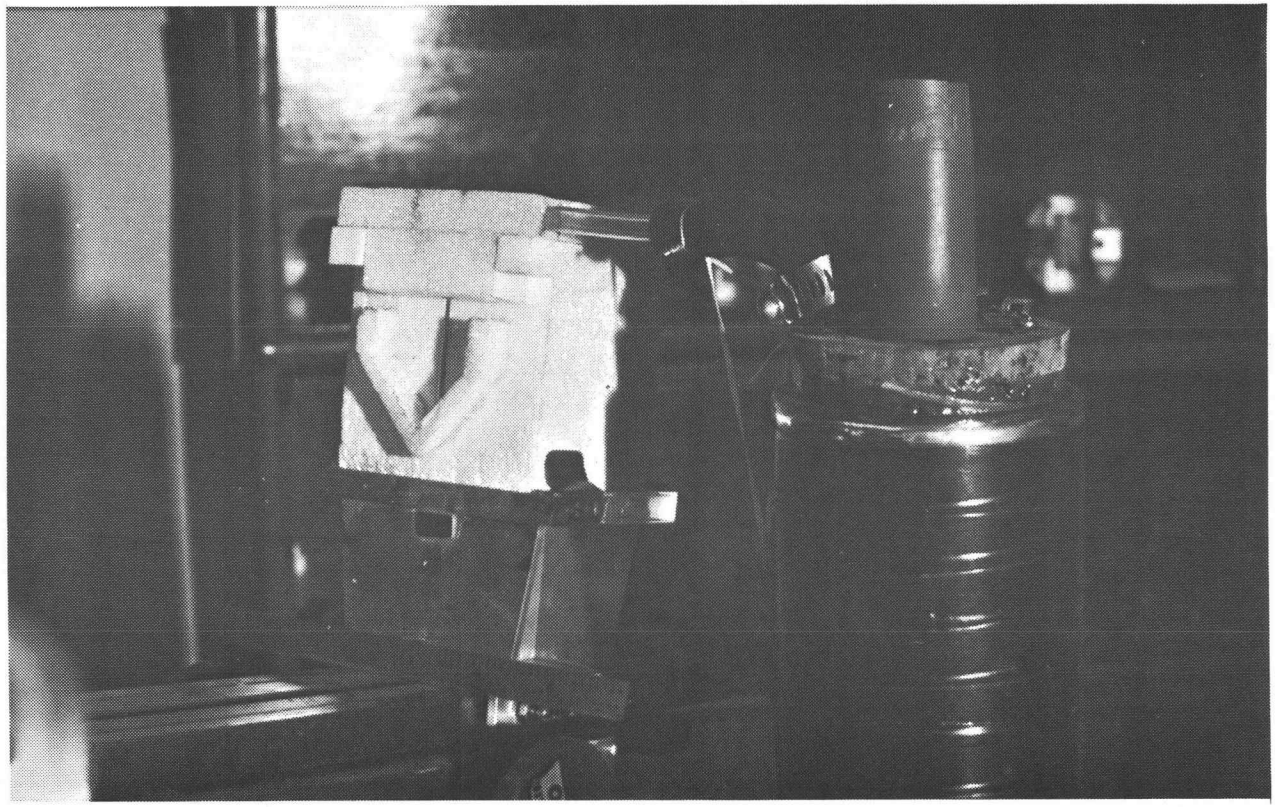

Figure 9. Styrafoam sample holder for X-ray.

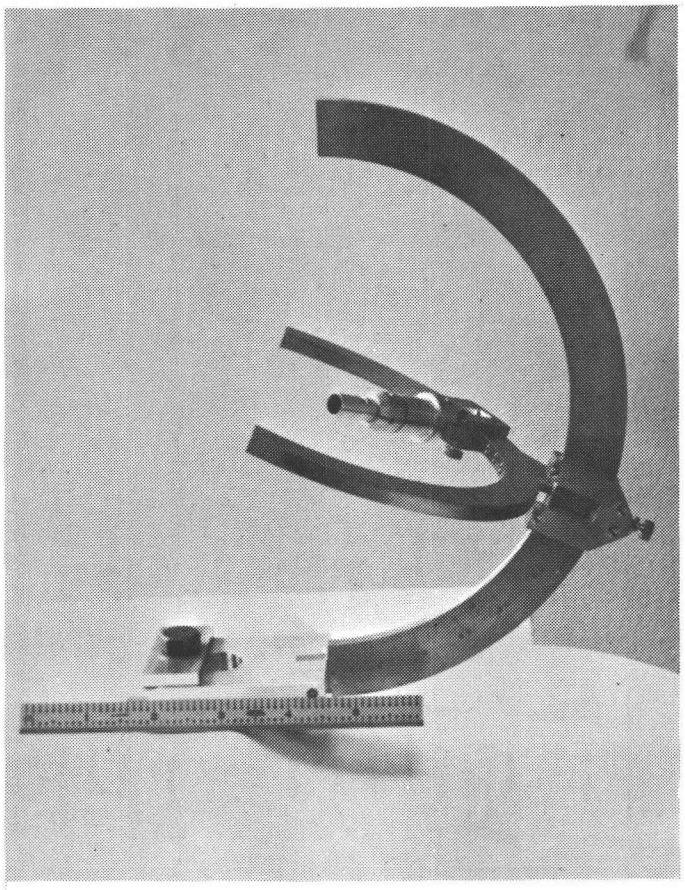

Figure 10. Large-angle back reflection goniometer.

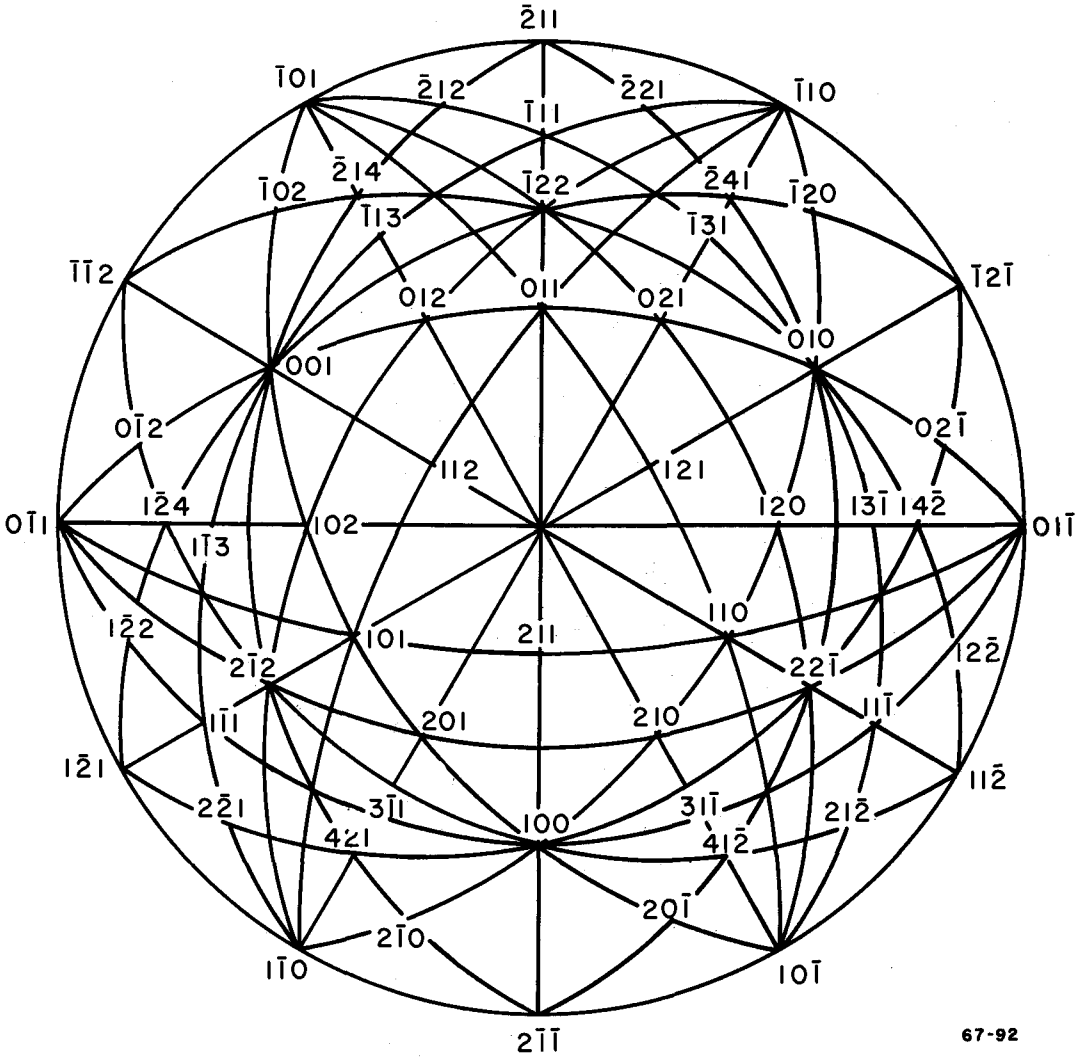

Figure 11. (111) standard projection for alpha mercury.

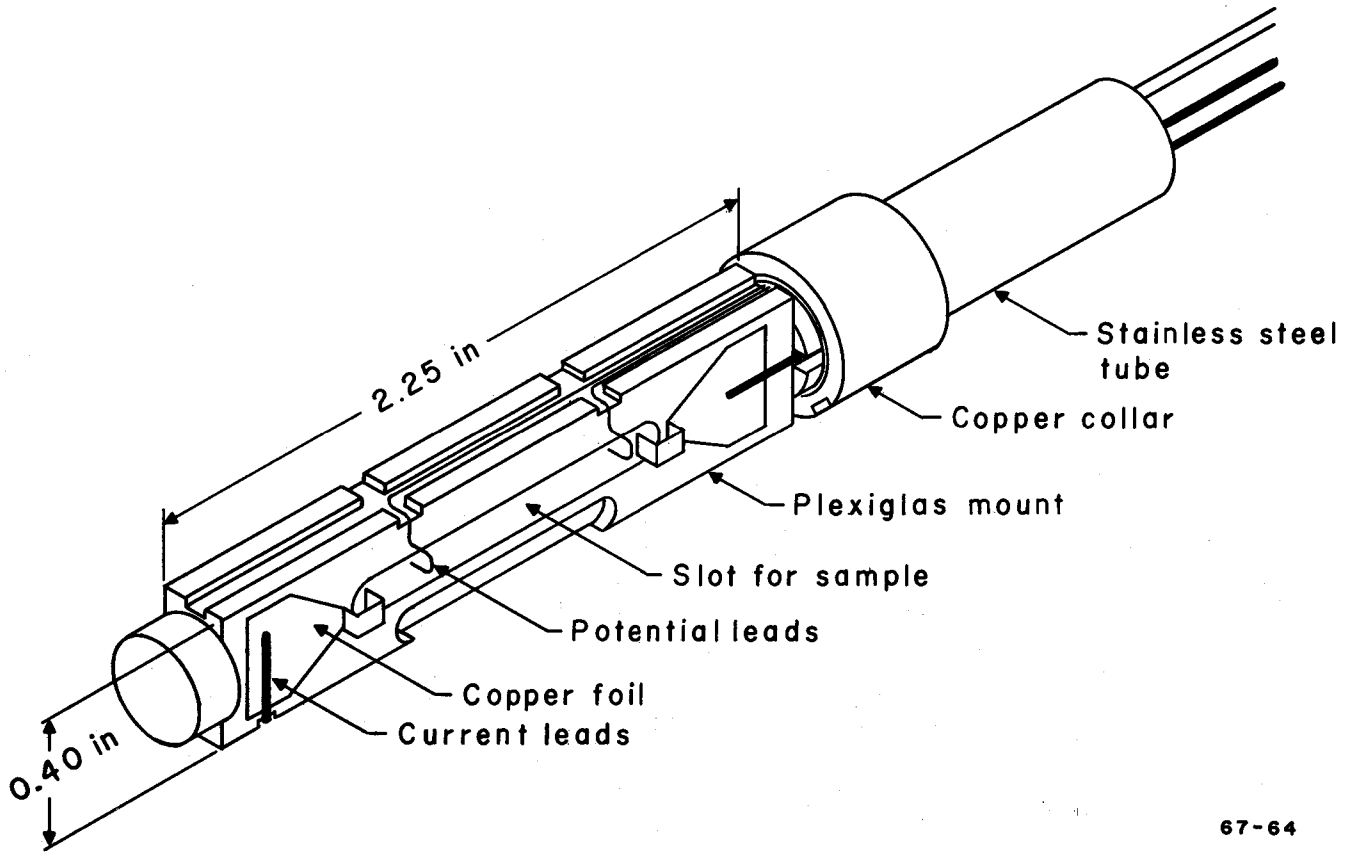

Figure 12. Universal sample mount.

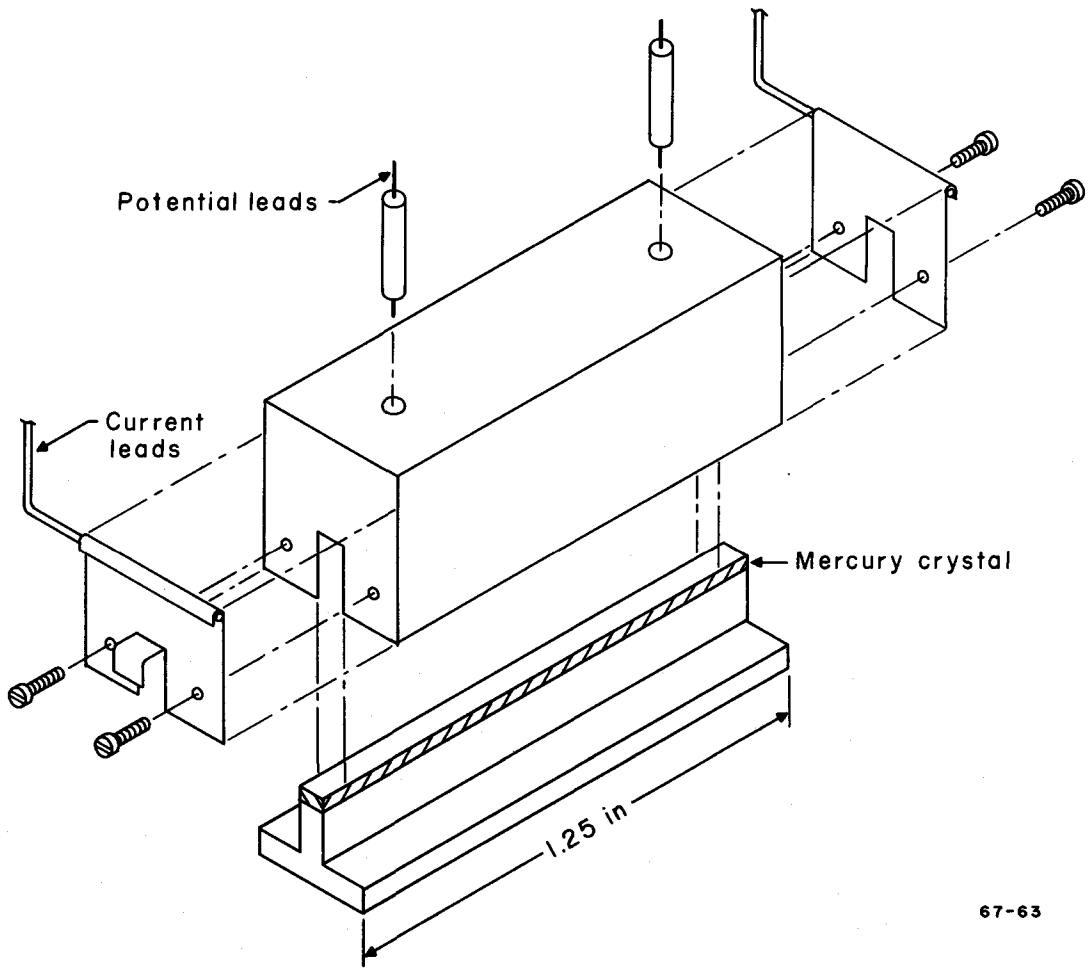

Figure 13. Holder for resistivity measurement at 77°K.

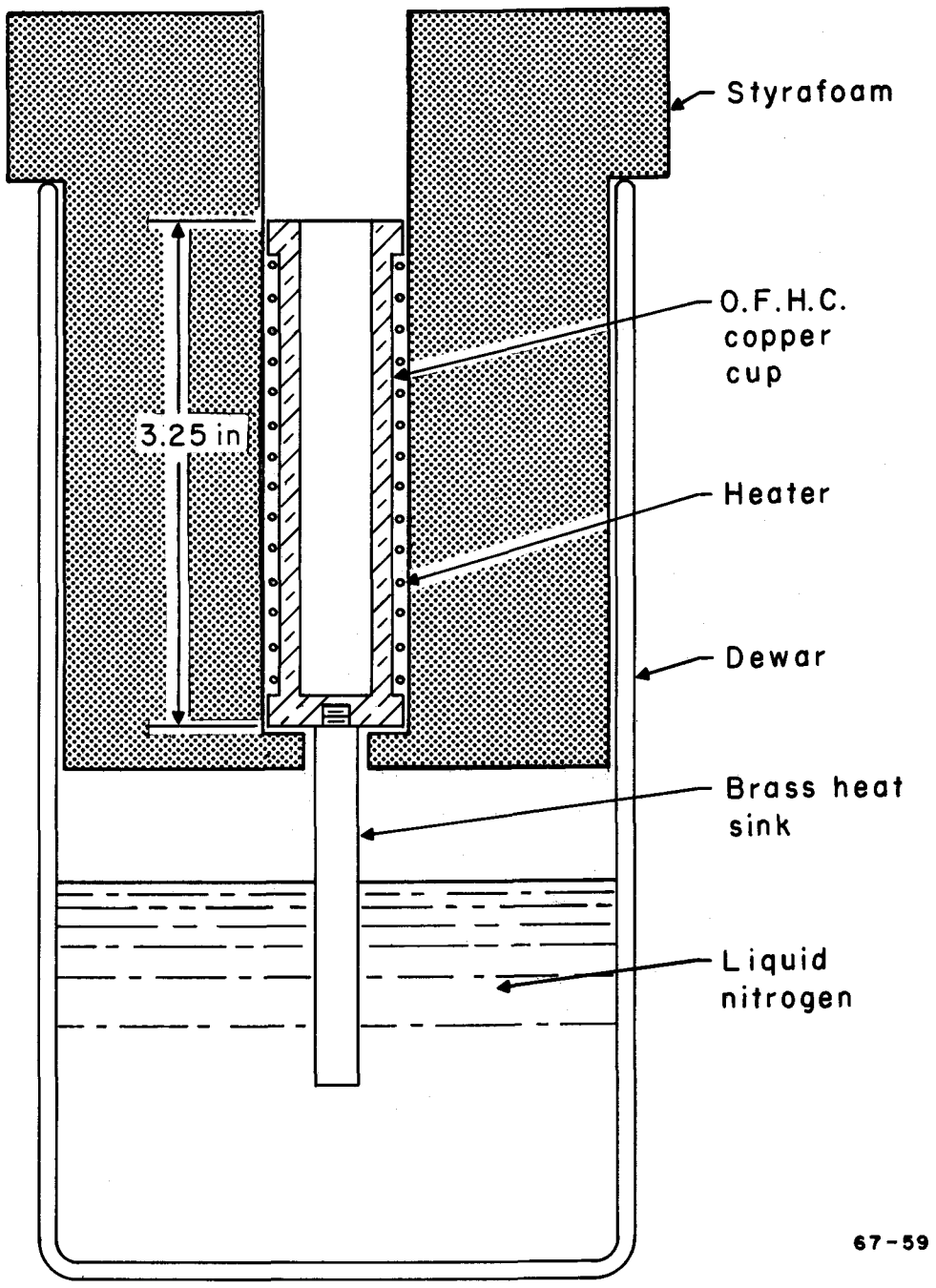

Figure 14. Holder for resistance versus temperature measurement 77°K to 220°K.

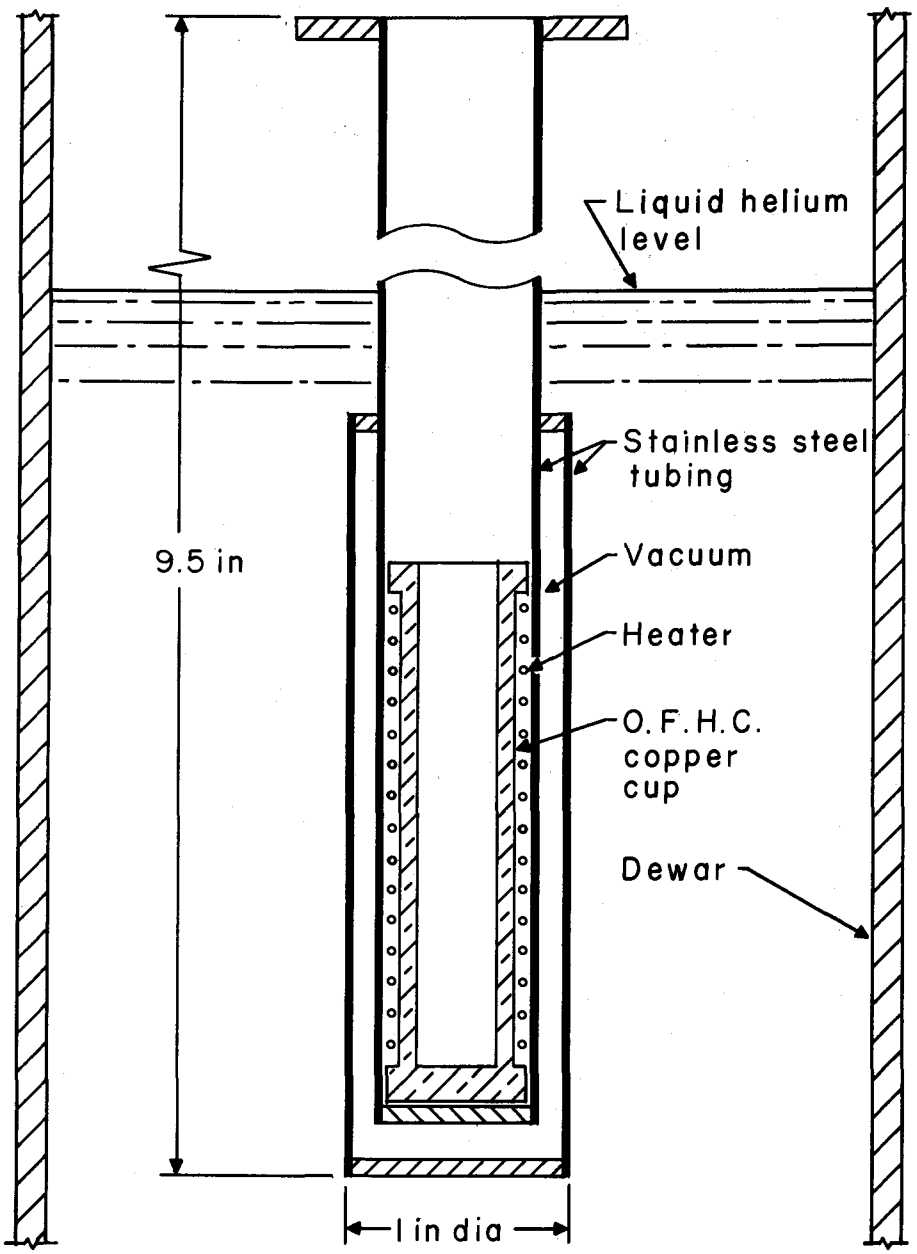

Figure 15. Holder for resistance versus temperature measurement 4.2°K to 40°K.

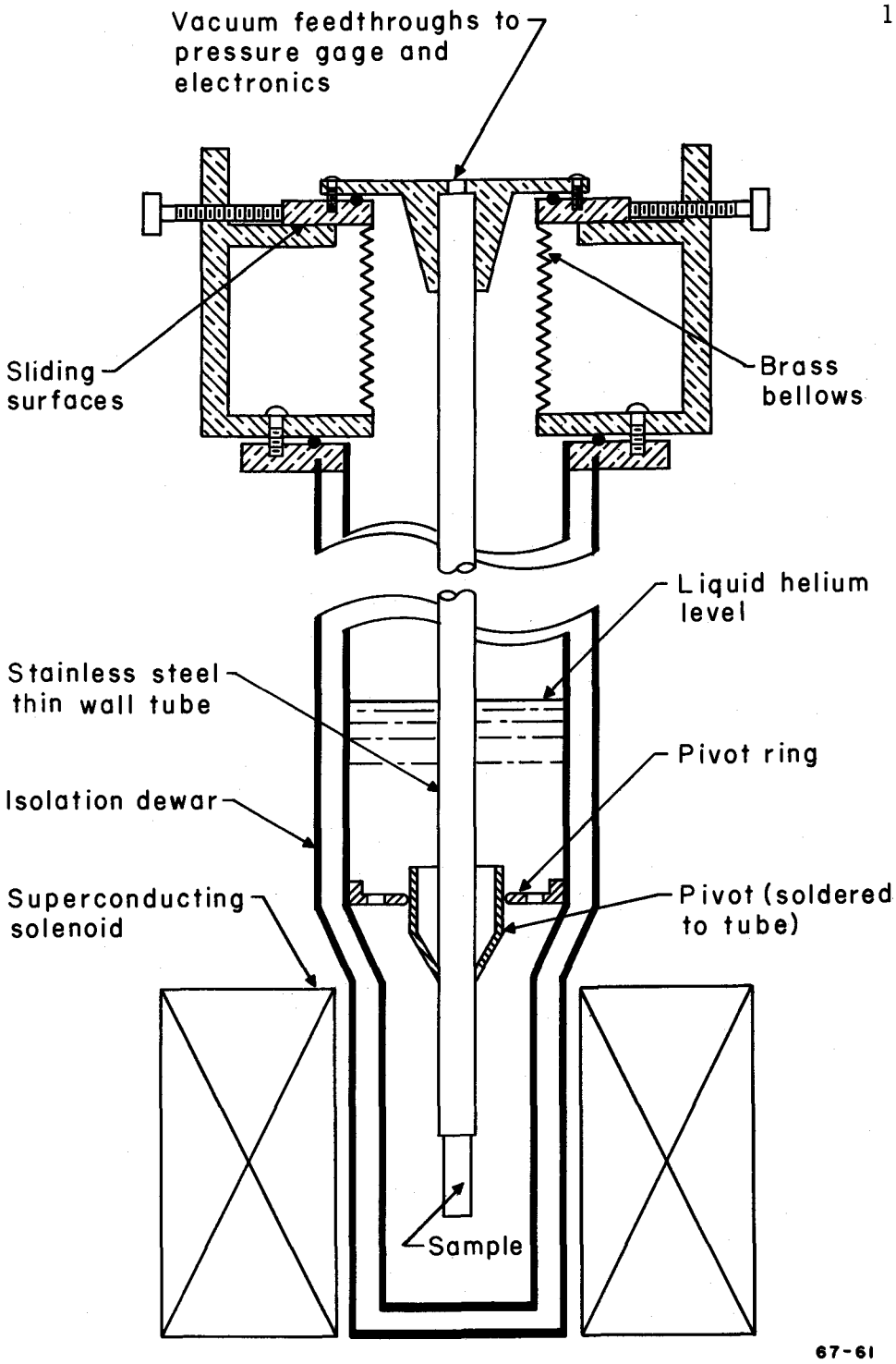

Figure 16. Holder for high field magnetoresistance measurement.

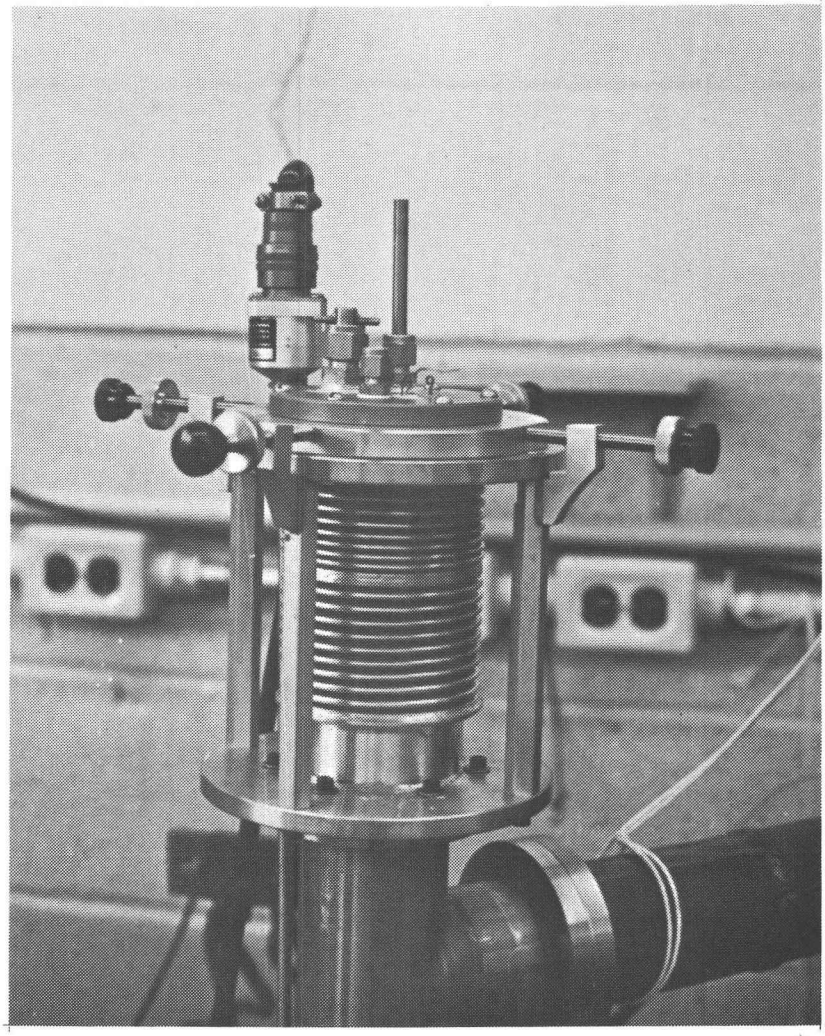

Figure 17. Bellows orienter for high field magnetoresistance measurement.

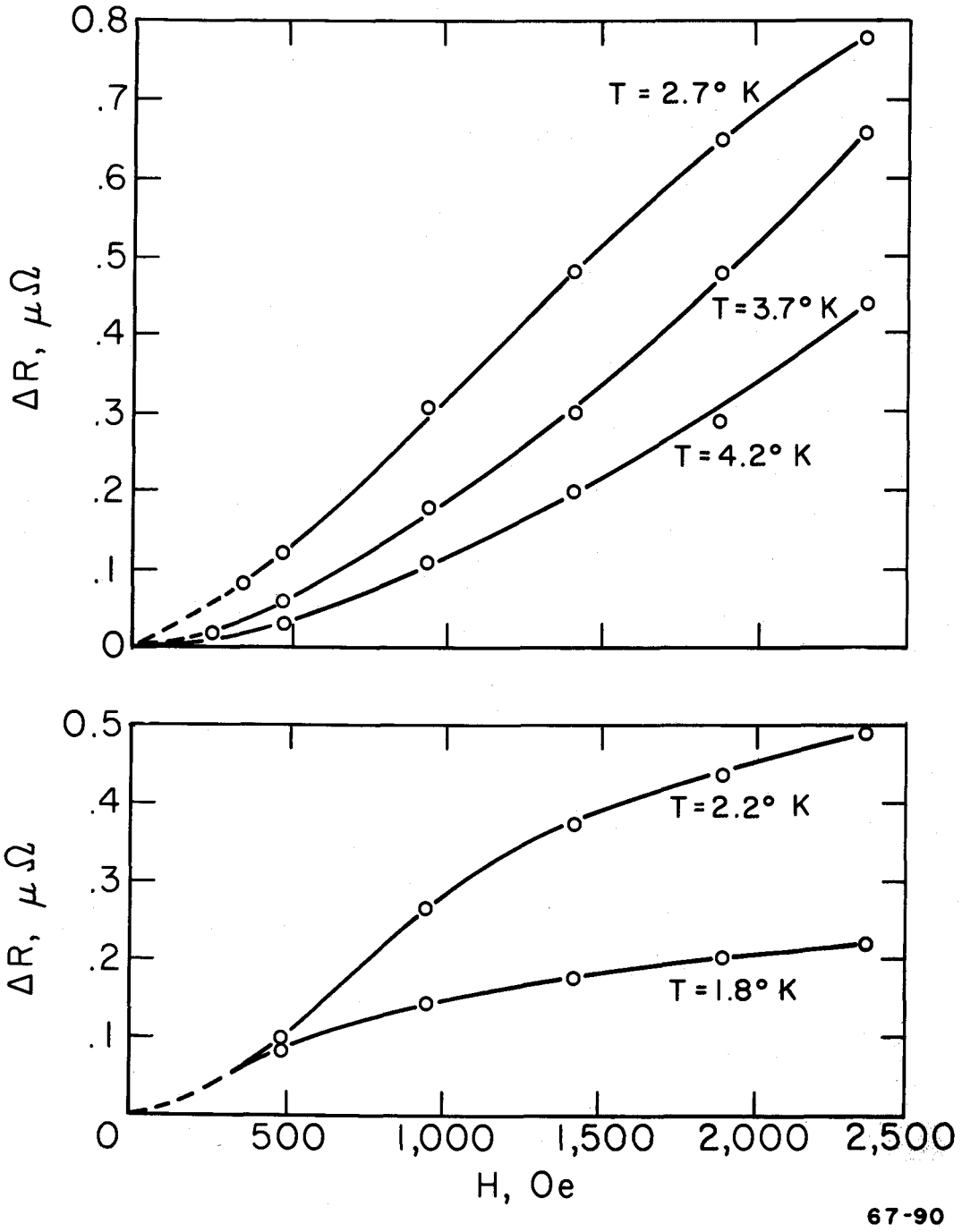

Figure 18. Variation of low field longitudinal magnetoresistance with temperature. Sample No. 83.

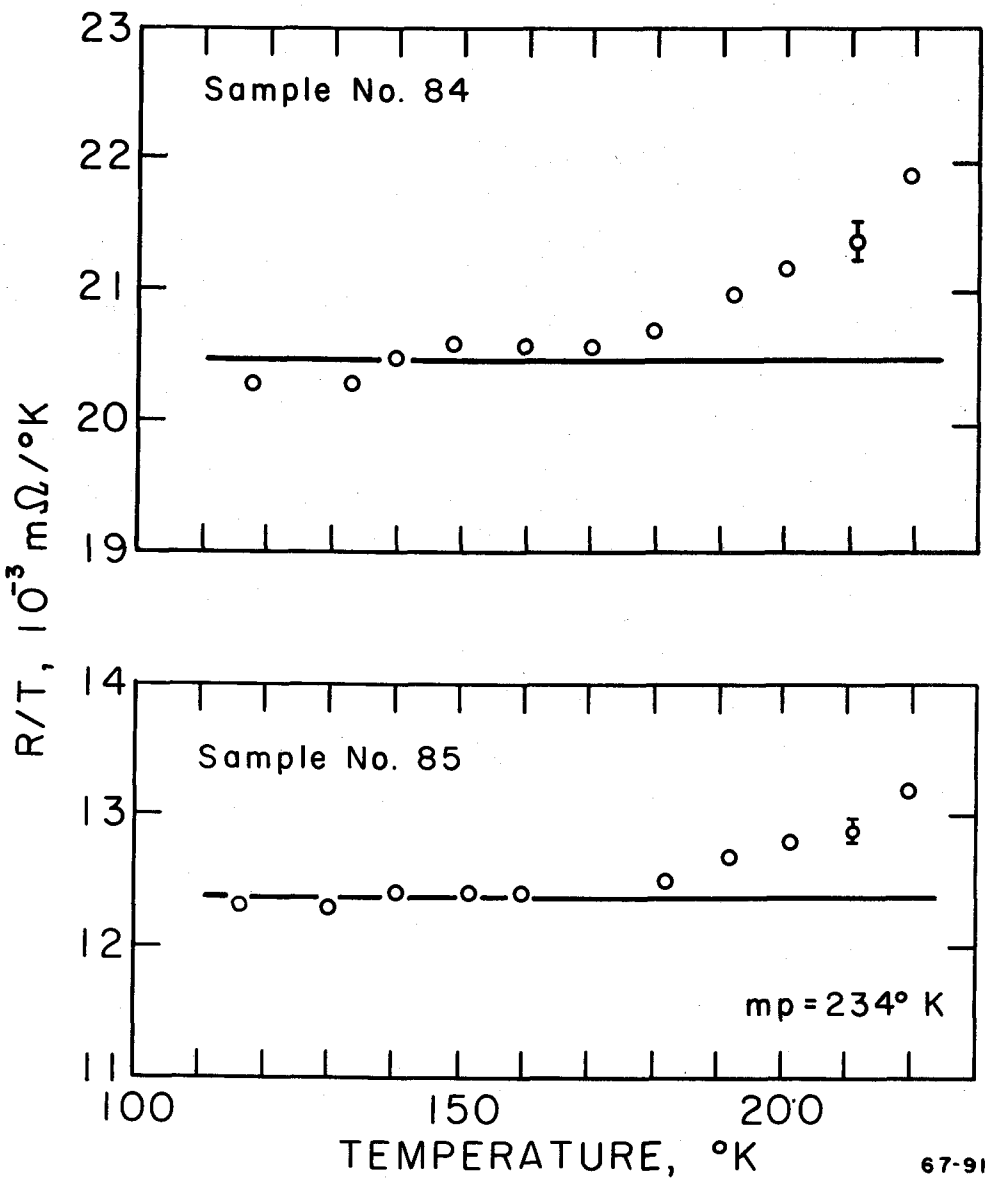

Figure 19. Departure of the resistance from a linear variation with temperature near the melting point.

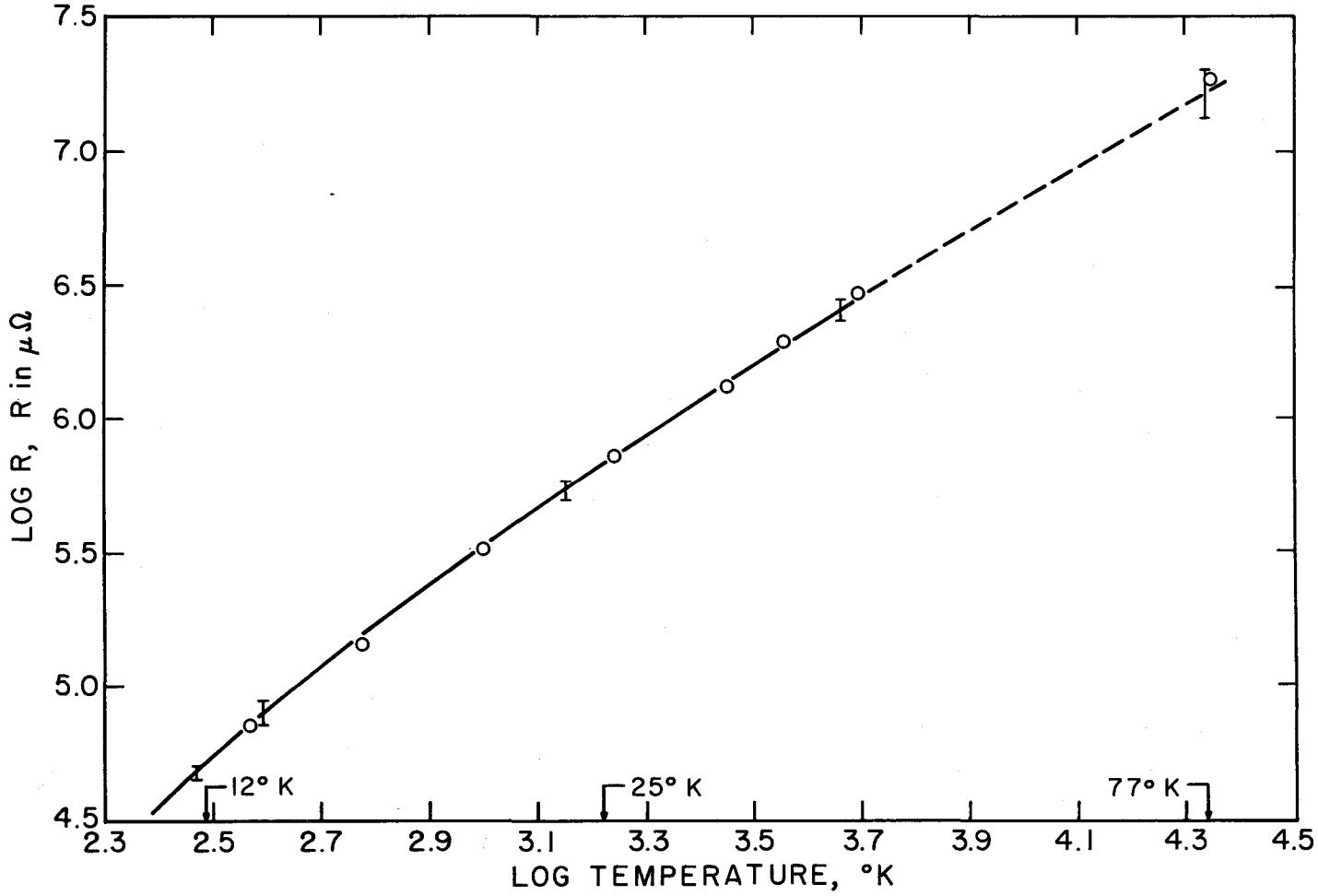

Figure 20. Resistance versus temperature in the range 10°K to 77°K. 67-94X

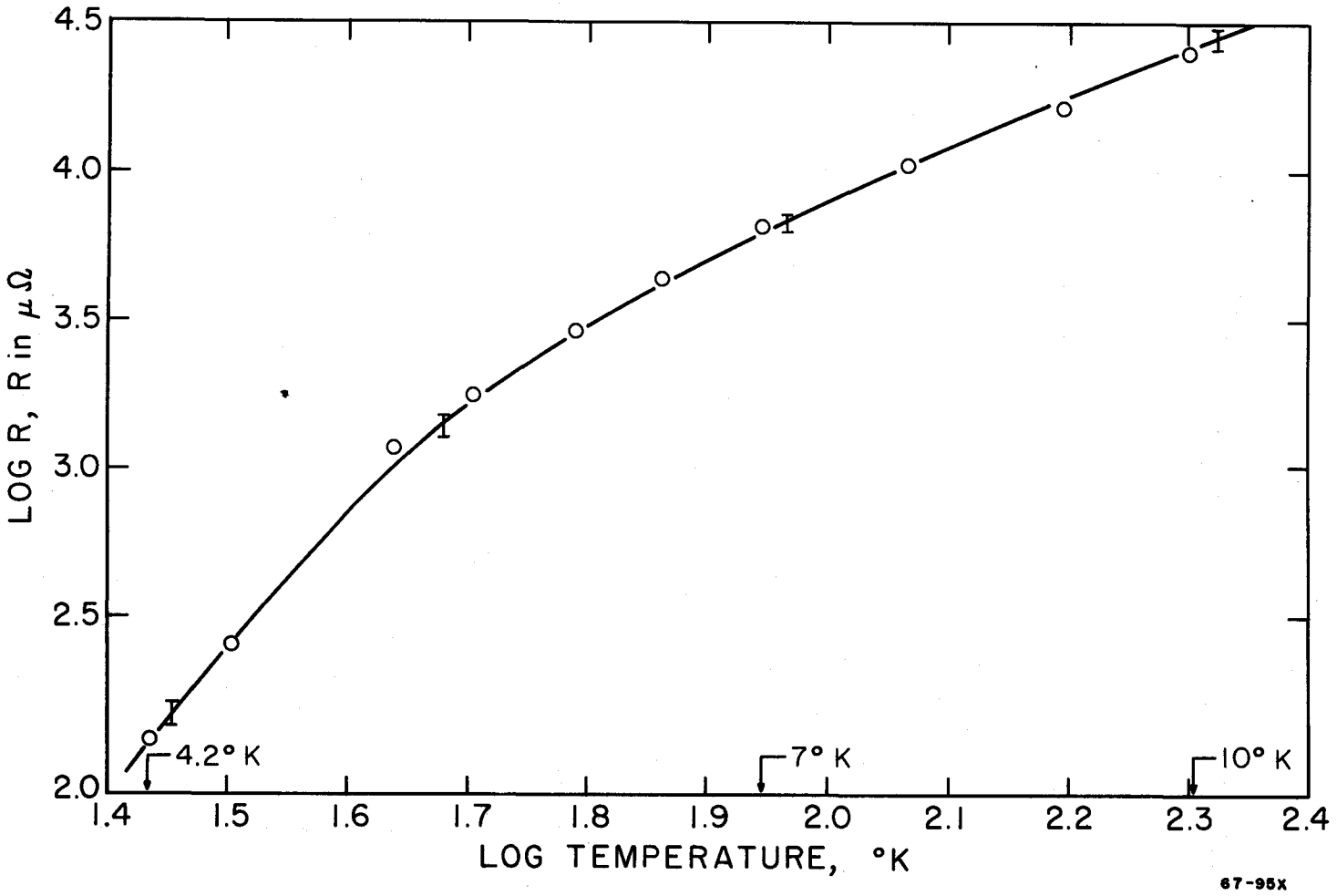

Figure 21. Resistance versus temperature in the range 4.2°K to 10°K.

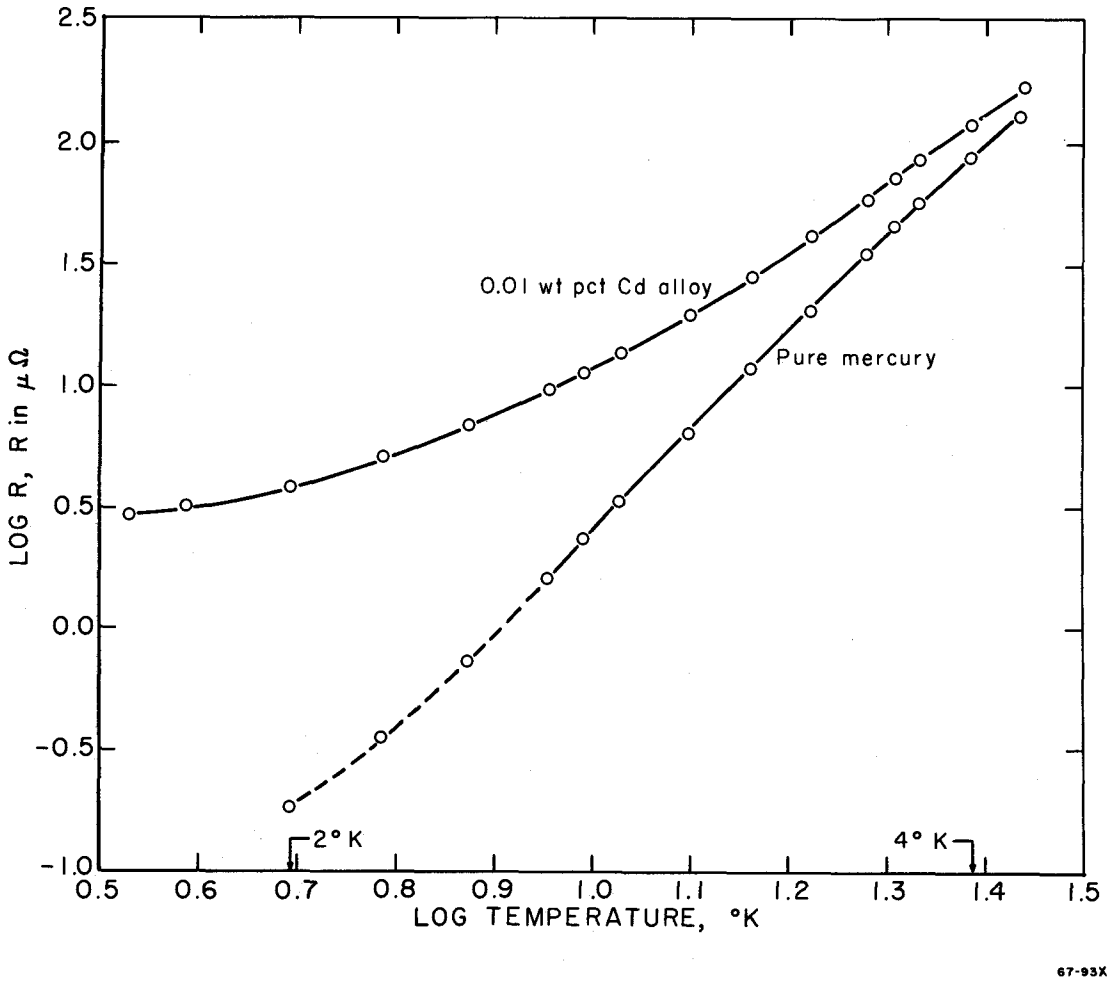

Figure 22. Resistance versus temperature in the range 1.8°K to 4.2°K.

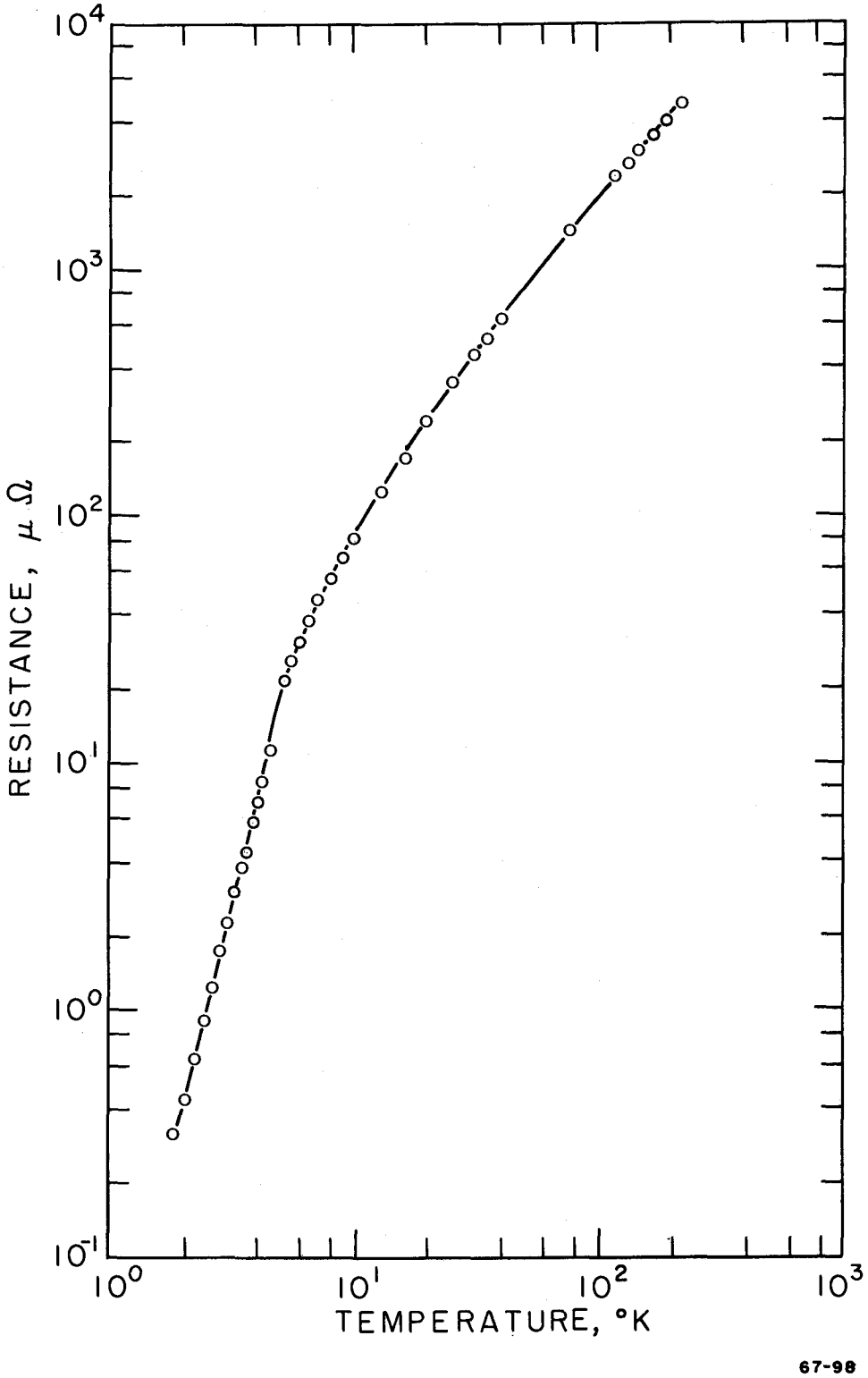

Figure 23. Resistance versus temperature 1.8°K to 220°K. Sample No. 84.

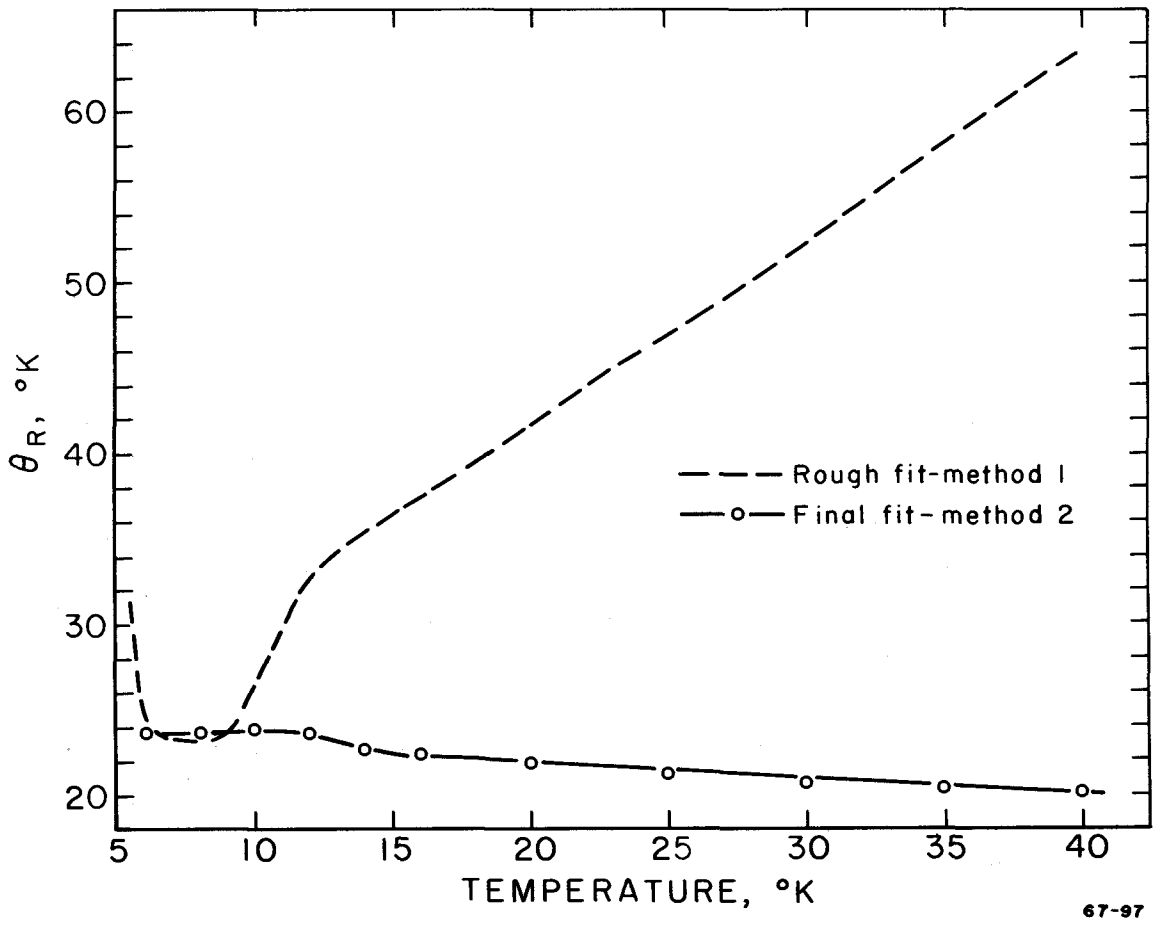

Figure 24. Calculated values of θ_R versus temperature to 40°K.

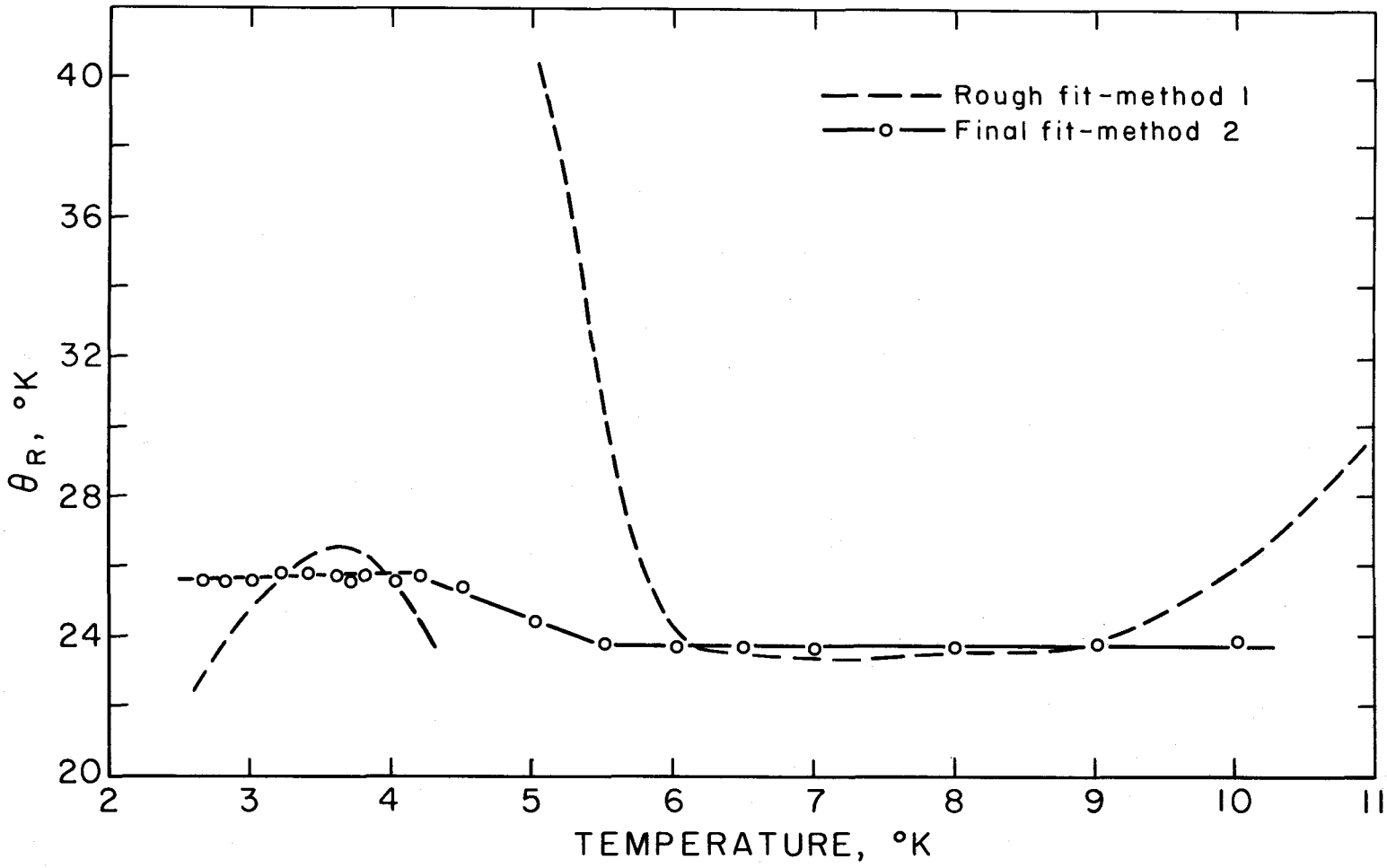

Figure 25. Calculated values of θ_R versus temperature at low temperatures. 67-96

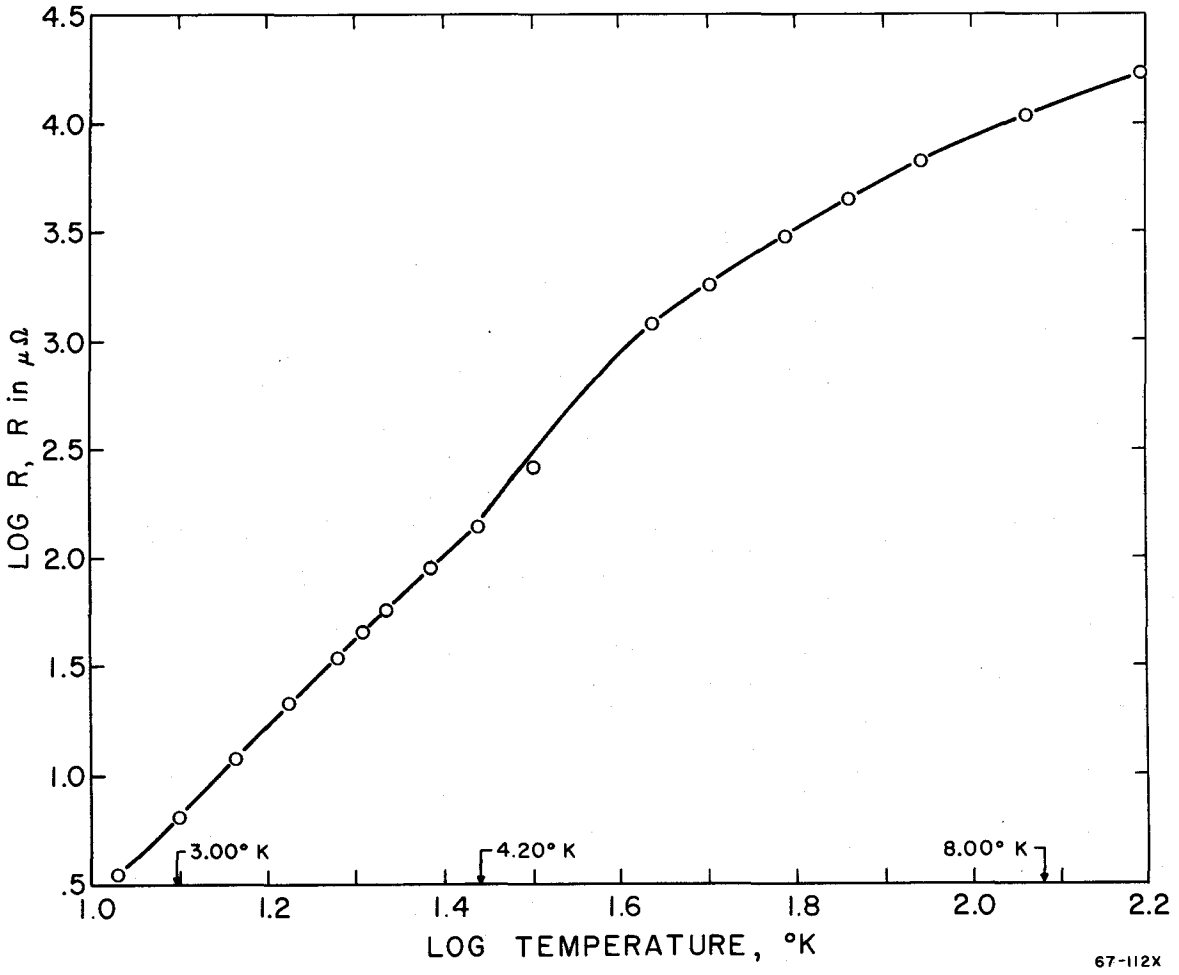

Figure 26. Anomalous change of slope near 4.2°K.

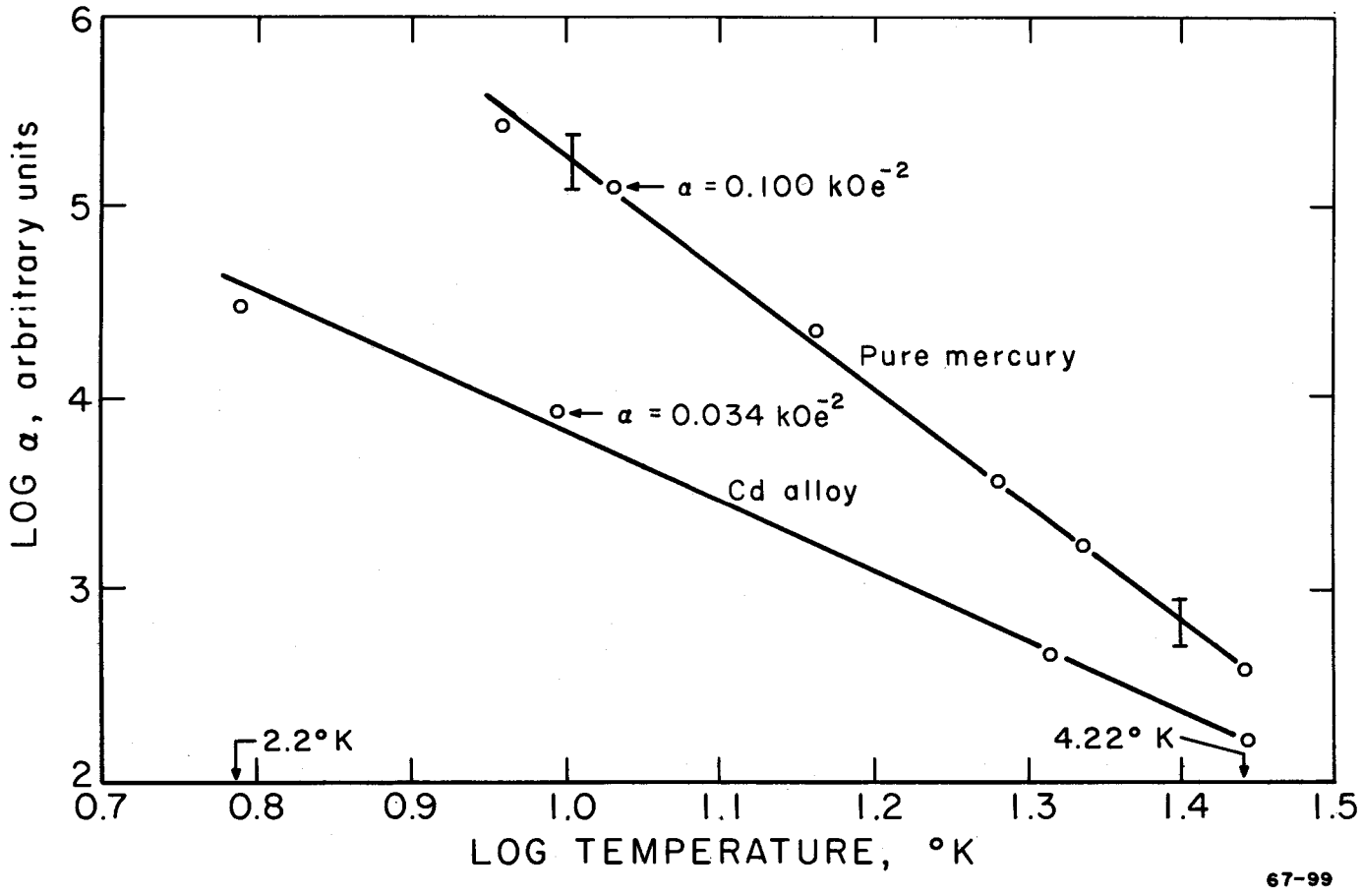

Figure 27. Low field longitudinal magnetoresistance coefficient versus temperature.

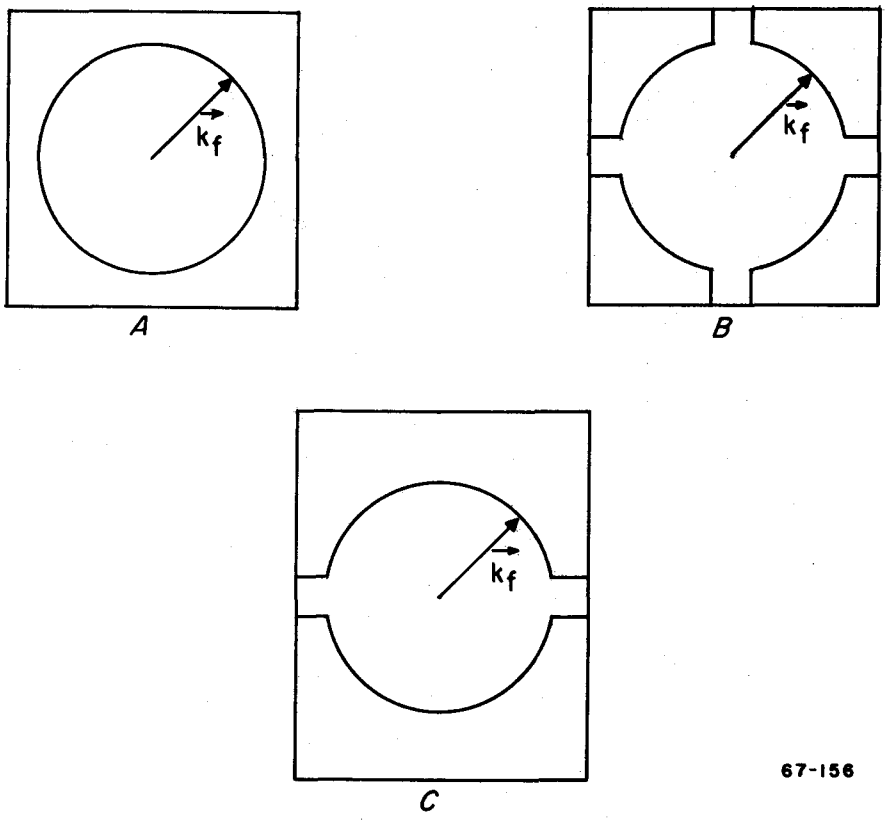

Figure 28. Fermi surface models for monovalent metals.

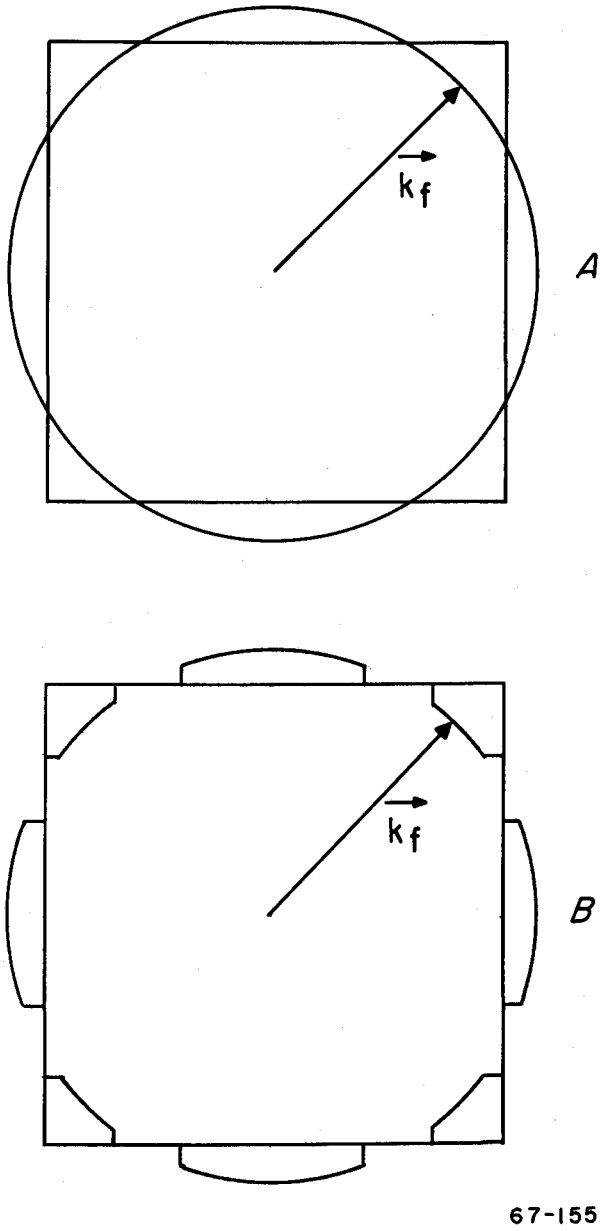

Figure 29. Fermi surface models for divalent metals.

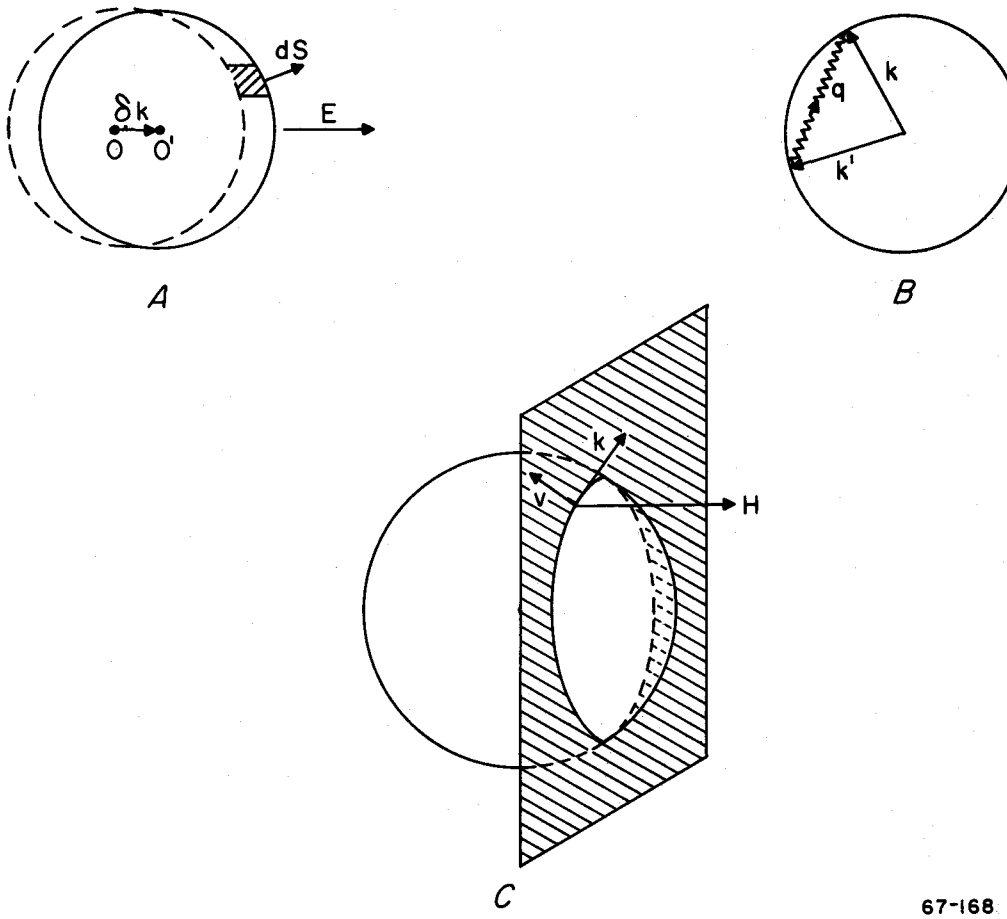

Figure 30. Transport processes on the Fermi surface.

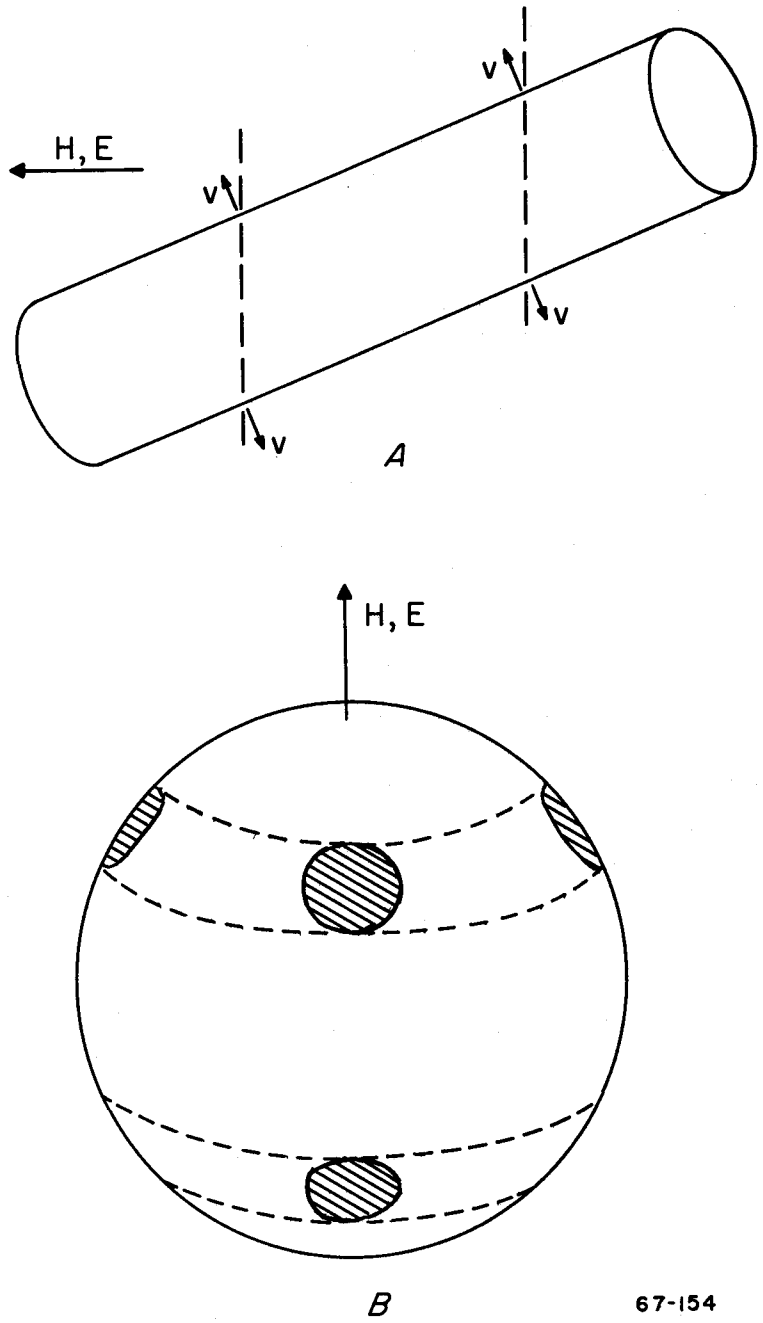

Figure 31. Fermi surface models showing saturation.

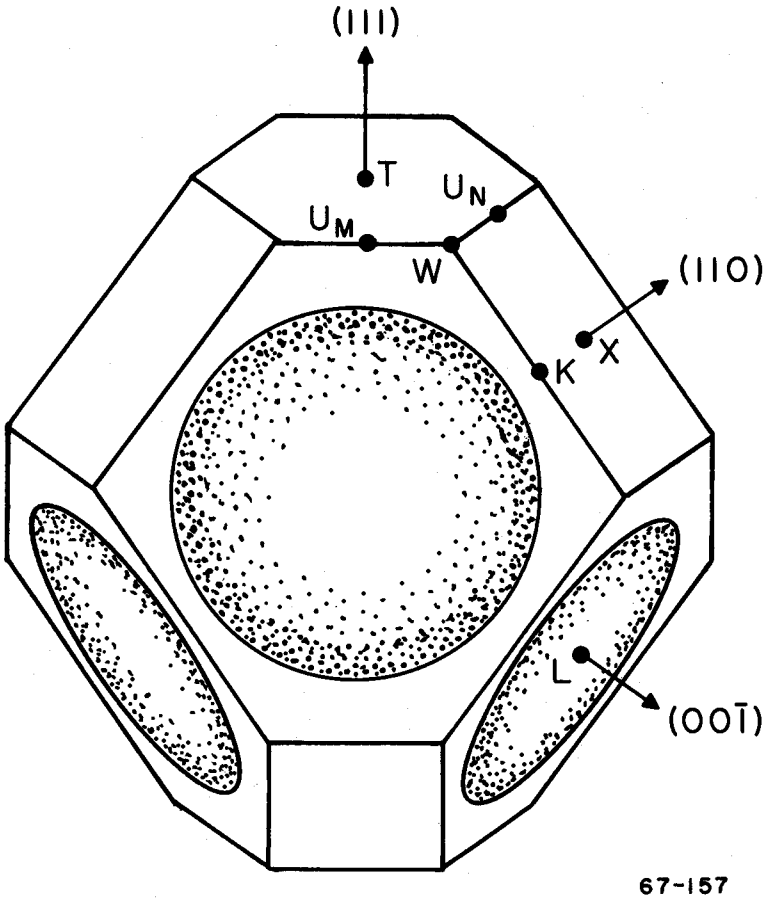

Figure 32. The first Brillouin zone for mercury.

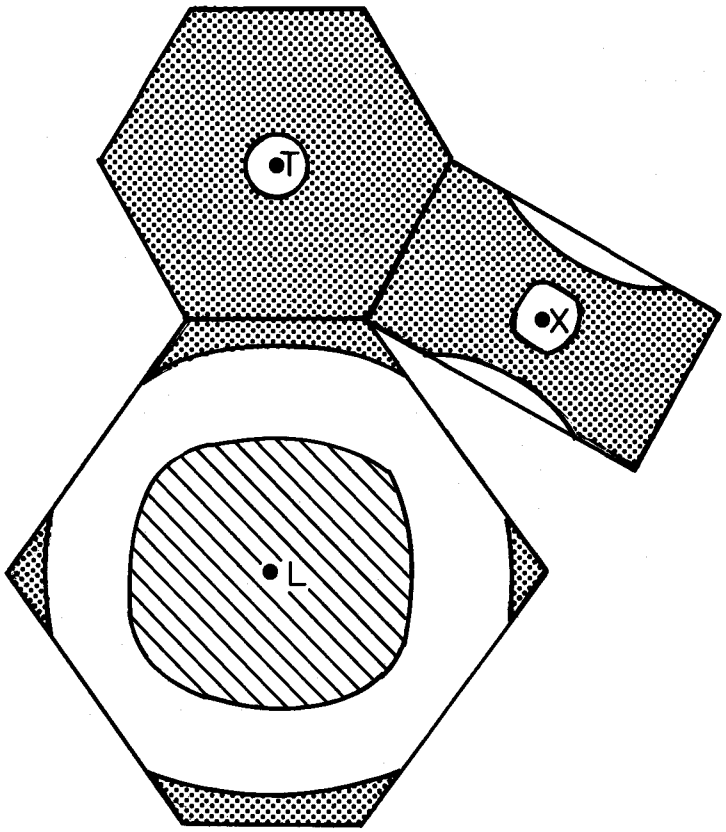

Figure 33. Surface modification by RAPW calculation.

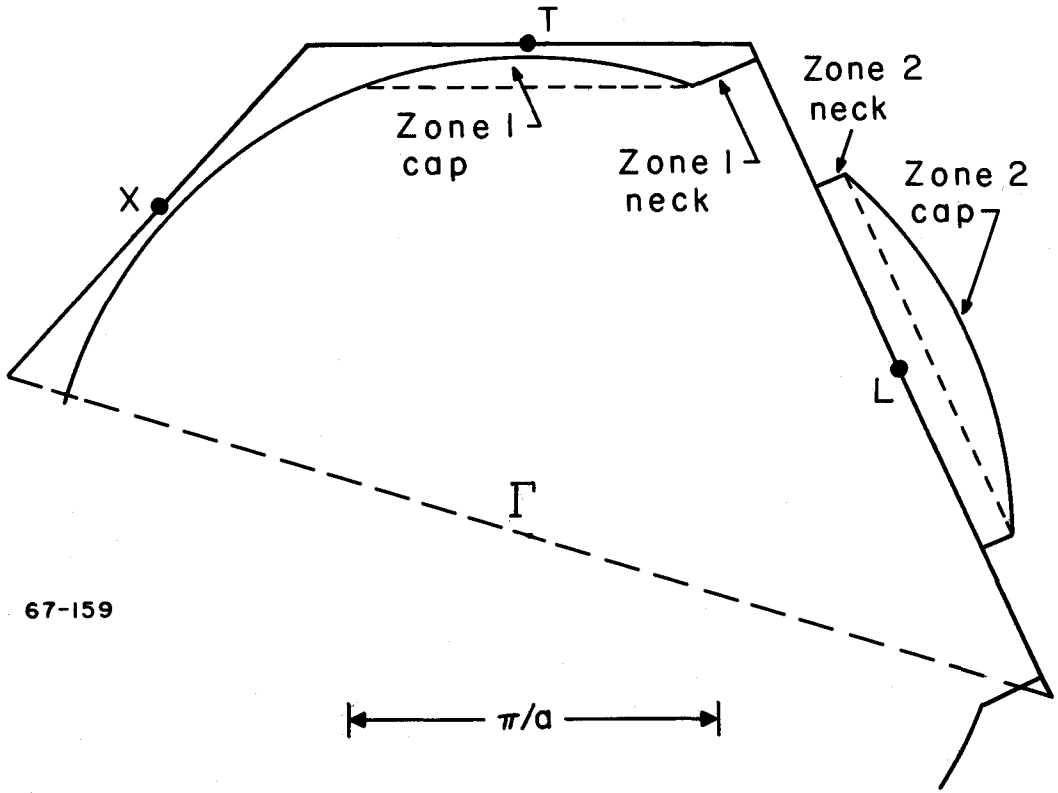

Figure 34. Model used for calculations.

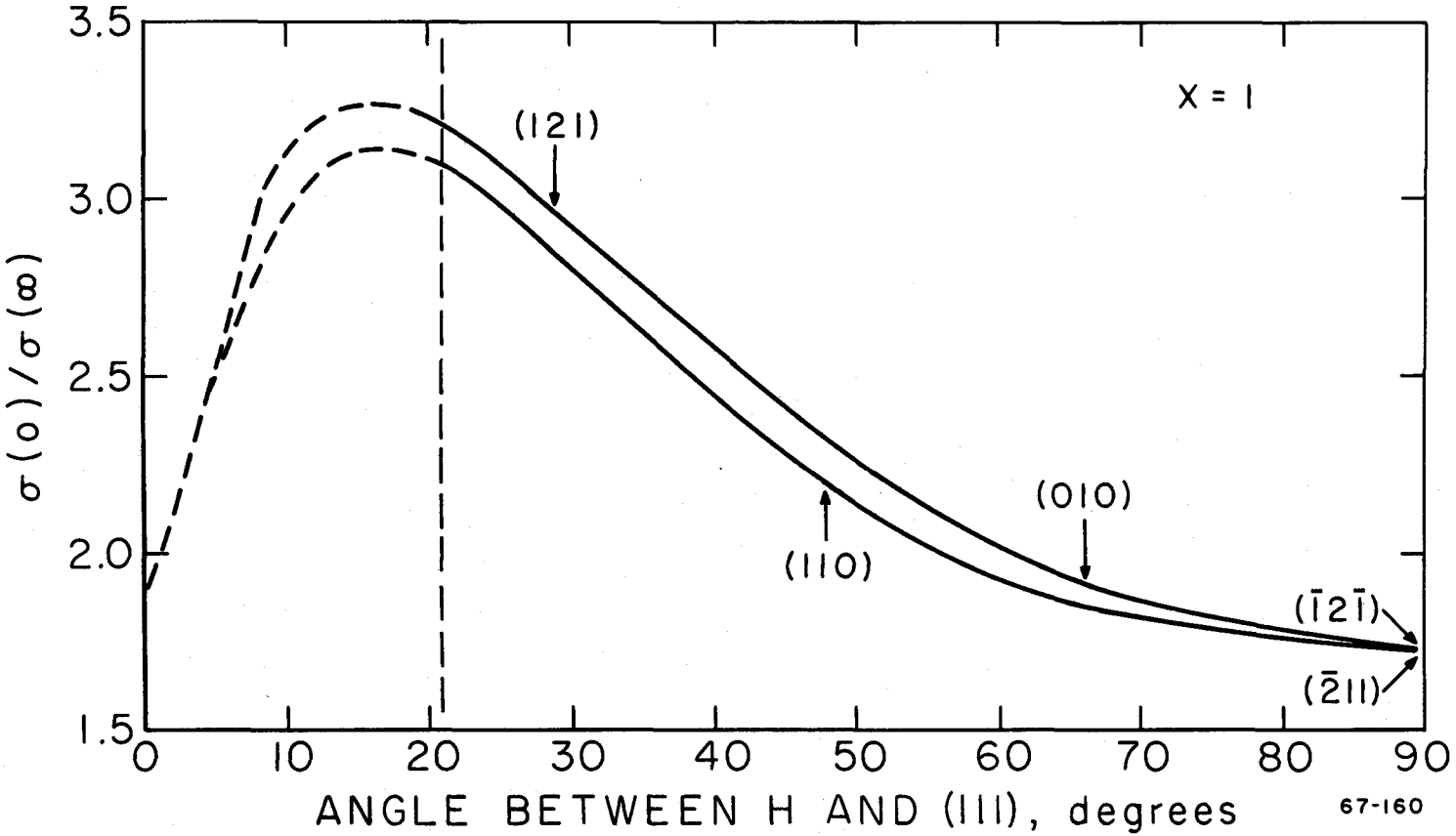

Figure 35. Calculated magnetoresistance for x = 1.

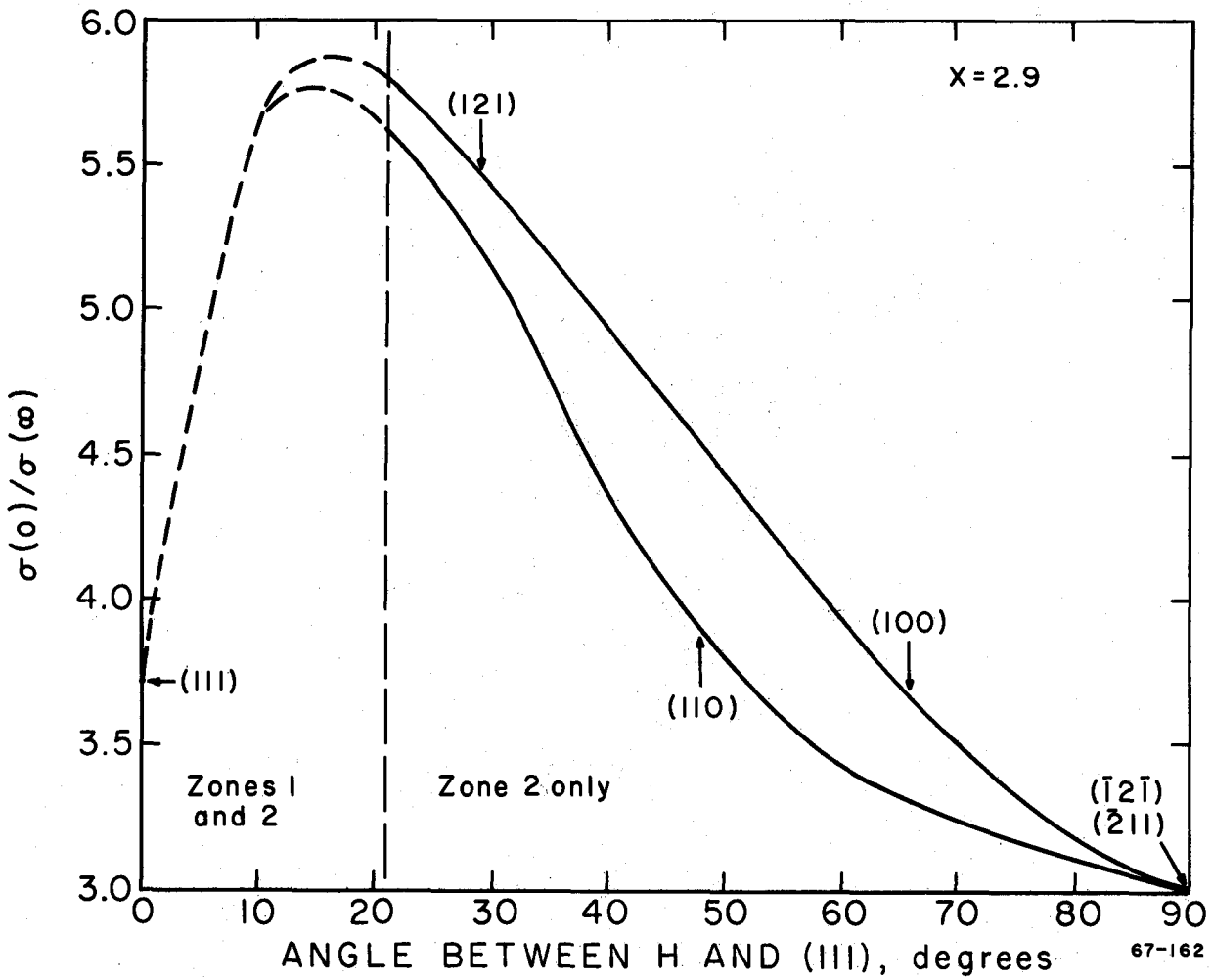

Figure 36. Calculated magnetoresistance for x = 2.9.

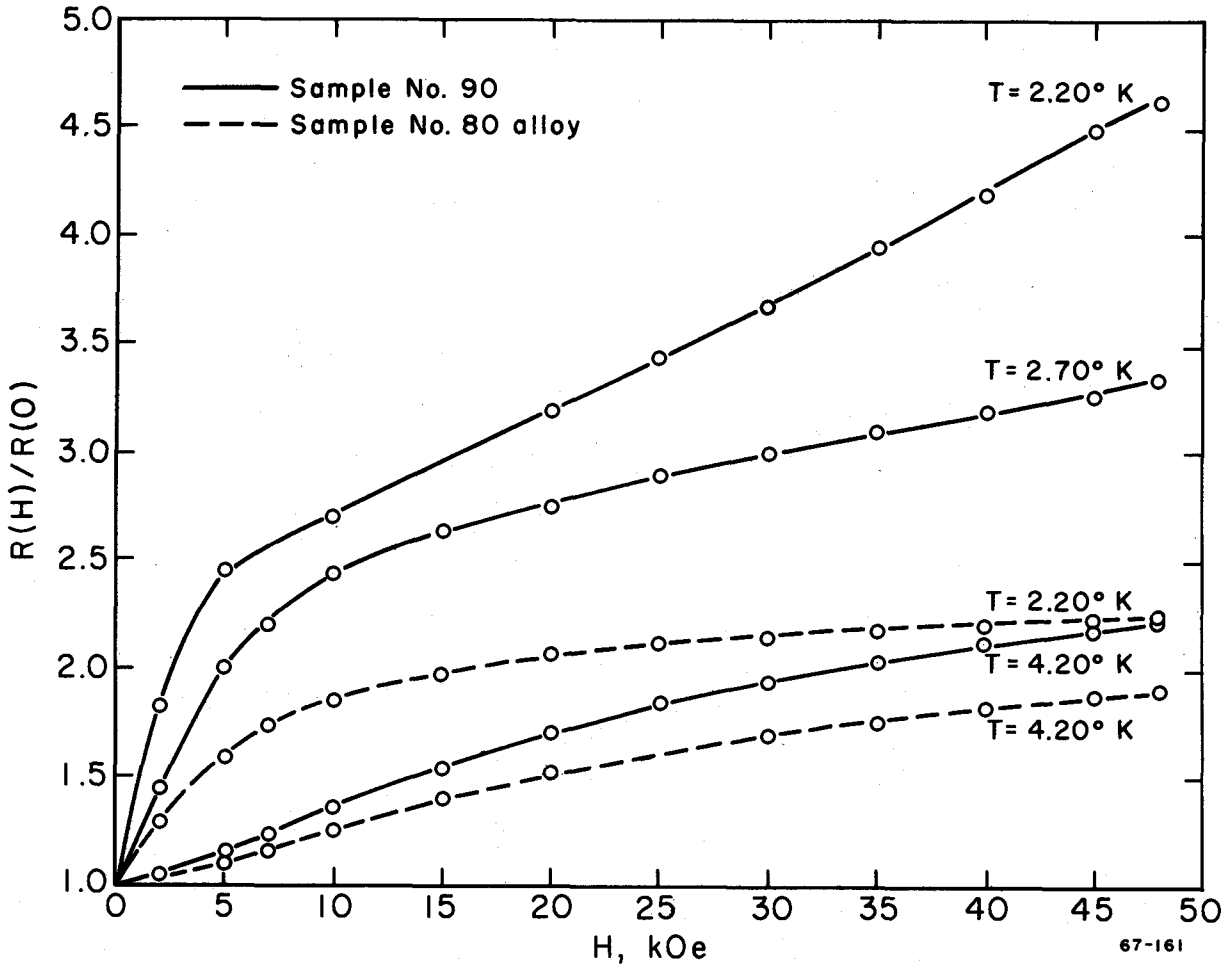

Figure 37. Effect of temperature on the magnetoresistance ratio.

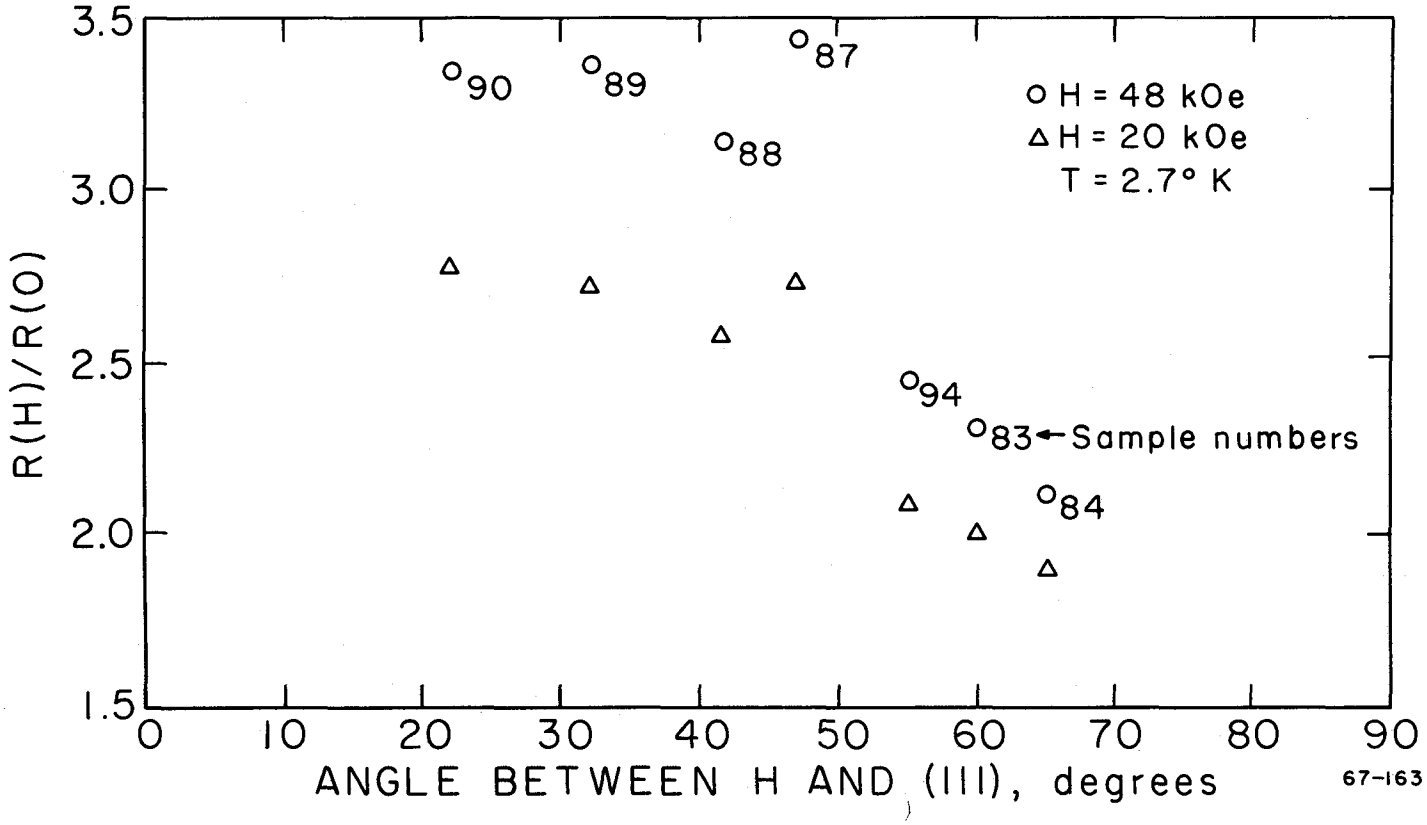

Figure 38. Magnetoresistance ratio versus angle at T = 2.7°K.

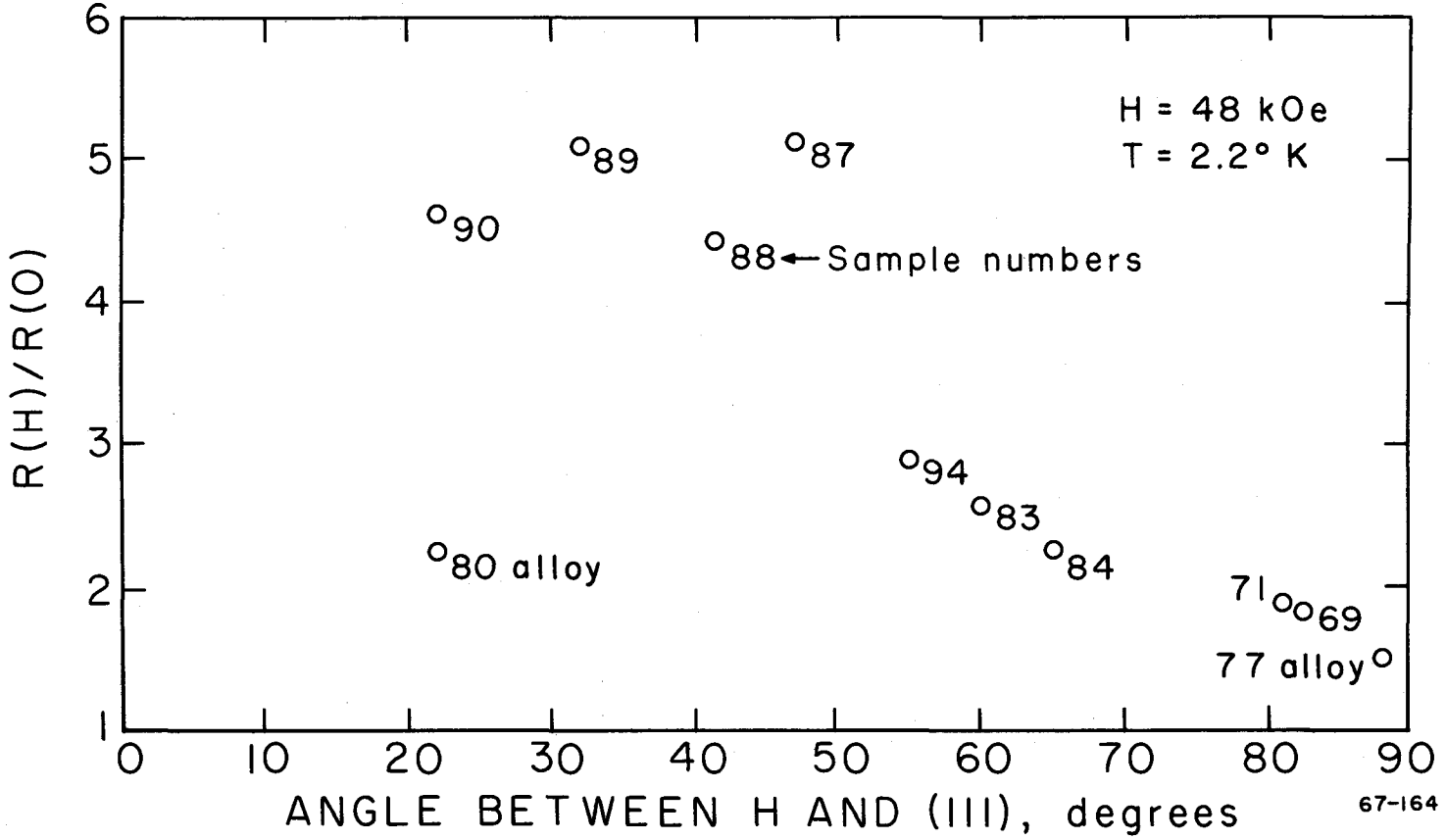

Figure 39. Magnetoresistance ratio versus angle at T = 2.2°K.

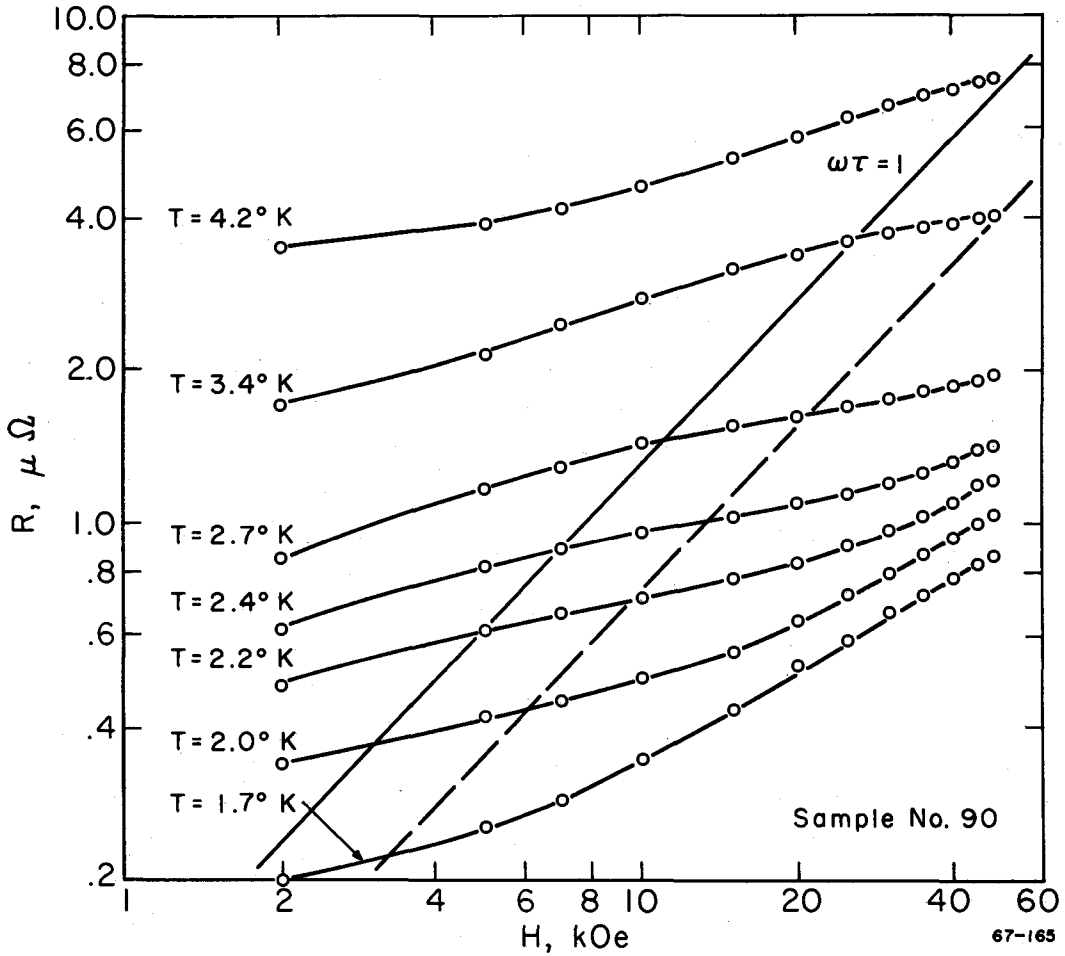

Figure 40. Temperature variation of magnetoresistance. Sample No. 90.

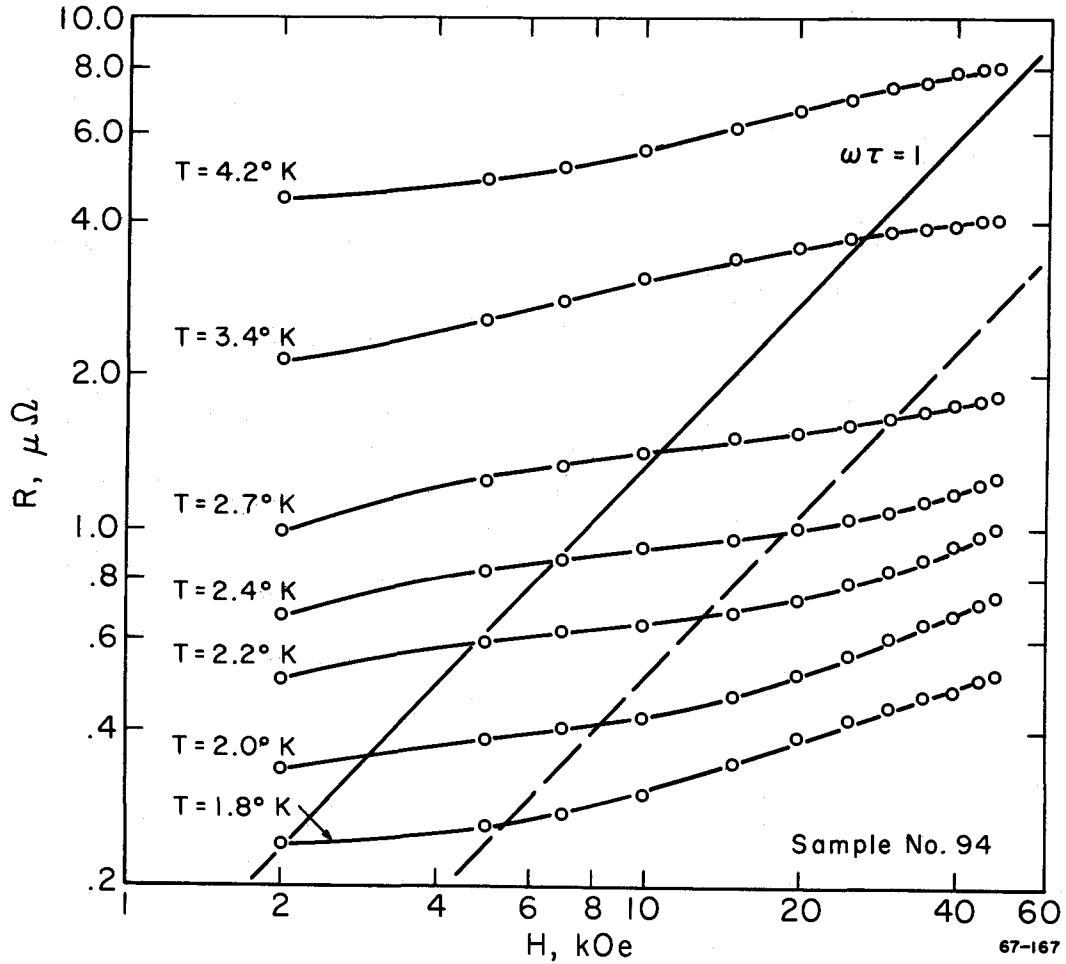

Figure 41. Temperature variation of magnetoresistance. Sample No. 94.

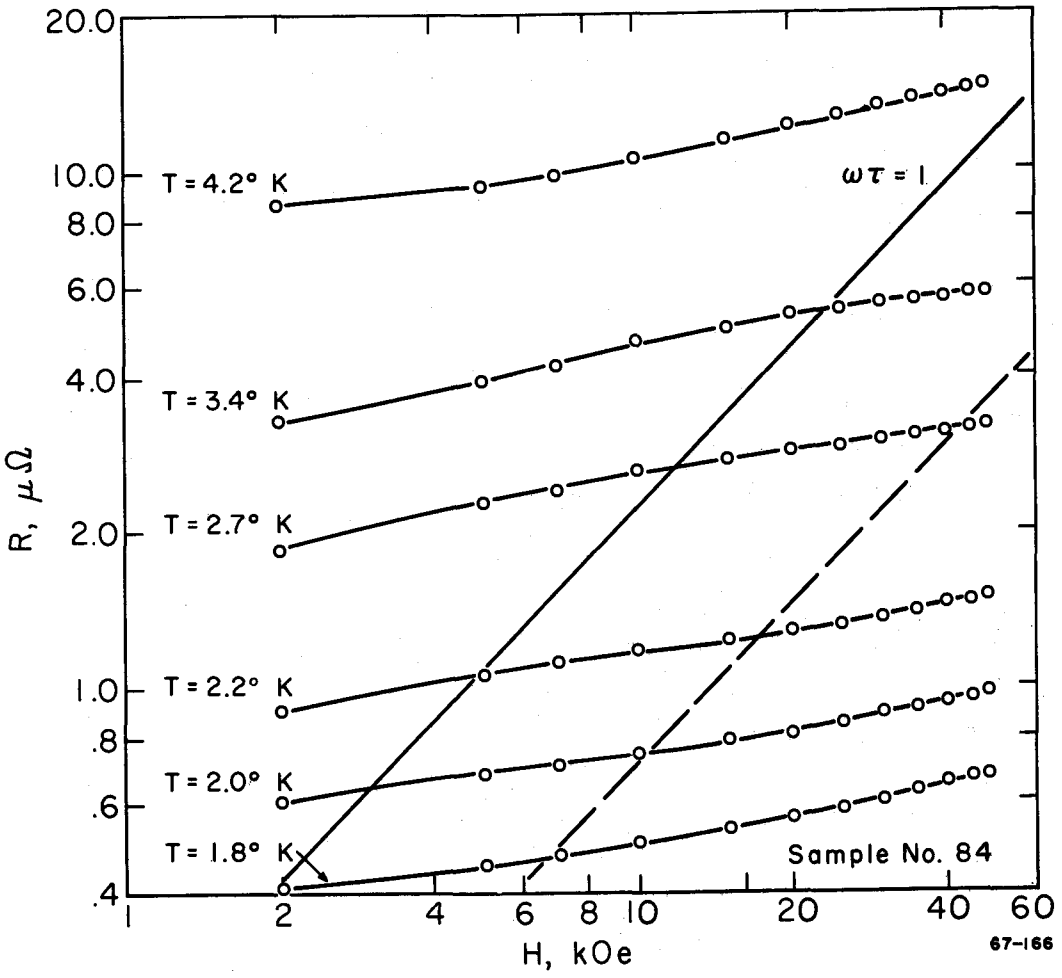

Figure 42. Temperature variation of magnetoresistance. Sample No. 84.

BIBLIOGRAPHY

Aleksandrov, B. N. 1963. Effect of the dimensions and purity on the electrical resistance of metals in a longitudinal magnetic field at He temperature. Soviet Physics JETP 16:871-878. (Translated from Zhurnal Eksperimental'noi i Teoreticheskoi Fiziki)

Aleksandrov, B. N. and I. G. D'Yakov. 1963. Variation of the electrical resistance of pure metals with decrease of temperature. Soviet Physics JETP 16:603-608. (Translated from Zhurnal Eksperimental'noi i Teoreticheskoi Fiziki)

Andrew, E. R. 1949. The size-variation of resistivity for mercury and tin. Proceedings of the Physical Society (London), Ser. A, 62:77-95.

Arko, A. C., J. Cotner and J. Weertman. 1963. Crystallographic angles for alpha mercury. Evanston, Illinois. 22 p. Northwestern Technological Institute. Technical Note No. 1.

Bacon, D. J., F. Heckscher and A. G. Crocker. 1964. Crystallographic angles for Hg, Bi, Sb and As. Acta Crystallographica 17:760.

Barrett, C. S. 1957. The structure of Hg at low temperatures. Acta Crystallographica 10:58-60.

Berlincourt, T. G. 1955. de Haas-van Alphen effect in arsenic. The Physical Review 99:1716-1726.

Boas, W. and J. K. Mackenzie. 1950. Anisotropy in metals. In: Progress in metal physics, ed. by B. Chalmers. Vol. 2. New York, Interscience, p. 90-120.

Brandt, G. B. and J. A. Rayne. 1965. de Haas-van Alphen effect in mercury. Physics Letters 15:18-20.

Brickwedde, F. G., H. Van Dijk, M. Durieux, J. R. Clement, and J. K. Logan. 1960. The 1958 He^4 scale of temperature. Journal of Research of the National Bureau of Standards, Ser. A, 64:1-5.

Bridgman, P. W. 1935. Polymorphism, principally of the elements, up to 50, 000 kg/cm^2. The Physical Review 48:893-906.

Bross, H. and G. Bohn. 1967. Theory of electrical resistivity of polyvalent metals. Physica Status Solidi 20:277-283.

Busey, R. H. and W. F. Giauque. 1953. The heat capacity of mercury from 15 to 330° K. Thermodynamic properties of solid liquid and gas. Heat of fusion and vaporization. Journal of the American Chemical Society 75:806-809.

Chambers, R. G. 1950. The conductivity of thin wires in a magnetic field. Proceedings of the Royal Society (London), Ser. A. 202:378-394.

Chambers, R. G. 1956. Magnetoresistance effects in the group I metals at high fields. Proceedings of the Royal Society (London) Ser. A. 238:344-357.

Condon, J. H. and J. A. Marcus. 1964. Fermi surface of calcium by the de Haas-Van Alphen effect. The Physical Review 134: A446-A452.

Cullity, B. D. 1956. Elements of X-ray diffraction. Reading, Massachusetts, Addison-Wesley. 514 p.

Datars, W. R. and A. E. Dixon. 1967. Magnetoresistance of crystalline mercury. The Physical Review 154:576-583.

Dingle, R. B. 1950. The electrical conductivity of thin wires. Proceedings of the Royal Society (London), Ser. A. 201:545-560.

Dishman, J. M. and J. A. Rayne. 1966. Transverse magnetoresistance of mercury. Physics Letters 20:348-349.

Dugdale, J. S. and Z. S. Basinski. 1967. Mathiessen's rule and anisotropic relaxation times. The Physical Review 157:552-560.

Fate, W. A. and R. W. Shaw. 1967. Amplitude-Independent ultrasonic attenuation in superconducting lead. Physical Review Letters 19:230-233.

Finnemore, D. K., D. E. Mapother and R. W. Shaw. 1960. Critical field curve of superconducting Hg. The Physical Review 118: 127-129.

Gorkun, Yu. I. 1961. Concerning the effect of current electrodes on the resistivity change in a magnetic field. Soviet Physics - Solid State 3:173-177. (Translated from Fizika Tverdogo Tela)

Grüneisen, E. 1945. Electrische Leitfahigkeit der Metalle bei tiefen Temperaturen. Ergebnisse der exakten Naturwissenschaften 21:50-166.

Gurzhi, R. N. 1965. Some features of the electrical conductivity of metals at low temperatures. Soviet Physics JETP 20:953-960. (Translated from Zhurnal Eksperimental'noi i Teoreticheskoi Fiziki)

Haas, W. J. de, G. J. Sizoo and H. K. Onnes. 1926. Measurements of the magnetic disturbance of the supraconductivity with mercury. Communications from the Physical Laboratory of the University of Leiden 16(180d):55-103.

Harrison, W. A. 1960. Electronic structure of polyvalent metals. The Physical Review 118:1190-1208.

Hasegawa, A. 1964. Effect of pressure on the electrical conductivity of alkali metals. Journal of the Physical Society of Japan 19:504-516.

Hoare, F. E. and J. E. Zimmerman. 1959. Helium temperatures from vapor pressure measurements. The Review of Scientific Instruments 30:184-186.

Jones, H. 1956. Theory of electrical and thermal conductivity in metals. In: Handbuch der Physik, ed. by S. Flugge. Vol. 19. Berlin, Springer-Verlag. p. 227-315.

Jones, H. and C. Zener. 1934. A general proof of certain fundamental equations in the theory of metallic conduction. Proceedings of the Royal Society (London), Ser. A. 144:101-117.

Juretschke, H. J. 1955. Symmetry of galvanomagnetic effects in antimony. Acta Crystallographica 8:716-722.

Justi, E. and K. Auch. 1963. Anderung des electrischen Widerstandes von Kalium bei 4, 2° K in gepulsten magnetischen longitudinalfeldern bis 110 kG. Zeitschrift Fur Naturforshung, Ser. A 18:767-768.

Justi, E. and J. Kramer. 1940. Galvanomagnetische Versuche uber den elktrischen Leitungsmechanismus des Bariums. Physikalische Zeitschrift 41:197-202.

Kao, L. and E. Katz. 1958. Phenomenological theory of anisotropic isothermal galvanomagnetic effects. Journal of the Physics and Chemistry of Solids 6:223-235.

Keeton, S. C. and T. L. Loucks. 1966. Electronic structure of mercury. The Physical Review 152:548-555.

Kelly, F. M. and D. K. C. MacDonald. 1953. On θ values in metals. Canadian Journal of Physics 31:147-164.

Kohler, M. 1938. Transversale und longitudinale Widerstandsanderung von Zweiwertigan Metallen Kubischraum Zentrierter Kristallstruktur. Physikalische Zeitschrift 39:9-23.

Lifshitz, J. M., M. I. Azbel' and M. I. Kaganov. 1957. The theory of galvanomagnetic effects in metals. Soviet Physics JETP 35:875-883. (Translated from Ahurnal Eksperimental'noi i Teoreticheskoi Fiziki)

Lifshitz, J. M. and V. G. Peschanski. 1959. Galvanomagnetic characteristics of metals with open Fermi surfaces. I. Soviet Physics JETP 35:875-883. (Translated from Zhurnal Eksperimental'noi i teoreticheskoi Fiziki)

Loucks, T. L. 1967. Augmented plane wave method. New York, Benjamin. 256 p.

MacDonald, D. K. C. Self-diffusion in the alkali metals. Journal of Chemical Physics 21:177-178.

Meaden, G. T. 1965. Electrical resistance of metals. New York, Plenum. 218 p.

Mott, N. F. and H. Jones. 1958. The theory of the properties of metals and alloys. New York, Dover. 326 p.

Newbower, R. S. and J. E. Neighbor. 1967. Anomalous resistance of pure gallium near 1.7° K. Physical Review Letters 18:538-540.

Onnes, H. K. and G. Holst. 1915. On the electrical resistance of pure metals, etc. IX. The resistance of mercury, tin, cadmium, constantin and manganese down to temperatures obtainable with liquid hydrogen and with liquid helium at its boiling point. Communications from the Physical Laboratory of the University of Leiden 13(142z):1-9.

Pearson, W. B. 1958. A handbook of lattice spacings and structures of metals and alloys. New York, Pergamon. 1038 p.

Pines, D. 1964. Elementary exitations in solids. New York, Benjamin. 299 p.

Pippard, A. B. 1947. The surface impedance of superconductors and normal metals at high frequencies. Proceedings of the Royal Society (London), Ser. A. 191:370-415.

Pippard, A. B. 1964. Longitudinal magnetoresistance. Proceedings of the Royal Society (London), Ser. A. 282:464-484.

Pippard, A. B. 1965. The dynamics of conduction electrons. New York, Blackie. 150 p.

Powell, R. L. 1966. Longitudinal magnetoresistance of copper. Boulder, Colorado. Various paging. (U. S. National Bureau of Standards Report No. 9176).

Putley, E. H. 1960. The Hall effect and related phenomena. London, Butterworths. 263 p.

Reuter, G. E. H. and E. H. Sondheimer. 1948. The theory of the anomalous skin effect in metals. Proceedings of the Royal Society (London), Ser. A. 195:336-364.

Rosenberg, H. M. 1963. Low temperature solid state physics--some selected topics. Oxford, Clarendon Press. 420 p.

Schriber, J. E. and C. A. Swenson. 1961. Superconductivity of α and β mercury. The Physical Review 123:1115-1122.

Schriber, J. E. and C. A. Swenson. 1962. The nature of the α-β transition in mercury. Acta Metallurgica 10:511-513.

Sckell, O. 1930. Die Anisotropie des electrischen Widerstandes von Quecksilberkristallen. Annalen der Physik (Leipzig) 6:932-956.

Slater, H. C. 1965. Quantum theory of molecules and solids. New York, McGraw-Hill. 563 p.

Smith, A. C., J. F. Janak and R. B. Adler. 1967. Electronic conduction in solids. New York, McGraw-Hill. 342 p.

Smith, P. L. and N. M. Wolcott. 1956. The specific heats of cadmium and mercury. Philosophical Magazine 1:854-865.

Sondheimer, E. H. 1950. The theory of the transport phenomena in metals. Proceedings of the Royal Society (London), Ser. A. 203:75-98.

Sondheimer, E. H. 1952. The mean free path of electrons in metals. Advances in Physics 1:1-42.

White, G. K. 1961. Experimental techniques in low-temperature physics. Oxford, Clarendon Press. 328 p.

White, G. K. and S. B. Woods. 1958. The thermal and electrical resistivity of bismuth and antimony at low temperatures. Philosophical Magazine 3:342-359.

Wilson, A. H. 1938. Electrical conductivity of the transition metals. Proceedings of the Royal Society (London), Ser. A. 167:580-593.

Wilson, A. H. 1965. The theory of metals. 2nd ed. Cambridge, University. 346 p.

Wycoff, R. W. G. 1963. Crystal structures. Vol. 1. New York, Interscience. 467 p.

Ziman, J. M. 1962. Electrons in metals. London. Taylor and Francis. 80 p.

Ziman, J. M. 1960. Electrons and phonons. Oxford, Clarendon. 554 p.

APPENDICES

APPENDIX A

The table on the following page contains information on each of the samples used in the course of the experiment. Detailed explanations of the symbols used are to be found in the main text. A brief explanation is given here.

Term	Explanation
A	Nominal cross section expressed as (width) x (thickness). Both dimensions are in mm. All crystals are 1.25 inches long. Potential leads are usually spaced 0.9 inches apart.
χ	Angle between the long axis of the sample and the crystallographic (111) direction in degrees.
ϕ	Angle between the projection of the long axis of the sample on the (111) plane and the $(\bar{2}11)$ direction. ϕ is negative measured clockwise from $(\bar{2}11)$, in degrees.
S. D.	Symmetry direction of Figure 11 nearest to the long axis of the sample.
Comp.	Composition of the sample. 5N = 99.999% Hg, etc. Weight % of solute is given for alloys.
RRR	Residual resistance ratio defined for Hg as R(77° K)/R(4.2° K).
R_{He}	Resistance measured at 4.2° K in $\mu\Omega$. Measurement made in zero magnetic field unless otherwise noted in which case H is given in kOe.
α	Low field magnetoresistance coefficient derived from R-H data at 4.2° K. Units are kOe^{-2}.
HFRR	High field resistance ratio defined as R(48 kOe)/R(0 kOe) measured at T = 4.2° K.

Information on Experimental Samples

Crystal No.	A	χ	ϕ	S. D.	Comp.	RRR	R_{He}	$10^3\alpha$	HFRR
60	.5x2	74	+22	$(\bar{2}14)$	7N	---	8.68	---	2.16
69	.5x2	83	-83	$(02\bar{1})$	7N	170	8.00	---	2.12
71	.5x2	81	-77	$(02\bar{1})$	7N	170	8.42 (H=.7)	---	2.02
72	.5x2	--	---	---	7N	171	7.88	---	---
73	.5x2	41	-46	(021)	7N	170	6.50	---	2.03
75	.5x2	56	- 9	(011)	7N	168	9.62	---	2.10
77	.5x2	88	-85	$(01\bar{1})$	.01% Ag	121	10.4 (H=.7)	---	1.75
80	.5x2	22	+ 4	(111)	.01% Cd	138	7.28	5.9	1.88
82	2x2	53	-36	(021)	7N	168	1.52 (H=1)	9.0	2.01
83	.5x2	60	- 6	$(\bar{1}22)$	7N	171	7.62 (H=1)	9.8	2.09
84	.5x2	65	+ 8	(010)	7N	168	8.40	6.4	1.68
85	1x2	24	-88	(121)	7N	171	5.10	9.3	2.16
87	1x2	47	-33	(021)	7N	171	3.48	8.2	2.16
88	1x2	42	-73	(010)	7N	173	4.81	8.8	2.12
89	1x2	32	-10	(011)	7N	172	3.31	8.3	1.90
90	1x2	22	-83	(121)	7N	171	3.38	7.8	2.22
94	1x2	55	-45	(021)	7N	169	4.31 (H = .7)	---	1.86

Approximate values for the resistivity are as follows:

$T = 77°K$	$\rho_{\perp} = 7.25 \mu\Omega$-cm	$\rho_{\parallel} = 5.50 \mu\Omega$-cm
$T = 4.2°K$	$\rho_{\perp} = 42.7$ nΩ-cm	$\rho_{\parallel} = 32.3$ nΩ-cm

APPENDIX B

CALCULATION OF MAGNETORESISTANCE FROM THE FERMI SURFACE MODEL

The First Zone Contribution

We consider a (111) orientation for simplicity. The contribution to σ from the first zone caps will not be affected by the magnetic field in this orientation. Consider the states created on the cylindrical first zone necks and on the small areas between the necks. As the field is increased these states will be driven into the zone boundaries quite quickly and reflected by a reciprocal lattice vector to the other side of the zone. Complete cancellation of the contribution to σ will occur only for orbits in planes through the points L on the zone. The necks of the mercury surface are very large and thus many orbits exist in the neck region for which exact cancellation due to the reflection does not occur. It is not possible to calculate the contribution from these orbits in any exact way. Following Pippard, but realizing that our approximation is not as valid as his, we assume that orbits passing through first zone necks do not contribute to the conduction. Note that this assumption leads to a zero contribution to the conductivity from the first zone for most orientations away from (111). There are several arguments which make this approach at least plausible. First, if there is any significant

contribution from the first zone it should not be nearly as orientation dependent as that of the second zone, and thus would result only in a constant added to the calculated values of $\sigma(0)/\sigma(\infty)$ due to the second zone. Second, if a first zone contribution of any size is assumed, the calculated $\sigma(0)/\sigma(\infty)$ values would be smaller than those actually observed for all orientations.

The Second Zone Contribution

Direct integration of equation 6-14 over the second zone lens orbits would have to be done numerically by computer and the approximate nature of the model does not warrant such an approach. The method used here is to find an "average" orbit on the lens for each orientation. We first calculate the net number of electron states created on each segment of the lens. This is proportional to $\vec{E} \cdot \vec{v}$ or, in our approximation, to cos θ integrated over the region of the lens segment where $-\frac{\pi}{2} \leq \theta \leq \frac{\pi}{2}$. Next we calculate the average velocity in the field direction for the lens segment by

$$\bar{v}_z = \frac{\int v \cos\theta \, dS}{\int dS} = v \, \overline{\cos\theta} \qquad \text{(B-1)}$$

by integration over the same part of the surface as above.

The evaluation of $\overline{\cos\theta}$ allows us to state an average θ for the particular lens segment (neck or cap) in question. Thus we can then

compute the actual length of the orbit on the segment.

Next we proceed to find the average value of v_z over the entire lens by considering the segments calculated above. Let the subscript s refer to the paths on the spherical caps and n refer to the necks. Consider the general "average" lens orbit shown below. The average velocity in the z direction is then

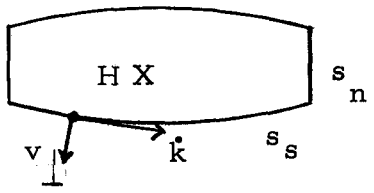

$$\bar{v}_z = \frac{v_{zs}\, t_s + v_{zn}\, t_n}{t_s + t_n} \qquad \text{(B-2)}$$

where t_i is the time spent in traversing the ith segment of the orbit. Clearly, $t_i = s_i/(ds_i/dt)$, $v_{\perp_i} = v_i \sin\theta_i$ and $v_{zi} = v_i \cos\theta_i$. Further

$$\hbar \dot{k}_i = \left(\frac{e}{c}\right) v_{\perp_i} H \qquad \text{(B-3)}$$

and

$$\dot{k}_i = \frac{ds_i}{dt} = -\left(\frac{1}{\hbar}\,\frac{e}{c} H\right) v_i \sin\theta_i . \qquad \text{(B-4)}$$

So that finally for the orbit

$$\bar{v}_z = \frac{v_{zs}\dfrac{s_s}{v_s \sin\theta_s} + v_{zn}\dfrac{s_n}{v_n \sin\theta_n}}{\dfrac{s_s}{v_s \sin\theta_s} + \dfrac{s_n}{v_n \sin\theta_n}} . \qquad \text{(B-5)}$$

If we assume $v_n = X v_s$, i.e., that the variation in the mean free path is due to variation of the Fermi velocity, we can write finally

$$\bar{v}_z = \frac{s_s \cot\theta_s + s_n \cot\theta_n}{\frac{1}{v}\left(\frac{s_s}{\sin\theta_s} + \frac{s_n}{X\sin\theta_n}\right)} . \qquad \text{(B-6)}$$

The total contribution to the conduction is just the net number of states created times this velocity. Note that these numbers will be different for every orientation. Also note that by our definitions s_s and s_c do not necessarily join--it is an average orbit in a mathematical sense.

The expression for the conductivity now takes the form

$$\sigma_{zz}(\infty) = \left(\frac{e^2}{4\pi^3\hbar}\right) \tau \bar{v}_z \sum_{i=1}^{2} \int \cos\theta_i dS_i . \qquad \text{(B-7)}$$

There are still two points to consider: First, finding s_s and s_n given θ_s and θ_n is a geometrical problem which is tedious but easily done and will not be discussed further. Secondly, the evaluation of the cosine integral of (B-1) over a lens segment would have to be done numerically because of the problem with limits for nonsymmetry orientations. The approximation made here for this integral is

$$\int_{\text{surface where } \theta > 0} \cos\theta \, dS \simeq \left[\int_{\text{entire surface}} \cos^2\theta \, dS\right]^{\frac{1}{2}} \Big/ \int_{\text{entire surface}} dS . \qquad \text{(B-8)}$$

We can check the validity of this approximation by doing an exact computation of $\sigma(0)$ for a spherical cap in the two extreme orientations where the left hand side of (B-8) can be evaluated exactly, namely when z is the polar axis of the cap and when z is perpendicular to the polar axis. The two equations of interest are

$$\sigma_{zz}(0)_{\text{exact}} = \left(\frac{e^2}{4\pi^3\hbar}\right)\tau v \int \cos^2\theta \, dS \tag{B-9}$$

$$\sigma_{zz}(0)_{\text{approximate}} = \left(\frac{e^2}{4\pi^3\hbar}\right)\tau \bar{v}_z \int \cos\theta \, dS \tag{B-10}$$

$$= \left(\frac{e^2}{4\pi^3\hbar}\right)\tau v \, \overline{\cos\theta} \int \cos\theta \, dS \tag{B-11}$$

$$= \left(\frac{e^2}{4\pi^3\hbar}\right)\tau v \left[\int \cos\theta \, dS\right]^2 / \int dS. \tag{B-12}$$

For the orientation z = polar cap axis, in arbitrary units,

$$\frac{\sigma_{\text{exact}}}{\sigma_{\text{approximate}}} = \frac{.123}{.121} \quad . \tag{B-13}$$

For the orientation z perpendicular to polar cap axis in the same units as (B-13),

$$\frac{\sigma_{\text{exact}}}{\sigma_{\text{approximate}}} = \frac{.006}{.005} \quad . \tag{B-14}$$

Thus we conclude that the approximation is quite good in the region where the contribution to σ is the greatest. We can then

combine equation (B-7) and(B-12) to give the form used in the calculation of the ratio plotted in Figures 38 and 39,

$$\frac{\sigma_{zz}(0)}{\sigma_{zz}(\infty)} = \frac{\sum_{i=1}^{2} v_i \left[\int \cos\theta_i dS_i \right]^2 / \int dS_i}{\bar{v}_z \sum_{i=1}^{2} \int \cos\theta_i dS_i} \qquad \text{(B-15)}$$

where the cosine integrals are evaluated by use of (B-8).